UCRL-53179-84
Distribution Category UC-20,20D

Fire Protection Research for DOE Facilities: FY 84 Year-End Report

H. K. Hasegawa, N. J. Alvares,
A. E. Lipska-Quinn, D. G. Beason,
K. L. Foote, S. J. Priante, and K. Staggs

Manuscript date: September 25, 1985

LAWRENCE LIVERMORE NATIONAL LABORATORY
University of California • Livermore, California • 94550

Available from: National Technical Information Service • U.S. Department of Commerce
5285 Port Royal Road • Springfield, VA 22161 • $10.00 per copy • (Microfiche $4.50)

Contents

Fire Protection Research for DOE Facilities: FY 84 Year-End Report

Abstract

Fire prevention is the ultimate form of fire safety and is the primary motivation of our program. DOE safety managers recognize the need to understand new fire risk conditions that can emerge as new energy-producing technologies are developed, and also the need to develop counter-measures to combat these changing fire risks. This Year-End Report contains data and analyses of the final year for 'Phase One' of the project "Fire Protection Research for DOE Facilities." Information presented here includes descriptions of: experiments to gain a better understanding of smoke transport and corrosive gas content of smoke along a horizontal path; experiments to understand the burning characteristics and heat production from electrical cable arrays; development of an enclosure fire model to define the hot-layer temperature for forced-ventilated rooms, and a logic diagram that defines allowable limits for enclosure fire model predictions; and procedures for parametric analysis of the reliability of the LLNL water-supply system, and an outline of our protocol for assessing fire risk in any size enclosure. Because this is the last report of this phase of our project, a synopsis of results from the efforts of previous years serves as an introduction.

Part 1: Introduction

Overview

This is the final year-end report for the project "Fire Protection Research for Department of Energy Projects" [Lawrence Livermore National Laboratory (LLNL) Project No. 6294-93]. In this report, we will describe the results of several parallel experimental and analytical project segments completed during FY 84. In most cases, these results build upon prior work and will require further refinement in FY 85 before assimilation into a final summary report, "The Protocol for Fire Risk Assessment for DOE Experimental Facilities." This Protocol will be published and distributed to DOE Headquarters after the end of FY 85, the termination date for Part I of this project.

The structure of this report is similar to the organizational structure of our project. The research concerned fire engineering, fire chemistry, fire risk assessment, fire modeling, and areas of suppression and detection, including fault-tree analysis. In FY 84, we have made significant progress in all of these areas, as summarized in this report. We describe the results and conclusions of our final series of forced-ventilated enclosure fire experiments, and also report our development of a model which is very successful for predicting temperature rise from forced-ventilated fires. Another section presents our conclusions on the corrosive potential of smoke, and the transport of smoke in long corridors from moderate fire sources. We discuss experimental results from small- and large-scale flame-spread studies on bunched and individual cable insulators, as well as the flame-spread response of cables exposed to external thermal radiation. Generic procedures of digraph/fault-tree analysis are discussed, using our analysis of the LLNL water-supply system as a test case. Finally, an outline of the fire-risk-analysis protocol is enclosed to show the importance of input data and assumptions on the validity of analysis.

Because of the relatively long duration of this project, and because of the many areas of research and analysis involved, we believe this final report

is the appropriate vehicle to review the results, accomplishments, and failures of our research during the entire project period. To this end, we enclose a narrative summary of the history, background, and philosophy of the project. The information is also presented in a brief form as Table 1-1.

Background

Our project, "Fire Protection Research for DOE Projects," has been active and productive since FY 78. The thrust of our research is to provide tools for fire risk assessment that are *predictive* rather than *responsive*. Instead of relying on the experience of past events, we attempt to analyze fire hazards based on a knowledge of materials behavior, materials configurations, environmental response, environmental influence, and feedback dynamics. Our approach was divided into three major areas:

(1) Defining the environment of concern.
(2) Establishing the engineering characteristics of contemporary fire-management procedures.
(3) Research into applicable fire risk analysis procedures.

Initially, we investigated all three areas simultaneously by surveying the existing literature, inspecting available facilities, and analyzing previously developed procedures. This exercise served to direct our program away from standard fire-protection techniques—which generally concern fire protection for the residential area—to address fire risk in large experimental facilities.

After defining the focus of our research, we began a systematic exploration of the fire-risk parameters in DOE experimental facilities. Our progress has been chronicled in 18 reports and papers published between 1979 and 1985. Five of these publications are "Year-End" reports, such as this one, which document our work for the previous fiscal year. A review of the abstracts and conclusions of the year-end reports will show the direction and emphasis of our research throughout the duration of this project.

Summary of Project

A brief description of our major publications since the beginning of this project provides a historical perspective on our research and accomplishments.

Fire Hazard Analysis for Fusion Energy Experiments (UCRL-82320—May, 1979)

This article described an analysis of fire risk parameters in a magnetic fusion facility, the 2XIIB experiment. The emphasis of this paper was to highlight our initial efforts.

- We conducted an analysis of the effectiveness of a dry pipe, pre-action fire management system. This dry-pipe system was initially selected to prevent the inadvertent release of water to the experiment. Our analysis was performed using fault-tree techniques which revealed that the dry-pipe system could malfunction with an 18% chance of unavailability. On the other hand, standard wet-pipe sprinkler systems have a tested reliability of 98%, and thus would be unavailable only 2% of the time. Our analysis also showed the risk of inadvertent water release to be minuscule.
- After a survey of LLNL facilities, we found that the major fuel load in large energy experiments is the insulation on electrical conductors and in electrical apparatus.
- We identified the existence of necessary and sufficient ignition sources throughout large facilities housing energy experiments.
- We reported a survey of enclosure fire models, and applied an empirical exponential-growth model to the estimated fuel load in the space we analyzed. The results varied widely, depending on which growth exponent was used.

FY 79 Year-End Report (UCID-18902—January, 1980)

During this period, we built on the preliminary work described in the previous paper.

- We confirmed the universality of our fuel-load assessment by questionnaire and survey of energy research laboratories throughout the world.
- We instituted a new fire-risk analysis in the building which housed the Shiva laser system. Preliminary data from our fault-tree investigation provided input into this analysis.
- We attempted to develop a system for smoke-aerosol analysis to define the smoke source term from flammable materials, particularly insulations and covers on electrical conductors.
- We began our chemical analysis of smoke from burning insulation materials.

- We developed procedures to define the corrosion potential of commonly used cable insulations and covers. By passing evolved gas from heated insulation materials through a buffered-water solution, we then compared the thermal parameters of the experiment to pH reduction in buffered water. We investigated the conditions for smoke corrosion using a small-scale portable test cell.

FY 80 Year-End Report
(UCRL-53179—May, 1981)

- We completed generic fault trees for the Shiva experiment. The Shiva facility contains wet-pipe sprinklers, independent smoke detectors, and a Halon 1301 detection/suppression system. We drew a fault tree for each of these three systems and then defined its reliability. We emphasize that these fault trees are generically drawn and can be used as patterns for new analyses. New analysis will require definition of the operational characteristics of low-voltage supply and control circuits before the fault-tree analysis can be completed.
- We tested and applied the Cal Tech enclosure-fire model to selected 2XIIB enclosures, assuming positive ignition. The results indicate no potential for fire growth in all but one of the analyzed enclosures. Assuming constant fire strengths, we determined the ceiling-layer temperature and the elevation of the layer interface. We used an *ad hoc* source term to define smoke concentration in the hot layer. We were unable to validate these results.
- We performed small-scale tests to measure ease-of-ignition and the production of excess pyrolyzates; these measurements allowed us to define insulation behavior and the production of flammable aerosols. The tests showed that the tested PVC cable was more difficult to ignite and produced less excess pyrolyzate than did the tested Neoprene. Our measurements of cable heat-release rates show a similar correlation at low exposure flux; this trend reverses at high flux.
- Measurements of hydronium-ion concentration show that, at all exposure fluxes, PVC produced a far greater amount of acidic product gases than did Neoprene.
- We continued our attempts to measure smoke-aerosol concentration and to produce dilution techniques, without success. Although many promising avenues were explored, all were found to have technological blocks.
- Smoke-chemistry advances in decomposition kinetics and the identification of pyrolyzate composition hinted at the mechanisms of retardants by chlorine-containing polymers. This analysis also demonstrated the difference in pyrolyzate production with exposure flux.

FY 81 Year-End Report
(UCRL-53179-81—July 1982)

- We began an effort to produce a simple but accurate enclosure fire in our test cell to be used for model validation. Since the test cell is forced-ventilated, we are able to simulate conditions that exist in many modern DOE laboratories. This initial work was done in cooperation with Los Alamos National Laboratory, who had similar interests under contract to NRC. These experiments yielded a great deal of information on enclosure fire parameters.
- We completed 13 forced-ventilated tests and attempted to make initial comparisons of data with model predictions.
- Other experiments conducted in the test cell involved preliminary tests of typical fuel arrays using vertically burning cables or stacked computer-tape containers.
- Several studies of extinguishant efficiency using CO_2, AFFF, Halon 1301, Halon 1211, and water sprays were performed against various fuels.
- A survey and analysis of contemporary early-warning, fire-detection sensors revealed that, as of 1981, the most innovative detection scheme combined both ionization and light-scattering sensors into one unit; aerosols produced by both flaming and smoldering sources could then be sensed with equal efficiency.
- We completed and published the fire risk assessment protocol for the Shiva fusion facility. This assessment integrated both tangible losses and intangible factors (such as programmatic delay) as well as indirect damage factors, such as smoke corrosion and thermal distortion of items not directly affected by the fire.
- We attempted to define the scope of fuel materials requiring analysis. A survey of electrical conductor designations in LLNL stock showed over 200 types. By using thermogravimetric analysis and differential scanning calorimetric analysis, we were able to identify 20 cable insulations and covers which have generically similar thermal properties to the 200 materials in stock.
- We conducted additional experiments to identify the mechanisms of retardants and plasticizers in PVC and Neoprene polymers by comparing their thermal behavior and decomposition kinetics to virgin-PVC and virgin-Neoprene (polychloroprene).

Table 1-1. Summary of background and progress of the project, "Fire protection research for DOE facilities."

Fiscal year	General Survey	Fire Engineering
1978	• Surveyed fuel load (LLNL) • Surveyed ignition source (LLNL) • Surveyed state of art—enclosure fire modeling	
1979	• Surveyed international and national fuel load — cable insulation and covers — computer tapes and readout paper • FY 78 paper, "Fire Hazard Analysis for Fusion Energy Experiments"	• Physical smoke analysis —dilution probe development
1980	• Surveyed range of ignition sources for DOE experiments — release of flammable liquid — high-power electrical sources — trash • FY 79 Year-End Report	• Further dilution probe development • Preliminary small-scale ignition tests • Excess pyrolyzates survey; general materials • Heat-release rates—PVC and Neoprene cables
1981	• State-of-art survey on smoke detectors, response sensitivity, and failure modes • FY 80 Year-End Report	• Began enclosure-fire validation experiments (forced ventilation) • Fire tests on three-dimensional arrays of computer tape cassettes • Began large-scale cable fire tests
1982	FY 81 Year-End Report	• Enclosure-fire validation experiments — reduced data, re-cast analysis — developed appropriate mass and energy balance factors • Ease-of-ignition small-scale ASTM/NBS protocol • Continued large-scale cable fire test
1983	• Surveyed DOE fire-protection and fire-safety engineers concerning fire-protection problems at their facilities. Set priorities of list of subjects suggested by these engineers at bi-annual meeting. • FY 82 Year-End Report	• Continued enclosure-fire validation studies — new procedures, new instruments — new experiments, new data • Continued large-scale cable flame-spread and heat-release rate test
1984	• FY 83 Year-End Report	• Conducted and reduced 83–84 enclosure-fire test series • Conducted radiation-enhanced small- and large-scale cable flammability tests • Fort Cronkhite smoke-production and spread-rate tests
1985	• FY 84 Year-End Report	• Finished data-reduction and analysis

Fire Chemistry	Detection/Suppression	Risk Analysis and Modeling
	• Fault-tree analysis, 2XIIB	• Exponential fire growth (Friedman) • Plume entrainment and ceiling-jet dynamics (Alpert)
• Chemical smoke analysis — initiated procedure for hydronium-ion determination — confirmed smoke corrosion of optics and electronics from PVC and Neoprene smoke	• Fault-tree analysis, Shiva — initiated procedure	
• Correlated hydronium-ion production to heat-release rate exposure conditions • Began thermal decomposition studies in cable insulations	• Fault-tree analysis, Shiva — wet-pipe sprinkler — detector-grid analysis — Halon 1301 control room	• Applied Cal Tech model to 2XIIB — ceiling layer height — ceiling layer temperature — smoke dilution (*ad hoc* source term)
• Procedure developed and implemented to delimit the inventory of cable types (200^+ found at LLNL). Investigated 20 representative types • Began studies on representative cables to define the mechanism of thermal degradation and the effect of additives	• Tested effectiveness of fire extinguishants on a variety of three-dimensional fuels and pooled-liquid fuels	• Total fire-risk assessment for Shiva facility
• Defined 20 representative insulation and cable covers for total LLNL cable inventory • Continued decomposition studies to define: — production of hydronium ions — effects of additives on decomposition		• Total fire-risk analysis of tandem mirror test facility completed
• Determined that heating rate of polymers has a minimal effect on the critical degradation temperature • Investigated presence of common and unique gases released by insulations and cable covers	• Digraphs and fault-tree analysis applied to LLNL water-supply system	• First model-validation exercise using forced-ventilated enclosure fire results
• Completed background library of thermal and chemical behavior of representative insulators and cable covers • Analyzed Fort Cronkhite data in terms of hydronium-ion loss in smoke remote from the fire source	• Constructed procedure for digraph and fault-tree analysis • Conducted tests of liquid nitrogen as a noncontaminating extinguishant for cable fires	• Outlined protocol for total fire risk assessment • LLNL simple temperature model
• Finished data-reduction and analysis		• Refined LLNL simple temperature model • Refined risk-assessment protocol regarding limits to model application

FY 82 Year-End Report
(UCRL-53179-82—September 1983)

- Advances in the procedures and precision of our enclosure fire experiments began to show a lack of predictive ability in contemporary forced-ventilated models. We found that the Cal Tech model fit our data better than did other available models. However, in rigorous comparison, none of the models gave very encouraging results. Simplification of the Cal Tech model to a closed-form integral equation allowed us to quickly compare our data with the predictions of the model and to adjust the model variables. We were unable to produce model modification factors which would unambiguously recreate actual fire parameters.
- We completed 27 model-validation experiments, varying the fire strength, ventilation rate, fuel composition, and fuel phase.
- We measured the ease-of-ignition of real cables, using a proposed ASTM method developed at the National Bureau of Standards. This procedure was similar to the method we used in FY 80, but the procedures were much more rigid. Results of these experiments showed that the ignition response was sensitive to the insulation composition and thickness, cable diameter, and electrical-conductor configuration. Due to these variables, we were unable to perform a reliable ranking.
- Six large-scale cable flame-spread experiments were performed in the test cell. These experiments indicated the importance of cable "packing" (the density of cables in a specific area) on the flame-spread rate. The greatest flame spread occurred when the ratios of surface area of all cables in the array volume is a maximum.
- We continued studies of the corrosive and noncorrosive chemicals produced during the main degradation phase of a large number of commercial plastic insulations and their virgin counterparts. We also studied how the heating rate in air affected the onset of initial decomposition of the various insulations.
- We applied the protocol for fire-loss assessment to the TMX-U experiment, a major new LLNL magnetic-fusion experiment.

FY 83 Year-End Report
(UCRL-53179-83—August 1984)

- Our major accomplishments of FY 83 were centered around the large-scale cable burn tests and the continued enclosure-fire model validation tests. Because of test-cell scheduling, the model validation tests were extended into FY 84. Because of better instrumentation and new insight into enclosure fire characteristics, this series of experiments contains the most precise data we have yet produced.
- We analyzed our FY 82 enclosure-fire validation data to assess the capabilities of the new generation of enclosure fire models, which had been modified to predict conditions in forced-ventilated enclosures. As before, this set of models could approximate some of the actual fire data trends, but not with encouraging frequency as fire conditions were changed.
- The results of cable fire tests showed general trends only, confirming previous data on cable packing and showing that flame-spread variation was never greater than 10:1 between all cable types tested. Our data does not show a clear correlation between flame-spread rate and heat-release rate.
- We demonstrated another application of fault-trees in a detailed analysis of the LLNL water-supply system. (A primary factor in the fire-fighting capability of all facilities is an unlimited water supply.) Our analysis used procedures we have developed and applied to fire-protection systems in several LLNL energy research facilities. Results of the analysis indicated the probability of the system being unavailable on demand was 3.6×10^{-4}. Actual experience shows that demand unavailability was 6.1×10^{-5}, in good agreement considering that the only unavailability data was recorded for completely empty systems.
- Fire chemistry efforts added to our database of combustion products from electrical insulations, and confirm that the rate of heating does not markedly affect the critical temperature at which insulation polymers decompose. However, the rate of heating does greatly change the nature and concentration of the degradation products.

List of Major Publications

1. J. R. Gaskill, "Smoke and Corrosivity," *Proceedings, Symposium on Flammability of Solid Polymer Cable Dielectrics*, Electric Power Research Institute, Palo Alto, CA, EL-1263 (1979).
2. N. J. Alvares and H. K. Hasegawa, "Fire Hazard Analysis for Fusion Energy Experiments," *Fire Safety Journal*, 2, 191–211 (1979/1980).
3. G. P. Naanep, H. E. Lambert, and H. K. Hasegawa, "Fire Protection Study of the 2XIIB Mirror Fusion Facility," submitted to *IEEE*, also available from Lawrence Livermore National Laboratory, Livermore, CA, UCRL-82277 (1979).
4. H. K. Hasegawa, N. J. Alvares, A. E. Lipska, H. Ford, and D. G. Beason, *Fire Protection Research for Energy Technology Projects; FY 79 Year-End Report*, Lawrence Livermore National Laboratory, Livermore, CA, UCID-18902 (1981).
5. A. Lipska, S. Priante, D. Beason, H. Ford, and S. Stover, *The Combustion of Reels of Magnetic Tapes*, Lawrence Livermore National Laboratory, Livermore, CA, UCID-18976 (1981).
6. H. K. Hasegawa, N. J. Alvares, A. E. Lipska, H. Ford, S. Priante, and D. G. Beason, *Fire Protection Research for Energy Technology Projects; FY 80 Year-End Report*, Lawrence Livermore National Laboratory, Livermore, CA, UCRL-53179 (1981).
7. N. J. Alvares, "Gross Mechanism of Smoke Aerosol Production from Solids, Liquids, and Gases," *Proceedings, Symposium Institute of Environmental Sciences*, 28th Annual Tech. Meeting, Institute of Environmental Sciences, Atlanta, GA (April 1982).
8. H. K. Hasegawa, N. J. Alvares, A. E. LIpska-Quinn, D. G. Beason, K. L. Foote, and S. J. Priante, *Fire Protection Research for Energy Technology Projects; FY 81 Year-End Report*, Lawrence Livermore National Laboratory, Livermore, CA, UCRL-53179-81 (1982).
9. H. K. Hasegawa, N. J. Alvares, A. E. Lipska-Quinn, D. G. Beason, S. J. Priante, and K. L. Foote, *Fire Protection Research for Energy Technology Projects; FY 82 Year-End Report*, Lawrence Livermore National Laboratory, Livermore, CA, UCRL-53179-82 (1982).
10. F. R. Krause and N. J. Alvares, *Experimental Simulation of Forced-Ventilation Fires*, Los Alamos National Laboratory, Los Alamos, NM, LA-UR-84-1691 (1982).
11. N. J. Alvares, A. E. Lipska-Quinn, and H. K. Hasegawa, "Thermal Degradation of Cable and Wire Insulation," *Symposium, Behavior of Polymer Materials in Fire*, American Society for Testing and Materials, Philadelphia, PA, ASTM STP 816 (1983).
12. N. J. Alvares and K. L. Foote, "Contrast Between Natural and Controlled Fires in Forced-Ventilated Enclosures," *Proceedings of the CSNI Specialist Meeting on Interaction of Fire and Explosion with Ventilation Systems in Nuclear Facilities*, Committee for the Safety of Nuclear Installations, April 25–28, 1983, Los Alamos National Laboratory, Los Alamos, NM; also available from Lawrence Livermore National Laboratory, Livermore, CA, UCRL 88588 (1983).
13. N. J. Alvares, "Experiments in Forced-Ventilated Enclosures to Validate Enclosure Fire Models," *Workshop on Modeling Pre-Flashover Fires*, Boras, Sweden, May 1983, CIB-W-14.
14. H. K. Hasegawa, N. J. Alvares, A. E. Lipska-Quinn, D. G. Beason, K. L. Foote, S. J. Priante, and K. Staggs, *Fire Protection Research for Energy Technology Projects; FY 83 Year-End Report*, Lawrence Livermore National Laboratory, Livermore, CA, UCRL-53179-83 (1984).
15. D. McGehee, "Radiative and Convective Heat Transfer in a Compartment Fire," Lawrence Livermore National Laboratory, Livermore, CA, UCID, in press 1985.
16. N. J. Alvares, K. L. Foote, and P. J. Pagni, "Forced Ventilated Enclosure Fires," special issue of *Combustion Science & Technology*, **39** (1984), published as *Fire Science for Fire Safety*, Robert S. Levine and Patrick S. Pagni, Eds. (Great Britain: Gordon and Breach, 1984), pp. 55–81.
17. H. K. Hasegawa and H. E. Lambert, "Reliability Study on the LLNL Water Supply System," *Proceedings, First International Symposium on Fire Safety Science*, Gaithersburg, MD, October 1985, also available from Lawrence Livermore National Laboratory, Livermore, CA (1985).
18. D. Beason, S. Priante, and A. Lipska-Quinn, *Corrosive Product Formation in Smoke from the Combustion of Polyurethane/Neoprene Cribs*, Lawrence Livermore National Laboratory, Livermore, CA, UCRL-92331 (1985).
19. K. L. Foote, P. J. Pagni, and N. J. Alvares, "Temperature Correlations for Force-Ventilated Compartment Fires," *First International Symposium on Fire Safety Science*, Gaithersburg, MD, October 1985, also available from Lawrence Livermore National Laboratory, Livermore, CA, UCRL-92818 (1985).

Part 2:
Fire Chemistry: Thermal Degradation of Cable and Wire Insulations

Introduction

Many facilities housing expensive electronic equipment are not protected against possible fires with early-warning smoke detectors. In order to design appropriate detectors, more information is needed about the fate of smoke which contains corrosive products from the combustion of various plastic cable and wire insulations.

Our previous laboratory efforts emphasized the fundamental aspects of thermal degradation of such insulations (Hasegawa et al., 1981, 1982). From the results of these studies, we learned the degradation temperatures of the materials, the rates of degradation, the nature of the various degradation products, and the influence of the additives used in the material formulations as well as the heating rate. Specifically, we found that all insulations generate detectable amounts of light hydrocarbons in the early stages of decomposition.

The insulations which form corrosive products (such as HCl from PVC and Neoprene, HF from Teflon, HCN from polyurethane, acetic acid from wood) do so at the onset of the early stage of degradation. The amount of corrosive products released into the environment is governed by the additives used in the material formulation (e.g., ZnO, MgO, Sb_2O_3 and $CaCO_3$).

We found that higher heating rates increase the rates of formation of light hydocarbons as well as corrosive products. This information, coupled with the concentration of corrosive products as a function of time after ignition and distance from the fire, is extremely useful in selecting or designing early-warning alarm systems.

Large-Scale Experiments

The primary goal of this study was to determine how far smoke which contains corrosive products will travel from the fire source. Our laboratory-scale experiments gave us little information about the fate of the smoke in terms either of the rate of travel from the source or of the concentration of corrosive products as a function of time from ignition and distance from the fire. We then studied burns in the LLNL full-scale fire test facility; however, the walls became rapidly coated with smoke after each burn, making it impossible for us to conduct a meaningful study of the fate of the smoke because outgassing from the accumulated products on the walls adversely influenced our results.

As a result, our large-scale experiments were conducted near San Francisco at Fort Cronkhite, former site of many defense batteries built during World War II. We chose the Battery Townsley because it was located in an unpopulated area overlooking the ocean side of the San Francisco Bay where appreciable breezes help dissipate degradation products from the area after termination of a burn. In addition, the tunnel was free of soot and large enough for us to effectively determine the fate of smoke from our burns. The section of the battery tunnel used for our test was 12-ft wide, 13-ft high, and 200-ft long, as shown in Fig. 2-1. One end of the tunnel was closed off by a wall made of 5/8-in. sheetrock attached to a 12 × 13 ft frame constructed of two-by-fours. The wall had a 6-ft door, which was opened at the conclusion of each test.

Experimental Procedure

The laboratory-scale and test-cell experiments which preceded the Fort Cronkhite tests allowed us to select optimal fuel compositions, sample configurations, and instrument design for grab-sampling the corrosive products present in the smoke. These tests indicated that a 50/50 mixture of Neoprene and polyurethane foam arranged in a 3- × 3-ft crib would produce optimal burn parameters for corrosive-product generation under the most severe fire conditions. The corrosive potential was measured in terms of pH change resulting from the formation of HCl from the burning Neoprene and HCN from the burning polyurethane. We also measured smoke density and weight loss of the burning Neoprene and polyurethane sample to better characterize the fate of the smoke. A 30-lb sample crib (Fig. 2-2) consisted of alternating layers of 2- in.-thick polyurethane sheets and 2-in.-diameter Neoprene pipe insulation. Each crib had eight layers of polyurethane and seven layers of Neoprene.

Five sampling stations positioned at 10, 45, 80, 115, and 150 ft from the fire were used to take grab samples of the corrosive products. Each sampling station (Fig. 2-3) contained five filtering flasks with 200 ml of water in each. The flask was connected to glass tubing positioned 1 ft off the ceiling of the tunnel. A glass-wool filter was

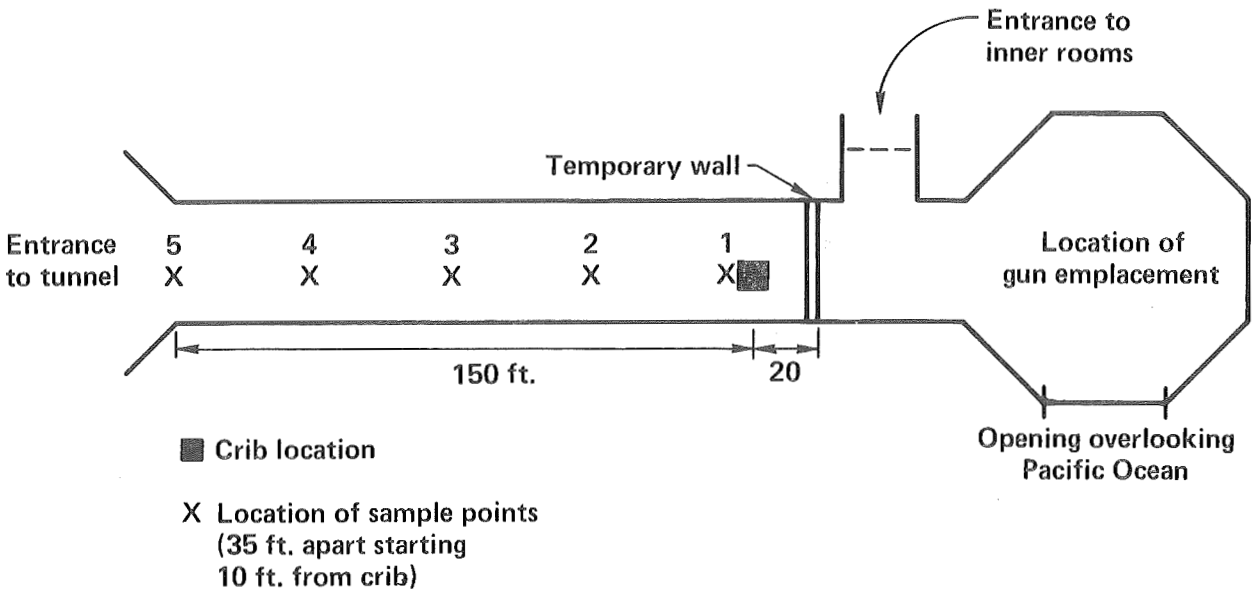

Figure 2-1. Drawing of experimental tunnel showing location of crib, sample station, and temporary wall.

Figure 2-2. Sample crib consisting of alternating layers of polyurethane sheets and Neoprene pipe.

placed between the filtering flask and the valve to prevent large particles of soot from contaminating the solenoid valve. The products were drawn into the flasks at a rate of 9 liter/min by a vacuum source controlled by solenoid valves and were sampled at each station for a one-minute duration at 1-min intervals starting one minute after the onset of burning. Samples were analyzed in a mobile laboratory after termination of each burn. By trapping soot particulates, we probably reduced the pH effect by excluding HCl adsorbed to soot surfaces. We did not monitor CO_2 in the combustion gases, which could form carbonic acid in the test flasks. Small-scale tests using polyurethane and Neoprene indicate that pH reduction by the formation of carbonic acid is overwhelmed by the acidic products from these materials.

The monochromatic transmission of a He-Ne laser beam through the smoke was measured at three places in the tunnel. A laser and photodiode system with a path length of 18 inches was mounted at the tops of sample stations 1, 3, and 5, and used to record light transmission through the smoke (Fig. 2-4). This system also allowed us to determine the time for smoke to travel the length of the tunnel. The systems were adjusted for 100% transmission before each run. Calibration was done in place with neutral-density filters to determine the light reduction vs voltage drop. A #1 neutral-density filter produced a drop of 100% to 10% transmission.

Weight loss of the burning material was measured with a simple three-point load platform. A 50-lb. load cell was used as one of the three points. The output was recorded every five seconds. We calibrated the instruments both in the laboratory and in the field to verify proper operation.

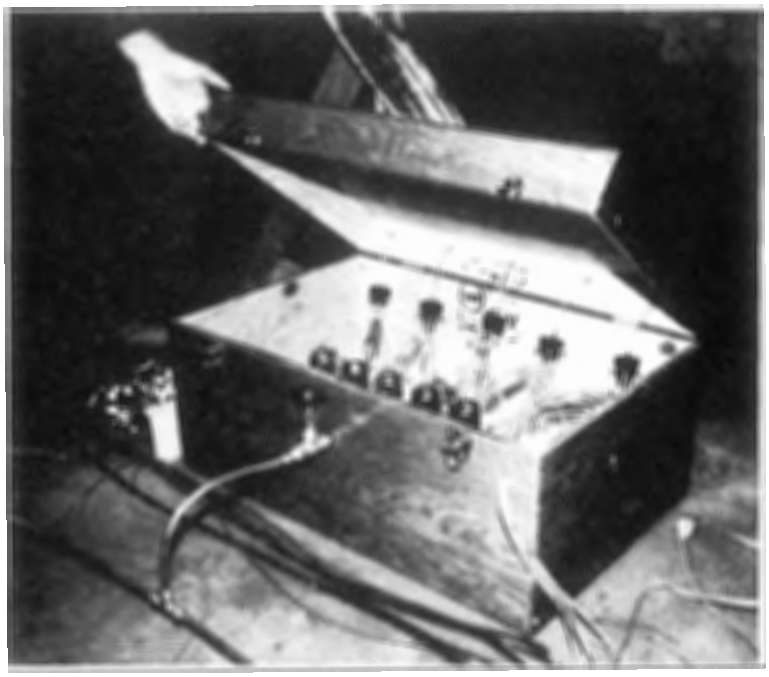

Figure 2-3. Gas-sampling rig showing sequential solenoids and corresponding water-containing flasks used to monitor pH change with time.

Figure 2-4. Residue of smoke pattern after burn at Fort Cronkhite. The laser and photodiode system can be seen in the foreground.

Results

Table 2-1 summarizes the results of the two burns. All stations registered a considerable drop in pH after one minute of sampling. As expected, the most pronounced pH change occurred at the sampling station nearest the fire, and the smallest pH change occurred at the most distant station. Most of the stations registered the greatest drop in pH less than four minutes into the burn, at which time the sample had lost about 50% of its weight. After this time, the pH began to climb again due to air dilution inside the test corridor.

Smoke-obscuration measurements revealed that there was an approximate 25% reduction in light transmission 120 seconds after ignition, and that the smoke density reached its equilibrium about 200 seconds after ignition. We found that the smoke travelled from Station 1 to Station 5, a distance of 140 ft, in 90 seconds, which indicates that under these specific burn conditions (a naturally ventilated corridor with a 1-MW fire burning at one end), smoke travels at a rate of about 1.6 ft/s. As expected, all of the smoke migrated to the upper level of the tunnel. The depth of the smoke layer was 4.8 ft at the closed (fire) end of the tunnel, and 2.6 ft near the open end, as determined by measuring the extent of residual smoke deposited on the walls (Fig. 2-4).

Figure 2-5 compares weight loss of the fuel, pH change, and smoke density (light transmission) as functions of time at Station 1 during the first test. At the time of the initial pH drop, there was very little weight loss, but at four minutes into the burn a 52% weight loss accompanied a pronounced pH change as well as a 55% reduction in light transmission. The overall weight loss at the conclusion of the test was 82%.

We combined the above results with those of thermogravimetric analysis (TGA) performed in the laboratory to estimate the amount of HCl formed from the burning Neoprene/polyurethane mixture. TGA was used to determine the pattern and rate of degradation of each plastic comprising the mixture. Each plastic was heated separately and as a 50/50 mixture in air at a heating rate of 115°C/min. The TGA results are shown in Fig. 2-6. Using the weight loss of the composite samples obtained from the Cronkhite test, and assuming that after six minutes all of the polyurethane was burned, we concluded that the remaining weight was unburned Neoprene. Taking the weight loss,

Table 2-1. Change of pH light transmission and weight loss of the polymers as a function of time for a burning Neoprene/polyurethane crib.

Test 1

Time	Station 1		2	3		4	5		Residual weight
(s)	pH	%T	pH	pH	%T	pH	pH	%T	(%)
0	5.46	100	5.46	5.46	100	5.46	5.46	100	100
60	5.46	100	5.46	5.46	100	5.46	5.46	100	98.2
120	4.03	78.6	3.97	4.08	85.6	4.24	4.43	83.8	87.9
180	3.55	40.0	3.74	3.65	63.3	3.88	4.08	75.5	66.8
240	3.56	49.7	3.94	3.79	57.5	3.87	4.34	61.1	47.7
300	3.41	46.5	3.87	3.84	63.1	3.98	4.59	62.1	30.9
360	3.71	62.6	3.97	3.90	64.1	4.13	4.86	63.6	18.1

Test 2

Time	Station 1		2	3		4	5		Residual weight
(s)	pH	%T	pH	pH	%T	pH	pH	%T	(%)
0	5.33	100	5.33	5.33	100	5.33	5.33	100	100
60	5.33	100	5.33	5.33	92.9	5.33	5.33	100	95.4
120	4.11	81.2	4.12	4.12	83.6	4.23	4.85	79.9	85.1
180	3.57	50.2	3.84	3.69	57.5	3.89	4.61	69.2	65.9
240	3.44	51.1	3.90	3.73	66.3	3.77	4.81	56.6	44.6
300	3.33	44.1	3.74	3.71	61.3	3.84	5.07	61.3	24.4
360	3.45	62.6	3.84	3.70	59.9	3.98	5.07	65.2	10.1

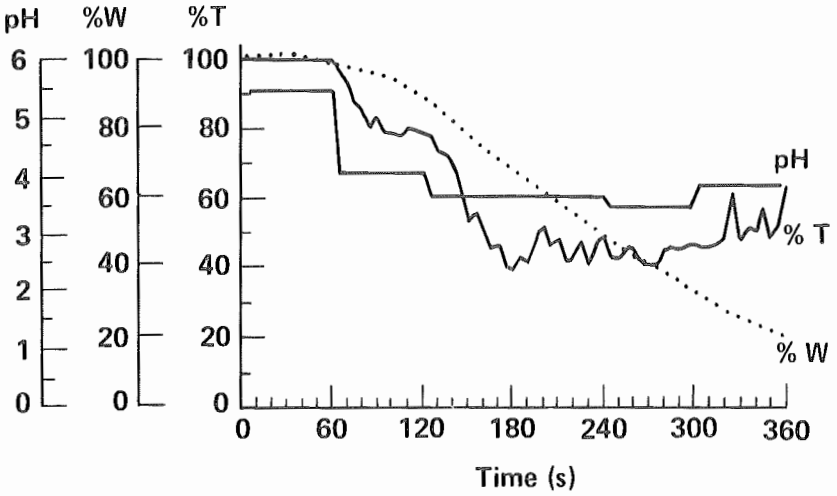

Figure 2-5. Evolution of smoke, pH change and weight loss as a function of time at Station 1.

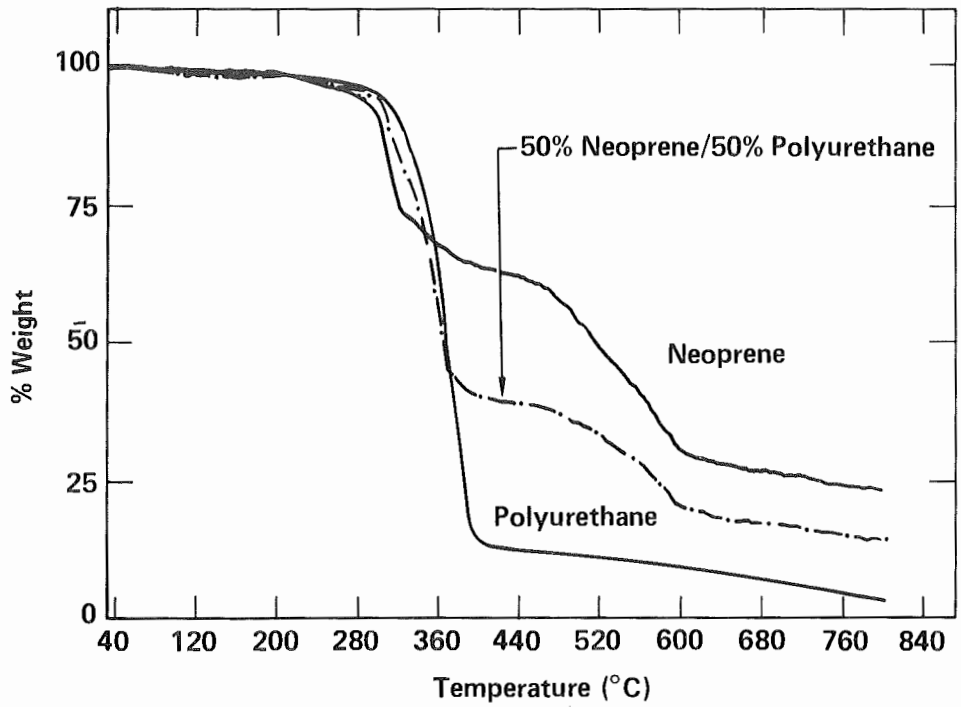

Figure 2-6. Weight loss of Neoprene, polyurethane and composite of 50% Neoprene 50% polyurethane.

plus the structural formula of the polychloroprene unit comprising the Neoprene polymer as well as the amount of additives used in the formulation, we estimated the amount of HCl formed. This simple approach can also be applied to estimating the amount of corrosive products formed from other materials. The results are summarized in Table 2-2. We see that formulations with even 20% additives appear to form substantial amounts of HCl, and we conclude that all acidic gases will travel with the rest of the smoke components at a rate of 1.6 ft/s.

Conclusions and Recommendations

Overall, we found that corrosive products are formed during the very early stages of degradation of the insulation materials. This correlates well with our previous findings which show that low-molecular-weight hydrocarbons are formed during the early stages of polymer degradation. We observed that smoke containing corrosive products will travel from a fire source (at a rate of 1.6 ft/s in this test) and has the potential to cause damage to corrosion-sensitive equipment. It is essential that facilities housing costly equipment be protected by smoke-detection systems capable of the earliest possible warning. Since existing smoke detectors are not designed to detect light hydrocarbons or corrosive gases, we suggest that a new smoke detector should be considered, designed specifically for detection of straight-chain light hydrocarbons or acid gases.

Table 2-2. Estimated HCl generation from a burning Neoprene/polyurethane crib after six minutes.

Fuel description	Initial amount of Neoprene and polyurethane (kg)	Initial amount of Neoprene (kg)	Amount of fuel lost (kg)	Amount of Neoprene lost (kg)	Amount of HCl formed (g)
50% Neoprene/50% polyurethane (pure Neoprene)	13.636	6.818	11.045	4.277	1749.6
50% Neoprene/50% polyurethane (Neoprene with 5% additives)	13.636	6.477	11.045	3.886	1589.7
50% Neoprene/50% polyurethane (Neoprene with 10% additives)	13.636	6.136	11.045	3.545	1450.0
50% Neoprene/50% polyurethane (Neoprene with 15% additives)	13.636	5.695	11.045	3.204	1310.7
50% Neoprene/50% polyurethane (Neoprene with 20% additives)	13.636	5.454	11.045	2.863	1171.2

Part 3:
Fire Experiments of Wire and Cable

Introduction

This section is a summary of the final series of small- and large-scale fire experiments conducted in FY 84. Several unique experiments were conducted during this period.

- Large-scale experiments on cables with brass and copper cores and polymethylmethacrylate (PMMA) jackets.
- Tests on cables that exploded when ignited.
- A large-scale fire extinguished with liquid nitrogen.

We completed our large-scale vertical cable burns with 13 experiments (some of which exposed the vertical cable array to flux from an external gas-fired radiant panel); in addition, we performed 55 cable flame-spread experiments using a small-scale radiant panel apparatus. Finally, we compared the large-scale results to the small-scale tests (which included thermogravimetric analysis).

Large-Scale Vertical Cable Experiments

These large-scale burns began in FY 82 and continued through FY 83. The results from the previous series indicated several important facts: for most cable types, the 50%-pack configuration (a two-layer bundle of 10–11 cables with a one-diameter space between adjacent cables) produced the highest heat-release rate. When exposed to the 5-W/cm^2 fire, most of the cable types were difficult to ignite, and once ignited, the flame-spread rate (FSR) was very slow; in most cases, the extent of flame spread was only a fraction of the vertical section, and heat-release rates remained low and peaked slowly. Finally, we found that fire performance depends on the cable diameter, the percentage of conductor, and the packing density. Multi-conductor cables generally have less fire resistance.

Our 1983 test series was performed for the following reasons:

- To obtain realistic cable fire data to be applied to fire risk assessment models. The three primary parameters were flame-spread rate (FSR), mass-burning rate ($\dot{m}_f$), and heat-release rate (HRR).
- To compare these data to results from our small-scale tests to assess the correspondence to real conditions.
- To obtain specific fuel and enclosure-fire parameters such as: temperature profile along the vertical surface, temperature distribution throughout the test cell, and enclosure ventilation changes from the heat-release rate.
- To define the change in cable fire performance by increasing the intensity of the exposure fire from the previous test series.
- To attempt to rank cable types according to their potential fire hazard.

Experimental Setup

Figure 3-1 shows the support structure for our vertical-cable tests. The bundle of electrical conductors is suspended from a steel cable threaded over two bicycle wheels to decrease friction and is attached to a counter-balanced load cell to dynamically monitor the specimen mass loss. Adjacent to the specimen is a vertical panel with half-meter increments for visually monitoring the flame spread. Calorimeters and radiometers are located at the ignition source, near the specimen bottom and at mid-height. Thermocouples attached to the specimens sense the temperature of the insulation in order to monitor heat transfer during flame spread. Note that these thermocouples were embedded in the insulation volume, and hence the temperature they sense is a bulk property of the material, dependent on insulation composition *and* thickness. Chromel-alumel thermocouples are also located at strategic points throughout the test cell to monitor temperature distribution throughout the enclosure. Gas analyzers located in the exit duct of the test cell are used to measure concentrations of oxygen, carbon dioxide, carbon monoxide, and total hydrocarbons with time.

Ignition Source. The primary ignition source for these tests was a premixed gas-and-air burner with gravel as a diffusion medium. This 30-cm-o.d. circular burner produced an exposure flux of 5 W/cm^2 at an energy-release rate of 20 kW on the underside of the horizontal section of the cable run (see Fig. 3-1).

Test Specimen. The test specimens for these experimental series were two-layer cable bundles formed into a perpendicular "Z" configuration, as shown in Fig. 3-2. Table 3-1 lists the

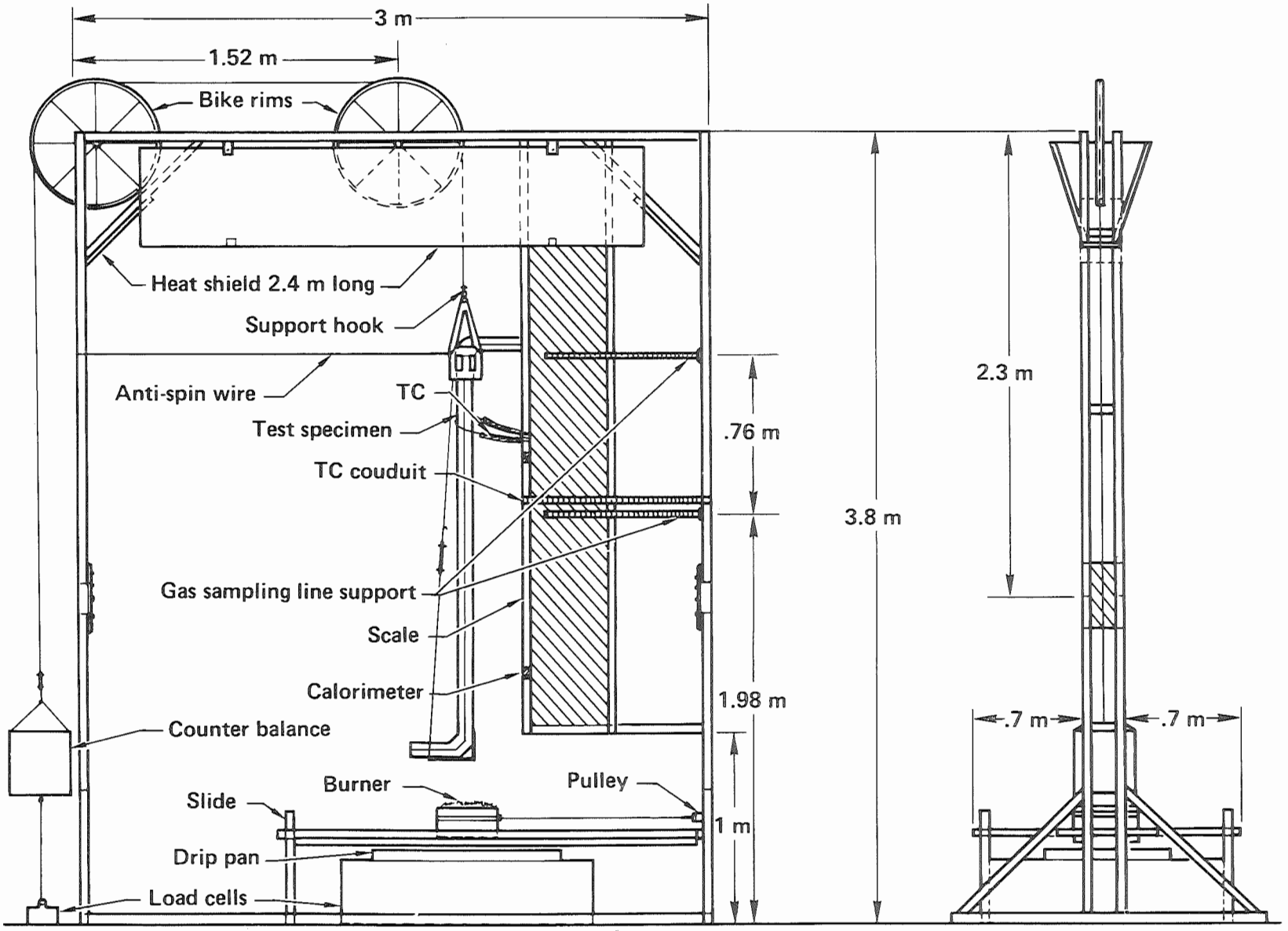

Figure 3-1. Experimental support structure for vertical-cable-burn experiments (TC = thermocouple).

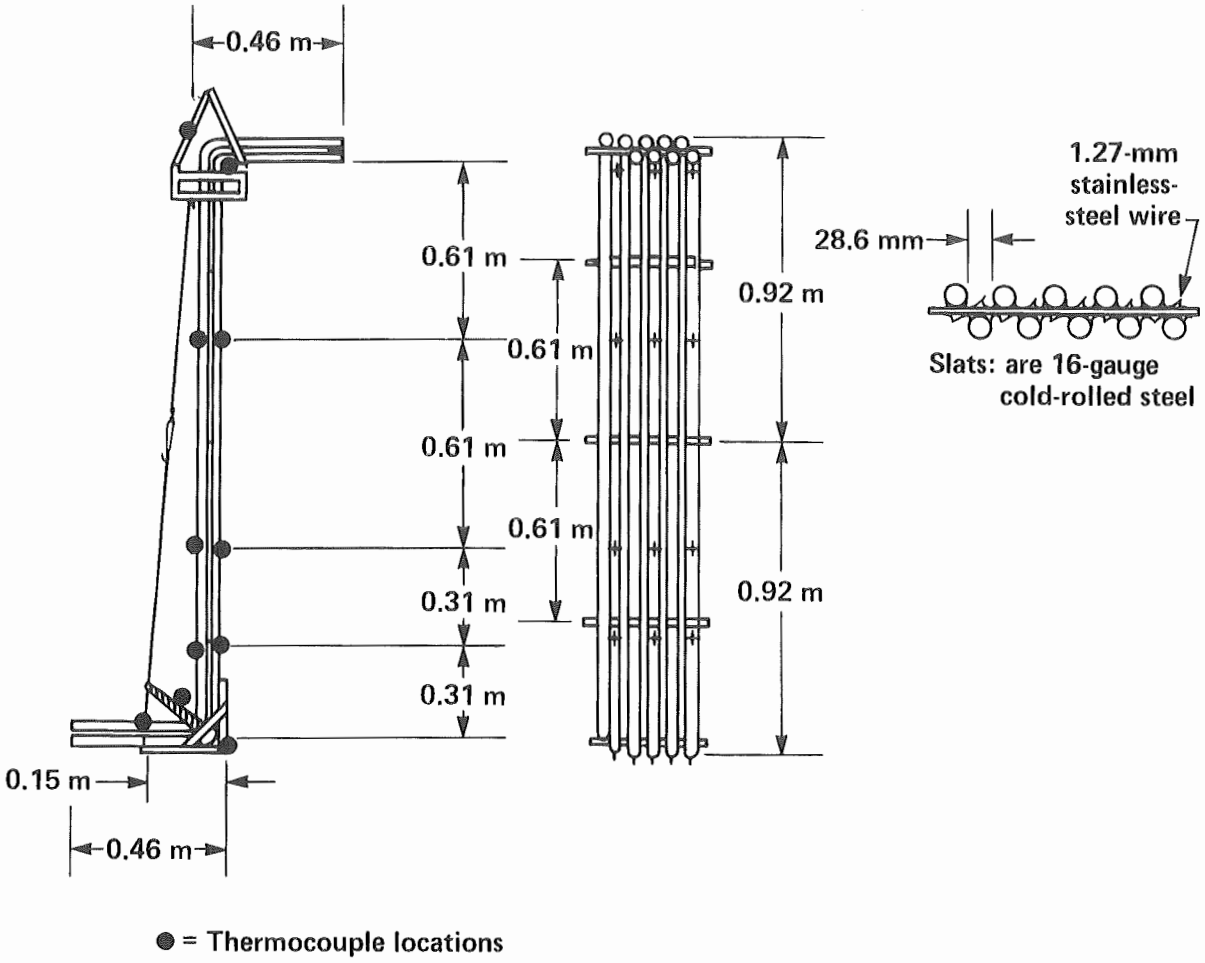

Figure 3-2. Configuration of the two-layer cable bundles used as test specimens for the large-scale cable burns.

Table 3-1. Physical characteristics of cables tested in FY 84.

Test No.	Jacket (% weight)	Insulation (% weight)	Conductor (% weight)	Cable o.d. (mm)	Total wt (kg/m)	Jacket thickness
84-1 84-2	EP rubber (25.5)	None	Copper (74.5)	22.2	1.32	4.37
84-3 84-4	Hypalon (17.2)	None	Copper (82.8)	20.2	1.30	3.05
84-5 84-6	Polyethylene (17.6)	Polyethylene (61.6)	Copper (20.8)	22.2	0.41	1.59
84-7 84-8	PVC polypropylene (25.5)	Copper (4.1)	 (70.4)	21.0	0.60	1.59
84-9 84-10	Rubber (Presto.) (22.4)	None	Copper (77.6)	21.2	1.25	3.85
84-1C 84-2C	Polyethylene (29.1)	Polyethylene (18.8)	Alum./copper (52.1)	12.7 12.7	0.16 0.16	1.59 1.59
84-3C 84-4C 84-5C	Polyethylene (22.6)	Polypropylene (17.4)	Copper (60.0)	22.2	0.48	2.5

cables chosen for the FY 84 tests and also their physical characteristics. These cables were selected to evaluate parameters that developed out of the previous test series, such as the performance of large multi-conductor cables. Although we attempted to purchase some of the previously tested cable types, we found that they had been replaced by newer generation cables. Only two rubber-jacketed cables of the same specification were still available. Based on what we had learned from the previous test series, we made the following modifications to our FY 84 experiments:

- The thermal flux from the premixed natural-gas burner was increased from 5 to 8 W/cm^2 by increasing the methane flow through the burner.
- All cable bundles were configured to the 50% packing density.
- Each cable type was exposed to two fire conditions—the gas burner alone and the gas burner plus a large-scale radiant panel which produced 0.5 W/cm^2 over the vertical section of the cable. Figure 3-3 illustrates the thermal flux distributions over the face of the radiant panel as seen by the cable bundle. The large-scale radiant panel is 0.9-m wide × 1.5-m high and is constructed from fourteen 15.2-cm × 30.5-cm radiant panels. This additional exposure was intended to simulate the effects of a developed fire nearby.

Experimental Procedure

The experimental procedure for these experiments depended on which of the two exposures mentioned above were used. These procedures are summarized in Table 3-2. When the gas burner alone was used, all monitoring instruments were started, using a 200–300 s baseline to record ambient conditions. The gas burner was then ignited at its preset level and shut off when we could visually determine that the cable bundle had sustained ignition; then the rate of flame spread was monitored from the time the flame attached to the vertical section of the cable run. After the specimen became fully involved, we allowed it to reach steady-state burning and then manually extinguished the fire.

We used a slightly more involved protocol when the large-scale radiant panel was added. As shown in Fig. 3-4, a quick-release curtain shields the test specimen from the radiant-panel exposure until the appropriate time. Initially, a 200-s baseline scan was run to record ambient conditions, then the radiant panel was brought up to its operating flux behind the curtain. At this point, the curtain was released, exposing the cable bundle to the radiant panel until the cable jacket temperature reached approximately 100°C, at which point the gas burner was ignited and the test formally started. As before, the burner was extinguished when sustained ignition was observed. We normally left the radiant panel on until the cable bundle became fully involved.

Results of the Large-Scale Vertical Cable Burns

Tables 3-3a and 3-3b summarize the key findings from our final series of large-scale burns. One part of the table lists data from the gas-burner exposure alone, and the other lists results from the burner and radiant-panel exposure. Two additional tests (84-1C and 84-2C) were run at the beginning of the series to validate the test apparatus. Since these cables were smaller than all the other cable types (12 mm o.d. vs 22 mm o.d.), the results cannot be compared to the other cable test results. All other cable diameters were comparable (between 20 and 22 mm). However, the data from the smaller cables illustrates the importance of cable size on burn characteristics. Interestingly, the heat-release rate seems to be independent of the flame-spread rate. The polyethylene/polypropylene (PE/PP) multi-conductor produced the highest heat-release rate of 1820 kW, and the polyvinylchloride (PVC)/PP multi-conductor cable had the fastest flame-spread rate at 0.40 m/min. Conversely, the rubber welding cable (Test 84-9) exhibited the lowest HRR, and the

Table 3-2. Experimental procedure with and without the radiant panel.

Ignition exposure	Preburn run (s)	First exposure	Second exposure	Third exposure	Fourth action	Fifth action
Without external flux	200	8 W/cm^2 burner	No	No	Terminate burner at sustained ignition	Terminate test after steady-state full involvement
With external flux	200	0.5 W/cm^2 behind shutter	0.5 W/cm^2 radiant panel	Initiate 8 W/cm^2 burner at cable jacket temp. 100°C	Terminate burner at sustained ignition	Terminate test after steady-state full involvement

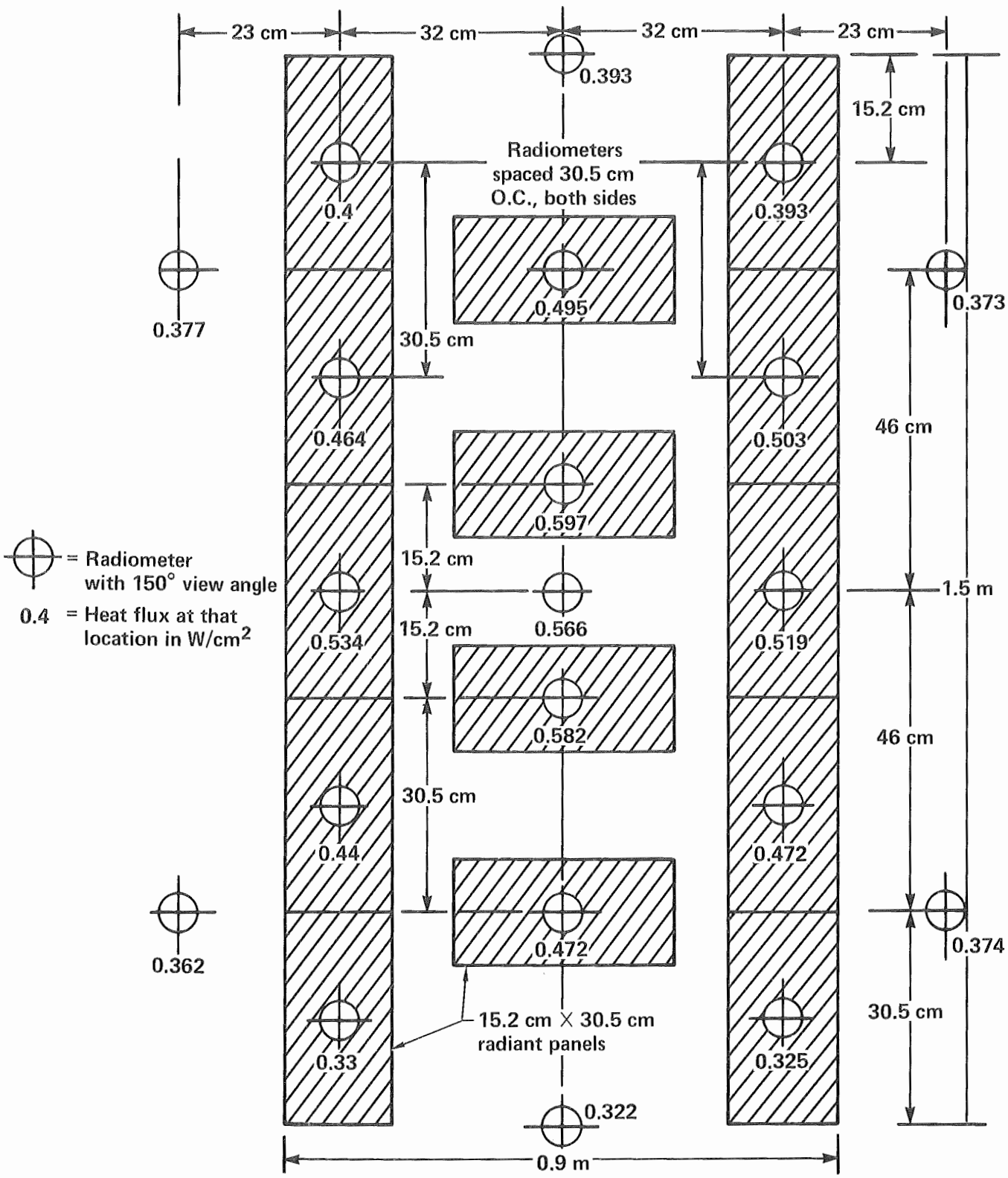

Figure 3-3. Thermal flux distributions over the face of the radiant panel.

ethylene propylene (EP) rubber welding cable had the slowest flame spread. Furthermore, we could not succeed in igniting the Hypalon cable even with the addition of the radiant panel. The PE/PE coaxial had the shortest time to ignition at 120 s, and the EP rubber had the longest at 470 s.

Figure 3-4. Large-scale radiant panel, showing the quick-release curtain that shields the test specimen until the start of the test.

The cable types have been ranked according to their relative fire performance for both large- and small-scale test series. Note that these rankings are not formal ratings for specific cables, but rather a means of comparing the results of the various tests for potential correlations. Tables 3-4a and 3-4b has been divided into two parts: tests using only the 8 W/cm^2 gas burner and tests using both the burner and the large-scale radiant panel. Both parts of Table 3-4 rank the large-scale results according to the five parameters listed. Criteria for rating these results are listed at the bottom of the table. The performance trends primarily show that the PE and PVC multiconductors rank highest (i.e., have the worst fire performance) in most categories, while the rubber, Neoprene, and Hypalon welding cables rank the lowest.

Table 3-5 illustrates the effects of the additional 0.5 W/cm^2 produced by the large-scale radiant panel simulating the exposure from a developed fire. The large increases exhibited by the PVC/PP and PE/PP multi-conductors show that

Table 3-3a. 1984 vertical cable burn summary of tests without 0.5 W/cm^2 radiant panel.

Test No.	TTI (s)	Peak $\dot{m}$ (g/s)	Peak HRR (kW)	Time to peak HRR (s)	Avg. HRR (kW)	FSR (m/min)	Cable type[a]
84-1C[b]	105	30.3	1316	550	257	0.38	PE/PE coaxial
84-2C[b]	65	35.6	1544	550	295	0.51	PE/PE coaxial
84-4C	125	21.3	923	850	151	0.19	PE/PP multicond.
84-1	990	14.3	646	1800	106	0.34	EP rubber
84-4	No ignition		—	—	—	—	Hypalon
84-6	160	18.7	810	850	150	0.29	PE/PE coaxial
84-8	265	10.8	489	1250	92	0.15	PVC/PP multicond.
84-10	350	7.9	356	1150	55	0.25	Rubber (Presto.)

[a] PE = polyethylene PVC = polyvinylchloride
PP = polypropylene EP = ethylene propylene
[b] Performance influenced by small diameter (12.7 mm) and large surface to volume ratio. Therefore their results cannot be compared to the rest of the cable types.

Table 3-3b. 1984 vertical cable burn summary with 0.5 W/cm^2 radiant panel.

Test No.	TTI (s)	Peak $\dot{m}$ (g/s)	Peak HRR (kW)	Time to peak HRR (s)	Avg. HRR (kW)	FSR (m/min)	Cable type
84-5C	125	41.9	1820	1000	251	0.37	PE/PP multicond.
84-2	470	14.2	642	2350	87	0.32	EP rubber
84-3	No ignition		—	—	—	—	Hypalon
84-5	150	22.7	987	1300	116	0.39	PE/PE coaxial
84-7	156	25.8	1168	1150	299	0.40	PVC/PP multicond.
84-9	180	13.4	606	1600	79	0.33	Rubber (Presto.)

Table 3-4a. Performance ranking of 1984 large-scale tests without radiant panel.

Test No.	Time to ignition (s)	Peak HRR (kW)	Avg. HRR (kW)	Peak $\dot{m}$ (g/s)	FSR (m/min)
84-4C	1	1	1	1	4
84-1	5	3	3	3	1
84-4			No ignition		
84-6	2	2	2	2	2
84-8	3	4	4	4	4
84-10	4	5	5	5	3

Table 3-4b. Performance ranking of 1984 large-scale tests with radiant panel.

Test No.	Time to ignition (s)	Peak HRR (kW)	Avg. HRR (kW)	Peak $\dot{m}$ (g/s)	FSR (m/min)
84-5C	1	1	2	1	3
84-2	5	4	4	4	5
84-3			No ignition		
84-5	2	3	3	3	2
84-7	3	2	1	2	1
84-9	4	5	5	5	4

Criteria for ranking:

Shortest time to ignition (TTI) = 1 Highest mass loss rate ($\dot{m}$) = 1
Highest heat release rate (HRR) = 1 Fastest flame-spread rate (FSR) = 1

they would vigorously contribute to a spreading fire, but may not appear as flammable when exposed to an incipient ignition source. Referring back to Table 3-3, the PVC/PP jumps from a slow FSR of 0.15 m/min (burner only) to 0.40 m/min (burner and radiant panel). The remaining cables show little or no change for the two exposures.

When looking at *percent* changes, little or no change can mean either that the cable resists fire fairly well (if it contributes very little to an incipient fire and only slightly changes when additional thermal energy is introduced), or that the cable is very flammable, because the incipient fire provided enough energy to get the cable fully involved and the addition of the radiant panel had little effect on anything but the time to ignition. Therefore, the actual values of HRR and FSR must be used to evaluate cable flammability. For example, although the PE/PE coaxial cable showed a slight percentage increase, its HRR without the radiant panel was fairly high. On the other hand, both rubber-jacketed cables had very low baseline HRRs, which means they are more fire-resistant than the PE/PE coaxial.

On the macroscopic scale, Table 3-6 summarizes pertinent test-enclosure and jacket-temperature data. The first columns list the maximum ceiling temperatures attained and the times of occurrence for each test. This information indicates whether a sprinkler head at the ceiling will activate and the approximate time it will do so. The table shows that all cable types produced ceiling air temperatures sufficient to fuse standard sprinkler heads, but the elapsed times vary. These times would be dependent on the heat transfer to the fusible link on the sprinkler head.

Another important factor listed in the table is the heat fluxes produced by the burning cable bundles. Heat flux values are taken at a distance of 0.3 m from the cable bundle at the top and the bottom, and a remote flux gauge is located at the wall approximately 2.4 m away. These values are listed in the table as calorimeter lower, upper, and wall, respectively. The heat fluxes produced by the burning cable bundle provide information on whether adjacent cable bundles or fuels will ignite and propagate the fire. It can be seen that all but the rubber-jacketed cables developed fluxes between 1.0 to 9.0 W/cm^2. The lower part of the cable run shows the highest value to be 9.0 W/cm^2 while the upper portion had a maximum of 6.5 W/cm^2. However, at 2.4 m the thermal flux drops to 0.02–0.15 W/cm^2. Results from our small-scale radiant panel tests show that the majority of cable types will ignite and spread flame when exposed to a piloted 1.0–2.0 W/cm^2 fire, and all cable types will spread flame rapidly at 2.5 W/cm^2. This being the case, our large-scale tests illustrate that cable bundles within 0.3 m of the burning cable will ignite (with a pilot flame) and propagate the fire.

Table 3-5. Effect of large-scale radiant panel.

Test	Cable type	HRR (%) increase	FSR (%) increase	TTI (%) decrease
84-4C, 84-5C	PE/PP	97	95	0
84-1, 84-2	EP rubber	0	0	47
84-5, 84-6	PE/PE	22	34	0
84-7, 84-8	PVC/PP	139	167	59
84-9, 84-10	Rubber	70	32	51

The remaining columns in Table 3-6 list the times to ignition and the jacket temperatures at ignition of the various cable types. Because these

Table 3-6. Key test-cell thermal data and cable-jacket temperatures at ignition.

Test No.	Maximum nominal ceiling temp. (°C)	Temp. elapsed time (s)	Cal. lower (W/cm^2)	Cal. upper (W/cm^2)	Cal. wall (W/cm^2)	Cal. elapsed time (s)	Cable temp. at ignition (°C)
84-1	225	1575	1.8	2.2	0.03	1550	200° ± 25°
84-2	210	1150	1.0	2.5	0.02	1125	200° ± 50°
84-3				No ignition			
84-4				No ignition			
84-5	325	500	2.5	3.5	0.04	500	175°
84-6	325	620	3.0	5.0	0.04	620	160°
84-7	300	710	1.75	3.8	0.04	570	110°
84-8	135	1050	1.0	1.0	0.05	1040	125°
84-9	175	960	0.25	1.0	0.07	940	125°
84-10	120	880	0.8	0.8	0.04	880	110°
84-1C	375	360	3.2	6.0	0.15	340	120°
84-2C	400	360	2.4	6.0	0.07	330	120°
84-3C	350	400	1.3	3.0	0.05	420	120°
84-4C	375	650	9.0	6.5	0.2	650	120°
84-5C	375	440	3.0	5.0	0.15	440	120°

ignition times are based on thermocouple readings rather than visual observation, they vary somewhat from the previously listed times. The actual jacket temperatures at ignition correlate fairly well with the values obtained from our small-scale radiant panel tests. We should, therefore, be able to determine the jacket temperatures at ignition using the small-scale test without the necessity of performing large-scale experiments.

Conclusions

Based on the results of the FY 84 series of large-scale experiments, we can draw the following conclusions:

- For almost all cables listed, increasing the ignition source intensity from 5 to 8 W/cm^2 decreased the time to ignition, increased the flame-spread rate, and considerably increased the heat-release rate.
- Augmenting the fire exposure with the large-scale radiant panel produced 100–150% increases in HRR and FSR for the more flammable cables such as PVC/PP and PE/PP multi-conductors, although this level of exposure had little or no effect on the less-flammable rubber welding cables. In the majority of the tests, ignition times were decreased by approximately 50%.
- The PE/PP and PVC/PP multi-conductors produced fires with the highest heat-release rates, confirming earlier findings that multi-conductor cables exhibit the worst fire performances. These were followed by the PE/PE coaxials. As in previous tests, the rubber- and Hypalon-jacketed welding cables showed the least fire threat.
- The high flammabilities of the multi-conductors and coaxials are a result of both the flammability of insulation materials and reduced heat losses due to a much lower conduction through the copper core. The weight of these cables is typically half that of a comparable stranded copper-core welding cable.
- With the exception of the Hypalon-jacketed cable (Tests 84-3 and 84-4) which did not ignite, all cable types produced ceiling-layer temperatures (125–400°C) in excess of that necessary to fuse standard sprinkler heads.
- Bulk jacket temperatures ranged from approximately 110–200°C, when sustained ignition was achieved. These data generally correlate to our small-scale radiant panel results.
- With the exception of the Hypalon cable and rubber cable (Tests 84-9 and 84-10), all cable types produced radiant heat fluxes with the potential to ignite (with pilot flame) similar cable materials within 0.3 m of the burning cables.
- The results from our 1984 tests confirm earlier predictions that, even though many of the cable types would contribute very little to an incipient fire, they would contribute quite readily to an already developed fire.
- Factors such as jacket temperature at ignition, ignition heat flux, heat-release rate, and flame-spread rate can be used as input for models in enclosure fire risk assessment. However, some

means must be found to predict the additive effects of burning multiple cable bundles.

Small-Scale Radiant Panel Experiments

We performed a series of small-scale cable tests using a radiant panel to assess possible correlations to our large-scale tests and to evaluate the following parameters:

- Flame-spread rate vs irradiance level.
- Flame-spread rate vs bulk jacket temperature.
- Flame-spread rate vs rate of heating.
- Threshold irradiance level for vertical (upward) flame spread.
- Contribution of the cable core to flame-spread rate.

Five of the seven cable types tested in the large-scale apparatus (see Table 3-7) were selected for small-scale tests to determine whether we could reasonably predict the fire performance of a specific cable type using small-scale tests. We expected to assess and correlate such parameters as flame-spread rate rankings, bulk jacket temperatures at time of ignition, and time-to-ignition rankings. To assess the effect of the conductor core on a cable's flammability, we tested two welding cables with and without their stranded-copper conductors.

We exposed each cable type to five irradiance levels (0.5, 1.0, 1.5, 2.0 and 2.5 W/cm^2) to evaluate the effect of increasing flux on the rate of flame spread and the time to ignition. We were not able to do this with the large-scale radiant panel because the maximum attainable heat flux was 0.5 W/cm^2. To determine a threshold ignition flux, each cable was exposed to the radiant panel until the bulk jacket temperature reached 100°C, at which point a pilot flame was applied. The primary reason for preheating the cables was to duplicate the conditions in the large-scale vertical panel tests.

The radiant panel is a modified ASTM E-162 set up, as shown in Fig. 3-5. Our modifications include:

- The stack and related hardware have been removed to reduce air turbulence across the specimen.
- The specimen was suspended vertically, rather than at a 30° incline.
- The pilot burner was repositioned from the top of the specimen to the bottom.
- A water-cooled sliding metal shutter was added between the radiant panel and the specimen to precisely control exposure times.
- Two thermocouples were attached to the midpoint of the cable specimen—one on the jacket surface, and one imbedded through the jacket to the conductor.

Experimental Procedure

Prior to each test series, the radiant panel was set to its operating temperature (monitored by a radiation pyrometer) and allowed to stabilize for thirty minutes. Following this stabilization period, the shutter was moved in front of the radiant

Table 3-7. Physical characteristics of cables (46 cm long) tested in small-scale radiant panel tests, 1984.

Cable	Jacket (% wt)	Insulation (% wt)	Conductor (% wt)	Cable o.d. (mm)	Total wt (kg/m)	Jacket thickness (mm)
Rg-214u coaxial	PVC (21.4)	Polyethylene (17.9)	Copper (60.7)	10.9	0.18	1.59
PVC multiconductor	PVC (25.5)	Polypropylene (4.1)	Copper (70.4)	21.0	0.60	1.59
Polyethylene multiconductor	Polyethylene (22.6)	Polypropylene (17.4)	Copper (60.0)	22.2	0.48	2.5
Rubber power. multiconductor	Neoprene (35)	Rubber (27)	Copper (38)	21.8	0.73	3.05
Rubber (Presto. W.C.)	Rubber (22.4)	None	Copper (77.6)	21.2	1.25	3.85
Diesel loc. 2/0 cable	EP Rubber (29)	None	Copper (71)	18.8	0.85	4.37
Diesel loc. Hatfield 4/0	Hypalon/rubber (22)	None	Copper (76)	23	1.37	3.97

panel, and the 46-cm-long specimen was hung in place. The shutter was then quickly moved out of the way and all monitoring systems were started. Each specimen was preheated until the bulk jacket temperature reached 100°C, at which point the pilot flame was applied and the test officially started. Time to ignition or flame attachment and rate of flame spread were monitored visually. We terminated the test when the flame had spread up the entire cable, or when it became obvious that the flame would no longer propagate.

Results of Small-Scale Radiant Panel Experiments

Table 3-8 summarizes the physical characteristics and ignition results from the cable types tested. The bulk jacket temperatures at piloted ignition are similar, with the rubber and Hypalon jackets slightly higher. Recall that this temperature is dependent on both materials' properties and thicknesses. In this case, results from the two rubber-jacketed cables without conductors show equal or higher temperatures at ignition compared with those of whole cables. This seems to indicate that the thermal thickness of the jacket material is the governing factor for ignition. Critical heat fluxes for ignition show that 1.0 W/cm^2 is generally the minimum required for sustained burning. Unfortunately, this prevented us from making direct comparisons to results from the large-scale tests using the large-scale radiant panel (0.5 W/cm^2). Again, the rubber-jacketed conductors required slightly higher ignition energies; the Hypalon required 2.5 W/cm^2 for ignition.

Table 3-9 lists the rate of flame spread as a function of input flux. Only the PE multi-conductor and the coreless Prestoflex rubber welding cable demonstrated flame spread at 0.5 W/cm^2. Most of the cables required at least 1.5 W/cm^2 for spread, but all ignited and produced rapid spread at 2.5 W/cm^2. When tested without cores, the two rubber-jacketed cables show an increase in flame-spread rate, unlike their ignition response, which helps to confirm the conductor's role in cable flame spread. These data are plotted in Fig. 3-6 to compare change in the flame-spread rate with increasing heat flux.

Times to piloted ignition as a function of input flux are summarized in Table 3-10. In general, the time to ignition decreases with increasing flux. However, since these times are so short toward the higher irradiance levels, the recorded times are probably questionable. This seems to be the case at 2.0–2.5 W/cm^2 where two cable types (rubber w/o core and PE multi-conductor) appear to have longer ignition times at 2.5 W/cm^2. However, since the time frames are only a matter of seconds, the recorded differences really do not exist. Using

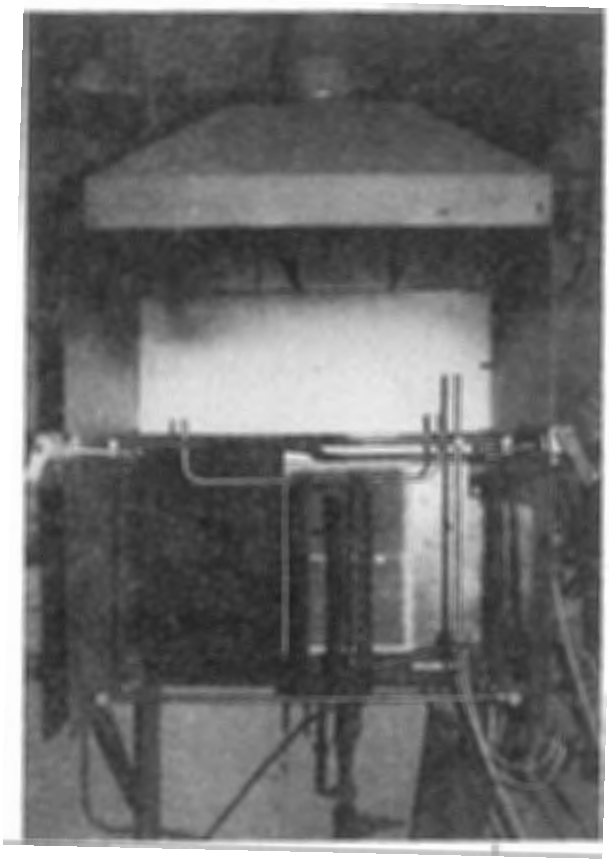

Figure 3-5. Radiant panel set-up for small-scale tests.

Table 3-8. Bulk jacket temperatures at piloted ignition and critical heat fluxes.

Cable type	o.d. (mm)	Total wt (kg/m)	Bulk jacket temperature at ignition (°C)	Critical flux (W/cm^2)
PVC multiconductor	21	0.60	120	1.0
PE multiconductor	22.2	0.48	120	0.6–1.0
Rubber weld (Presto)	21.2	1.25	130	1.0
Rubber weld w/o core (Presto.)	21.2	0.28	120–140	0.6–1.0
EP rubber (2/0 cable)	18.8	0.85	130	1.5
EP rubber (w/o core)	18.8	0.25	150–160	1.5
Hypalon Diesel 4/0	23	1.37	170	2.5

the values at 1.5 W/cm^2 (the lowest flux where all cables ignited), the PE multi-conductor has the shortest time to ignition, followed by the PVC multi-conductor and the PVC/PE coaxial. These three cables are the only ones which ignited at the lowest flux of 0.5 W/cm^2; all the rubber-jacketed cables had longer ignition times. The two cables tested without cores produced inconclusive results with one igniting at a shorter time and the other at a longer time.

Figure 3-7 is a multiple plot of the flame-spread rate as a function of preheating temperature for the PVC multi-conductor cable. The flame-spread rate increases as the preheating temperature increases. Although the data is not included here, we also found that increasing the heating rate increased the flame-spread rate. Again, the multi-conductor and coaxial cable exhibited the highest rates of spread.

Table 3-9. Flame-spread rate as a function of input flux.

Cable type	Heat flux (W/cm^2)	Flame-spread rate (m/min)	Flame-spread rate w/o core (m/min)
PVC multiconductor	1.0	0[a]	
	1.5	0.39	
	2.0	1.11	
	2.5	1.47	
PVC/PE RG 214u	1.5	0.18	
	2.0	0.46	
	2.5	0.55	
PE multiconductor	0.5	0.06	
	1.0	0.09	
	1.5	0.19	
	2.0	0.32	
	2.5	0.53	
EP rubber	1.5	0[a]	0[a]
2/0 cable	2.0	0.36	0.40
	2.5	0.58	0.78
Rubber	0.5	—	0.06
4/0 Presto.	1.0	0[a]	0.10
	1.5	0.09	0.18
	2.0	0.16	0.30
	2.5	0.24	0.46
Neoprene	1.5	0[a]	
Powercord	2.0	0.14	
	2.5	0.29	

[a] Flame attachment but no spread.

Conclusions

Table 3-11 ranks cables according to their flame-spread rates and times to ignition. The fastest flame spread and the shortest time to ignition were ranked #1. These values were taken at a heat flux of 1.5 W/cm^2, the lowest irradiance level at which all cable types ignited. The table shows that under both criteria the multi-conductors and the coaxial produced the worst fire performance. The rubber-jacketed cables were again the better performers, and the small-scale test successfully identified the rubber and Hypalon materials as good performers.

In retrospect, we see that several factors probably had a significant effect on the actual numerical comparisons for FSR, ignition temperature, etc. (excluding ranking) between large- and small-scale tests:

Table 3-10. Time to ignition[a] vs input heat flux.

Cable type	Input heat flux (W/cm^2) 0.5	1.0	1.5	2.0	2.5	
EP rubber 2/0	—	—	16	28	12	time to ignition (s)
EP rubber without core	—	132	33	18	10	
Rubber 4/0 Presto.	—	22	22	6.6	6	
Rubber (Presto.) without core	100	19	8	10	11	
Neoprene powercord	—	58	16	6	6	
PVC multiconductor	39	9	10	7	5	
PE multiconductor	40	9	5	4	5	
PVC/PE coaxial RG 214u	154	71	6.6	7	6	

[a] From pilot flame application.

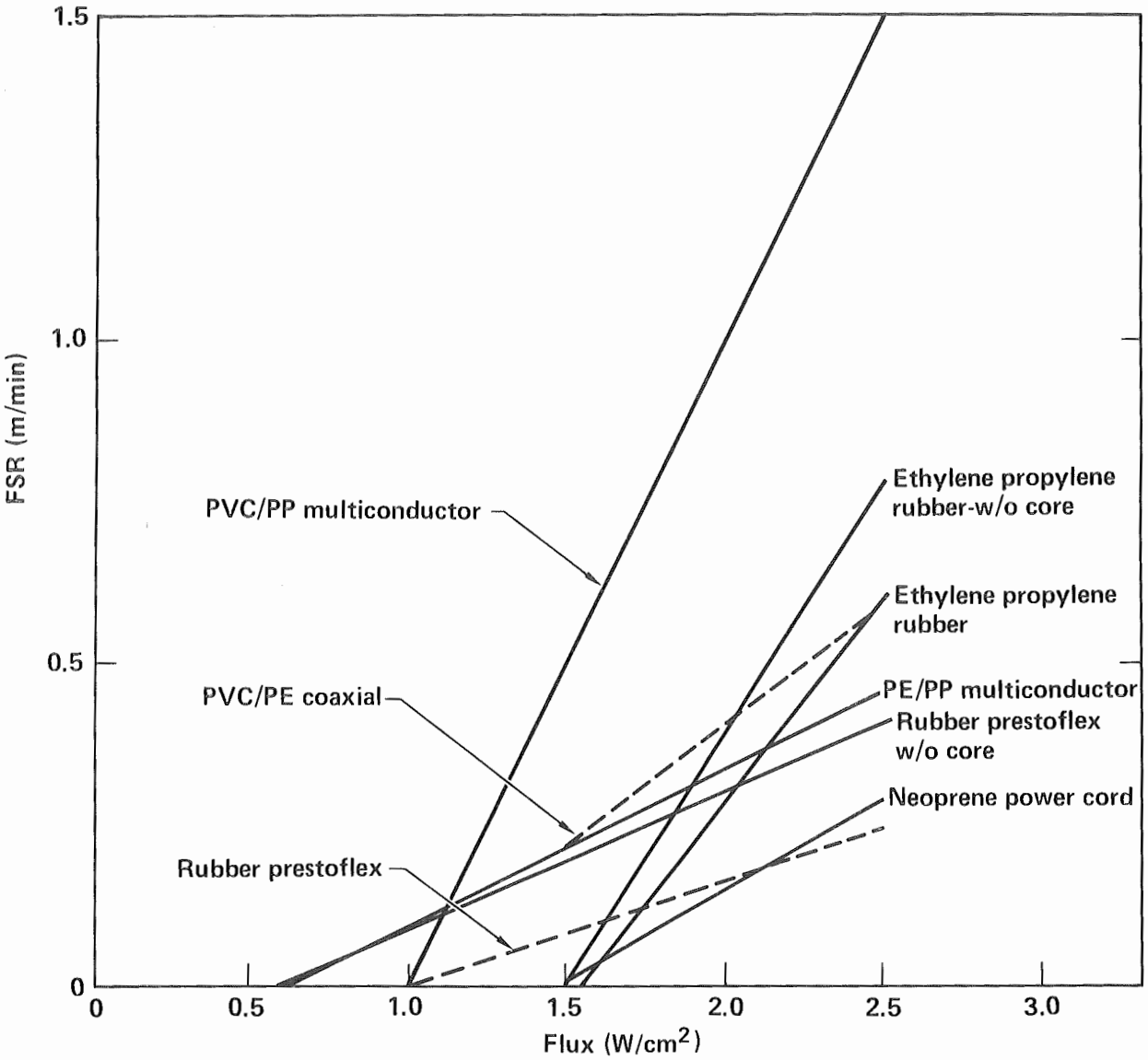

Figure 3-6. Rate of flame spread vs input flux for various types of cables tested.

Table 3-11. Small-scale radiant panel ranking at 1.5 W/cm^2.

Cable type	Rate of flame spread (m/min)	Rank[a]	Time to ignition (s)	Rank[b]
PVC multiconductor	0.39	1	10.2	3
PE multiconductor	0.2	2	4.8	1
PVC/PE coaxial RG 213u	0.18	3	6.6	2
Rubber 4/0 Presto.	0.09	4	22	5
EP rubber	0[c]	5	16	4
Neoprene powercord	0[c]	5	16	4

[a] Fastest flame spread = 1.
[b] Shortest time to ignition = 1.
[c] Flame attachment but no spread.

- The small-scale radiant panel used only a single cable, while the large-scale experiments used a two-layer cable bundle. In the large-scale case, the center cables are insulated on three sides by other cables, which could account for ignition at the low heat flux of 0.5 W/cm^2. Conversely, the absence of other cables around the small-scale test could require higher irradiance levels for ignition and flame spread.
- In the large-scale tests, the specimens are configured into a perpendicular "Z" which positioned a horizontal section of the cable bundle directly over the gas burner ignition source. As this section ignited and contributed to the fire, it provided an undefined additional exposure to the vertical cable section above it. In contrast, only a

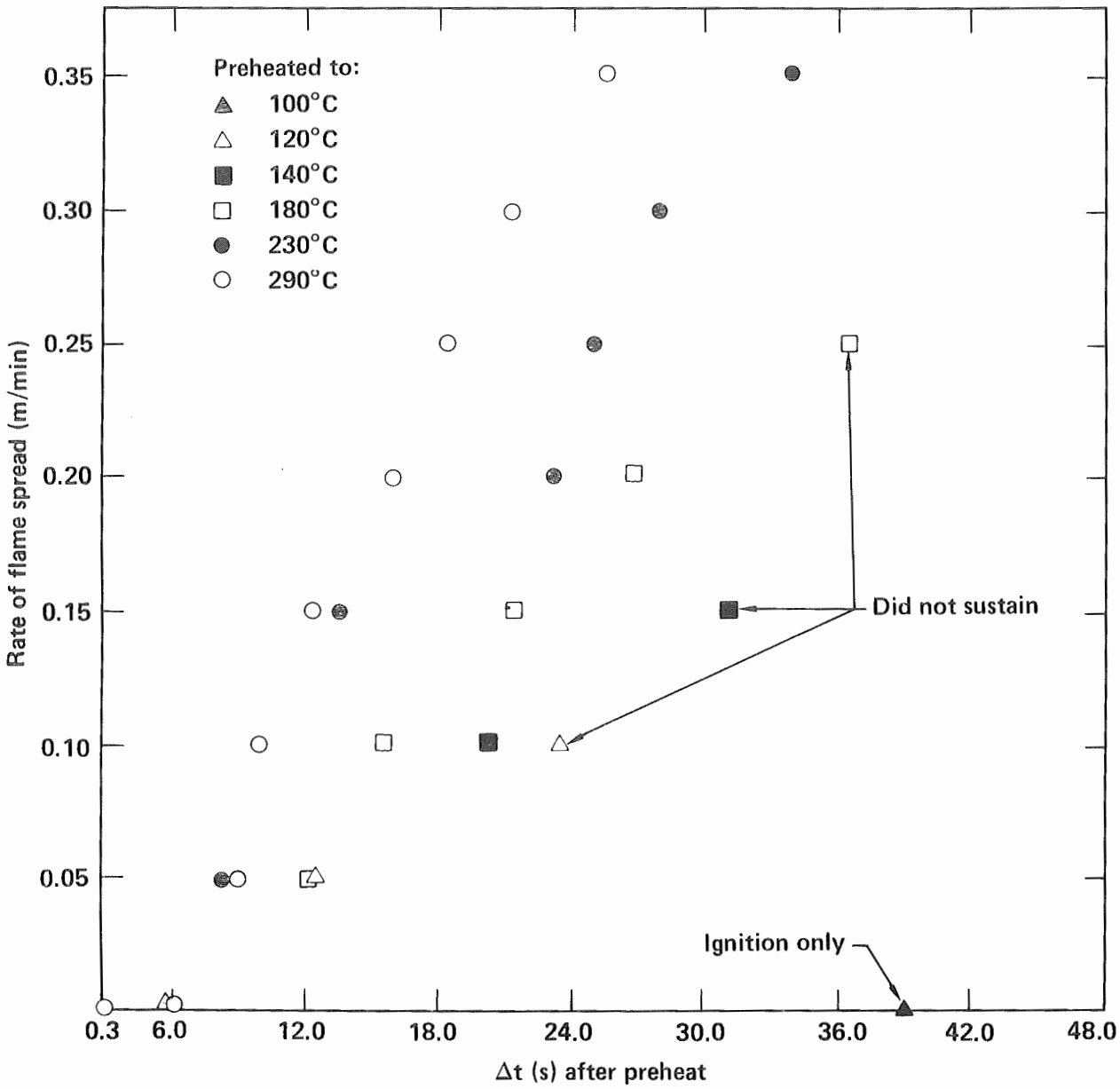

Figure 3-7. Flame spread rates, showing the effects of preheat temperature on the cable specimens.

vertical section of cable was used in the small-scale test with no horizontal section to augment the pilot flame. This could explain the requirement for higher ignition fluxes and slower flame-spread rates in the small-scale tests.

We feel that these differences would be significant enough to affect the correlation of the actual data points between the large- and small-scale tests. However, it appears that the small-scale radiant panel test can be used to evaluate the relative fire hazard of cable-insulating materials. The advantage of this test method is that a battery of parameters can be evaluated quickly and inexpensively, allowing the use of several parameters to support the conclusions of an evaluation. In terms of useful input for fire models, two pieces of data could probably be used directly—the jacket temperature at ignition and the critical ignition flux. A missing and important factor for model input is the aggregate heat-release rate, however, which can only be obtained from the large-scale experiments.

Comparison of Large-Scale Results to Small-Scale Results

We performed thermogravimetric analysis (TGA) to determine the onset of thermal degradation which could give an indication of a cable insulation's flammability. Table 3-12 summarizes the results of tests conducted on all the cable types used in the 1984 large-scale experiments. Two different heating rates were used, 160°C/min and 10°C/min (the former is closer to real fire heating conditions). The weight of material which had not burned by the end of the run is listed as "residual weight." Finally, the "in" and "out" on the multiconductor cables correspond to the onset temperature for insulation on the inside conductors and jacket material, respectively. The last column ranks the cable types at both heating rates, with the lowest onset-of-degradation temperature as rank #1. At a heating rate of 160°C/min, the worst performer would be the PVC/PP multi-conductor and the best would be EP rubber material.

Table 3-13 lists the four cable types used in all three tests (the small-scale radiant panel, TGA, and large-scale vertical cable tests). The table is a comparison of rankings on the basis of each of the listed criteria. It should again be emphasized that the results from the various experiments are ranked only to enable us to make dimensionless comparisons among the different test methods. It is *not* a formal hazard ranking of specific cables.

As before, rank #1 indicates the highest flammability in terms of highest HRR, fastest FSR, shortest time to ignition, and lowest temperature for the onset of thermal degradation. The small-scale radiant panel results are the most encouraging in comparison to the large-scale test. The rates of flame spread are ranked identically, and times to ignition are similar. The HRR is also similar to the small-scale FSR ranking. Although the TGA ranking correlates directly to the large-scale FSR and is similar to the HRR, comparison of the remaining cable types not included in this table produced a number of results totally inconsistent with the large-scale results. This is not surprising because TGA uses a very small amount (10 mg) of homogeneous material heated in air without an ignition source. In general, the physical characteristics of the cable as a whole has a significant effect on cable fire performance. By the nature of TGA, these effects cannot be accounted for. Knowing this limitation, however, the TGA can still be used as an initial screening tool, and we can evaluate its results using the small-scale radiant panel. In order to accurately define a cable's fire response, the cable must be tested as a complete assembly. This is one of the dangers of attempting to extrapolate various fire-response characteristics from a small-scale test which does not consider the complete cable.

Finally, the information in Table 3-14 (based on our test series) summarizes cable-fire data for

Table 3-12. Onset of thermal degradation as a function of two heating rates.

Cable type	Used in test No.	Onset (°C) heating rate 160°/min	10°/min	Change[a]	Residual weight (%) 160°/min	10°/min	Rank[b]
PE/PE coaxial	84-2C	430.8	332.49	98.31	1	0	3/4
PE/PE multiconductor	84-3C, 4C, 5C	431.5	376.32	55.2	0	0	4/6
EP rubber	84-1, 2	446.36	398.65	47.7	57.6	57	7/7
Hypalon	84-3, 4	363.03	290.37	72.7	25	22	2/2
PE/PE	84-5, 6	435.62[c] 415.92[d]	373.26 357.9	62.34	0	0	5/5
PVC/PP	84-7, 8	355.67[c] 392.16[d]	290.1 300.99	65.6	14	9.8	1/1
Rubber (Presto.)	84-9, 10	445.33[c]	308	137.33	56.5	56.5	6/3

[a] Change in temperature of onset of degradation between the two heating rates.

[b] Lowest degradation temperature = 1.

[c] Outside jacket material.

[d] Multiconductor jacket material.

model input and for the ranking of generic cable fire performance. The peak heat-release rates averaged over our entire test series for the cable materials are listed.

The following are insights into the effect of physical characteristics of single cables and cable bundles:

- Our tests show that the more tightly and densely a cable bundle is packed, the more fire resistant it is. If the cable run is a single layer with a reasonable space between cables, there does not appear to be enough heat reinforcement to sustain a significant fire.
- Multi-conductors and coaxials displayed the worst fire performance. Our data indicates that these cables have significantly less copper conductor to absorb the thermal energy from the exposure fire and that the insulating materials add fuel to the burning cables.
- Welding cables, because of their high conductor content (relative to jacket material), displayed the best fire performance.
- There is an inverse relationship between cable diameter and fire-response properties.

Unique Large-Scale Experiments

As mentioned in the beginning of to this section, some unique large-scale experiments were performed in FY 84. The following section describes these tests and the results we found.

Large-Scale Experiments of Polymethylmethacrylate (PMMA) Tubes

We attempted to define the effect of cable core density on its mass-burning rate and its flame-spread rate. We obtained 19-mm o.d. clear PMMA tubes along with 1.82 m lengths of 14.3-mm diameter aluminum and brass rods. The density of brass is three times that of aluminum (8.5 vs 2.7 g/cm^3) and aluminum has half the thermal conductivity of brass. We constructed 1.82-m test specimens in our 50%-pack vertical cable configuration, using PMMA tubes to simulate jacket material with aluminum rod cores and brass rod cores. Our initial thoughts were that the differences in thermal conductivity and density of the two metals should give us insight into how the amount of conductor affects cable fire performance. However, after conducting three tests with each core material, we concluded that the PMMA masked the conduction effect because of its high flammability; i.e., the plastic would become fully involved in the fire before the metal cores could influence the fire. Figure 3-8 is a multiple plot showing almost identical mass-loss rates for brass and aluminum cores. Similarly, times to ignition and rates of flame spread showed no substantial difference. A different polymer, such as PVC, should be used to simulate jacket material to allow the core to influence the fire.

Table 3-13. Comparison of small-scale to large-scale tests.

Cable type	Large-scale tests			Small-scale radiant panel		TGA
	HRR	FSR	TTI	FSR	TTI[a]	
PVC/PP 84-7 (multi.)	2	1	2	1	2	1
PE/PP 84-5C (multi.)	1	2	1	2	1	2
Rubber 84-9 (Presto.)	4	3	3	3	4	3
EP rubber 84-2	3	4	4	4	3	4

HRR = heat release rate
FSR = flame-spread rate
TTI = time to ignition
TGA = thermogravimetric analysis

[a] Taken at 1.5 W/cm^2.

Tests of Exploding Cables

We obtained approximately 60 partial spools of coaxial cable from our salvage area to evaluate the effects of changing certain parameters in test-cell ventilation and exposure fire. This type of cable has an o.d. of 13 mm with a polyethylene jacket, solid aluminum shielding, and a foamed polyethylene dielectric. According to our cable-specifying personnel, at least 304,800 m of this coaxial cable is currently used to connect LLNL's main computer network. We performed two experiments (Tests 84-1C and 84-2C), one with a 5 W/cm^2 exposure fire and a second using 8 W/cm^2. In both cases, the cable ignited quite readily, produced rapid flame spread, but then some sections began to explode violently. This phenomenon enhanced the burning, which in

Table 3-14. Summary of cable fire data.

Cable type	HRR	FSR (m/min)
Polyethylene and polypropylene	1.25 mW	0.38
Polyvinylchloride (coaxial)	510.00 kW	0.38
Rubber	345.00 kW	0.31
Hypalon	170.00 kW	0.23
Neoprene	20.00 kW	0.09

turn accelerated flame spread and the production of molten, flaming polyethylene. The explosions were caused by pressure produced by melting and vaporizing the polyethylene confined within the solid aluminum shielding by the non-molten polyethylene. Results from these experiments show that this cable type should be well-protected from sources of ignition wherever it is used.

Extinguishment of a Large-Scale Cable Burn

One of our tasks for this project is to evaluate unique extinguishing techniques for fires in DOE facilities. Research personnel are constantly concerned about water damage from fire-protection systems to their expensive electronics. We used large-scale cable test 84-10 to study the effectiveness of liquid nitrogen (LN) for extinguishing cable fires. Three separate spray nozzles—one positioned at the top, mid-height, and bottom of the burning specimen—were installed to release the LN. When the cable bundle had become fully involved and reached steady state, the LN was released, extinguishing the fire in approximately two minutes, using 24 liters of liquid. This technique may be a possibility in unoccupied areas or evacuated areas, and would provide an excellent non-contaminating agent for areas where water or other extinguishants are not practical.

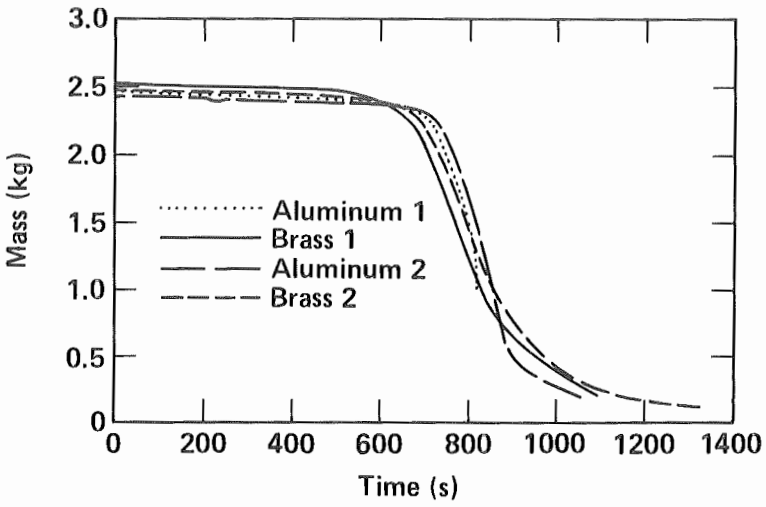

Figure 3-8. Mass-loss rates for cable specimens with brass or aluminum cores.

Part 4:
Risk Analysis: Fire Models in Forced-Ventilated Enclosures

Introduction

Codes and regulations are generally formulated by consensus, based upon well-established procedures for rating materials and designs. DOE research facilities, however, are developing new technologies which raise unique fire-protection problems. Designs and materials associated with R&D facilities are constantly evolving, resulting in unusual conditions and environments. Fire protection procedures must, therefore, be frequently reviewed to insure applicability and relevancy to current technological developments.

Advances in fluid mechanics, heat transfer, chemistry, and the rapid growth of computer speed and memory all contribute to an increased understanding of fire phenomenology. This allows the development of new procedures for predicting fire growth, heat-release rates, and smoke-release rates. We are developing and testing mathematical models of enclosure fires under a wide variety of conditions. Within limitations, these models can provide an added dimension of fire risk prediction, reducing the need for frequent and expensive full-scale testing.

Our primary goal is to develop procedures for risk analysis in enclosures containing and supporting large-scale experiments. These procedures should also be useful for fire risk prediction under many other circumstances. The central part of this analysis will be a mathematical model designed to predict several important time-dependent parameters of enclosure fires. Before our procedures can be adopted by the community of DOE fire-protection specialists, however, they must offer substantial improvement over current methods in speed, accuracy, ease of analysis, reduced ambiguity, and flexibility. The procedures described in this report are still preliminary, but it is clear they will provide a definite improvement in our ability to assess fire risk parameters.

Overview of Risk Analysis

A great deal of information is necessary to do a thorough risk analysis of any research facility. The information-gathering process is the most time-consuming portion of risk analysis. At present, the following information is required for a facility fire risk analysis:

1. Specific mission of facility.
2. Construction detail (specifically potential fire zones).
3. Existing or proposed fire management system.
4. Identification of the "critical" component and/or space.
5. Potential ignition source(s).
6. Location of items that could be degraded or destroyed by heat or smoke contamination.
7. Location, stability, or mobility of critical items.
8. Enclosure geometry and communication.
9. Ventilation dynamics.
10. Distribution of flammable materials.
11. Flammability of materials.

As we gain experience, this process can be shortened by prioritizing or ignoring parameters that balance or cancel, or that do not appreciably change throughout the time of interest. A more complete description of the required and desired information is attached as Appendix A of this report.

The cornerstone of our risk analysis is the fire modeling procedure. The actual data to be input to the enclosure fire model (8–11 in the above list) will always be required to complete this part of the analysis. The fire model we have developed is based on our experience with forced-ventilated enclosure fires, described below.

Forced-Ventilated Enclosures

At the start of this project, available risk analysis procedures were exclusively designed to analyze conditions in small, naturally ventilated enclosures. In naturally ventilated enclosures, the air supply is exterior to the enclosure, with flow coming through an opening in the room. No mechanical air-moving process is involved. However, our primary interest is in modeling fires in forced-ventilated enclosures.

Most DOE laboratory facilities provide forced air supply via extraction, or negative-pressure, ventilation systems. Here, the air motion is supplied by fans downstream from the serviced enclosures. A balanced air supply is generally provided upstream of the enclosure, especially in

large facilities. This procedure permits easier containment of possible laboratory-released contamination by keeping enclosures at lower pressures relative to their surroundings, and by providing proper conditions for the insertion of fine particulate filters and scrubbers downstream from protected enclosures.

Because of our need to analyze fire risk in forced-ventilated enclosures, we began a cooperative program with various researchers involved in model development. We planned and carried out a series of forced-ventilated enclosure fire tests to provide data for modelers, who in turn agreed to provide analysis for some benchmark conditions.

Forced-Ventilated Enclosure Fire Experiments

A generic enclosure fire is schematically shown in Fig. 4-1. The fire is located symmetrically in a regular enclosure, entraining air for combustion and into a plume. Air required for combustion is heated by exothermic reaction such that the density in the combustion gas volume directly above the fire is much less than that of the surrounding air. A buoyancy plume is produced, and as these hot gases rise, air is entrained, diluting and cooling the combustion products. This mixture collects in the ceiling space as a relatively well-mixed and homogeneous layer.

Our previous experiments in the test cell were designed to produce heat, combustion gases, and smoke as a challenge to downstream duct and filtration components. These tests involved fires of both solid- and liquid-phase fuel arrays, burning without control, and responding to environmental and enclosure interactions. These initial tests gave us a qualitative understanding of fire behavior in forced-ventilated enclosures. Test-cell instrumentation was sparse, however, since we directed our research to conditions in the downstream duct. Thus, before we could supply data precise enough for model validation, we had to equip our test cell with instrumentation capable of sensing and recording the requisite data.

Since we intended to provide simple, definitive data for the purpose of validating mathematical models, we needed to reduce unnecessary variables and control transient phenomena. Previous experiments showed that typical fuels burn at rates controlled by a variety of factors, such as initial mass, shape, heat-feedback, and oxygen concentration. We can avoid these complexities by using a fuel that can be metered at a preselected supply rate. We accomplished this by using natural gas flowing through porous bed burners or various liquid fuels sprayed radially into a heated metal pan. We kept the extraction rate constant by adjusting the downstream dampers and fan speed and by removing all filters. Also, a few models we surveyed required a constant heat-release rate $\dot{Q}$ as the primary input. While models are generally

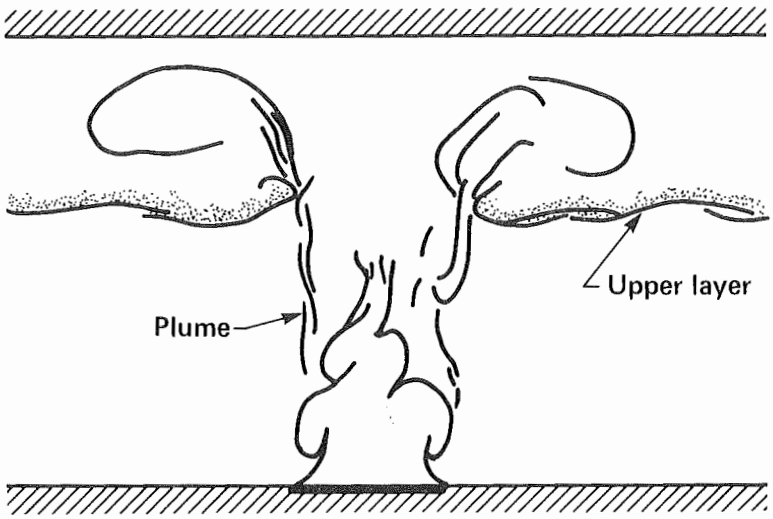

Figure 4-1. Schematic of a typical enclosure fire illustrating the fire plume and the hot upper layer.

capable of operating with a variable $\dot{Q}$, this is an unnecessary complication, particularly for initial validation purposes. Figure 4-2 is a schematic of the test cell, modified for enclosure-fire model validation.

Fire Experiments

In the first quarter of FY 84 we completed 35 forced-ventilated tests which represented a wide range of fire strengths and ventilation rates. The effects of several new parameters, such as the position and elevation of the fire source and the inlet and outlet ducts, were also explored. A listing of these fires and a full description of the tests can be found in our FY 83 Year-End Report (Hasegawa et al., 1984).

Previous research has yielded basic background information regarding fires in forced-ventilated enclosures (Hasegawa et al., 1981, 1983). It was determined that approximately 80% of the energy from such fires is absorbed into the enclosure walls, that two times the stoichiometric amount of air is needed to ventilate such fires, and that forced-ventilated fires require about 2000 s to reach quasi-steady-state equilibrium.

The 1983/1984 test series has, without question, produced the best forced-ventilated enclosure fire data to date, and has in turn provided much-needed insight into the significant parameters of such fires. The FY 84 tests differ from previous tests in that they were run longer, and only one test was done per day, allowing the test cell to cool to a uniform temperature. Improvements in the test setup, calibration, design, instrumentation, and data reduction have made these results more reliable and more consistent than earlier data. For a detailed description of the improvements in our test procedure, see the FY 83 Year-End Report.

An important step in the reduction of the 1983/1984 data was the "validation balancing" done after each test to insure that all data were consistent. We used the same method as in previous years, whereby all the gas species, temperatures, and mass flows were checked for consistency. This was routine because of improvements

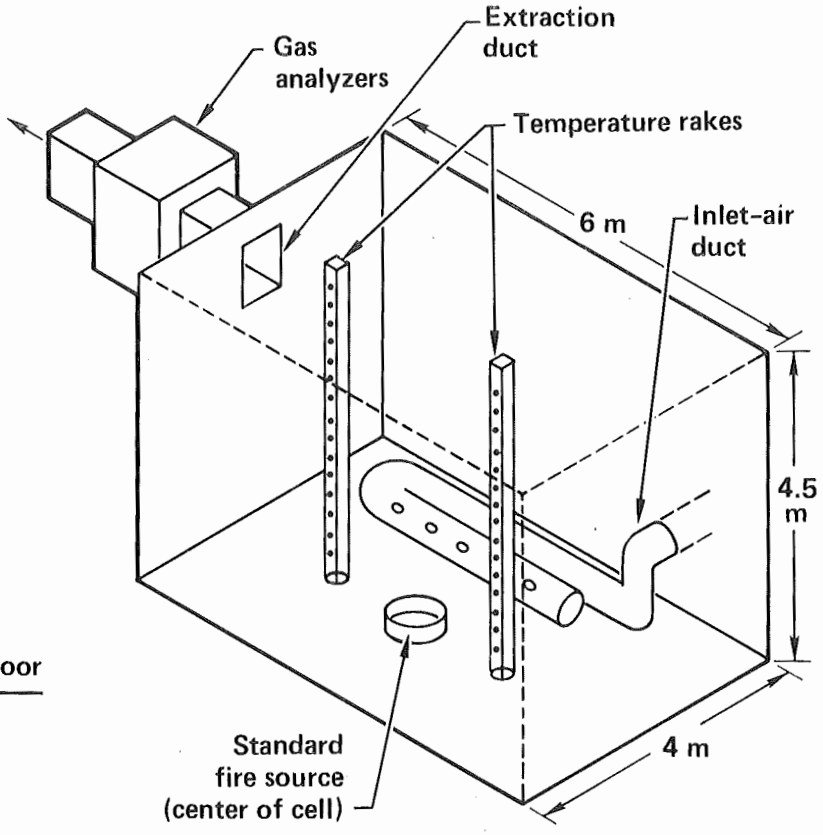

	Walls	Ceiling/Floor
ρ (kg/m^3)	1440	1920
k (W/m°K)	0.39	0.63
c (J/kg°K)	1000	1000

Figure 4-2. LLNL fire-test cell, showing the forced-ventilated ducting, instrumentation, wall properties, and fire-source location.

in measuring the inlet and exit air flows, though the sheer bulk of data increased the time required for the balancing procedures.

Characteristic Test Results

The results of this procedure for nine characteristic tests are summarized in Table 4-1, which consists of four sets of data taken at 500, 1000, 1500, and 2000 seconds. These tests represent a range of under- and over-ventilated fires. All of these tests had the fire in the center of the room on the floor with inlet air introduced at the floor and evacuated near the ceiling. Several temperatures are listed: the ambient air temperature measured by a thermocouple (TC) in the inlet duct, the exit gas temperature measured by a TC at the entrance of the exit duct, and the average test-cell air temperature measured by 30 small TCs on two vertical rakes. The 40-second average upper-layer temperature, as calculated from the top four TCs on each rake, is a time-dependent temperature average based on data-scanner frequency (for these experiments, the data is scanned every five seconds); thus, the 40-second upper-layer temperature average is the average of data taken 20 seconds before and after the recorded time. The ceiling temperature in the center of the room above the fire was measured by TCs embedded in the ceiling surface layer. The 40-second average of the hot-layer interface height is calculated from the vertical rake TCs using a method developed by Steckler (Quintiere, Steckler, and Corley, 1984).

The last nine columns contain data validated by the balancing procedure mentioned above. Since this data reflects steady-state information, we have not listed our results at early times (500 s and 1000 s). The amount of energy absorbed into the walls, floor, and ceiling is listed as a percent of the validated heat-release rate of the fire.

The bulk of our analysis and work has involved the steady-state data at 1500 and 2000 s, which refines some conclusions reported earlier. The amount of energy lost to the enclosure walls was very high (up to 91% if the ventilation rate was low, as in Test 5 at 2000 s). The average amount of energy absorbed by the walls was 86% ± 5% (80% was reported in our previous Year-End Report). The high density and conductivity of our enclosure construction accounts for this large heat loss and also for the relatively low upper-layer temperatures, e.g., at 2000 s the highest temperature recorded was 304°C in Test 1.

We previously reported that more than the stoichiometric ventilation rate was required to provide adequate air for our fire sources (Alvares, Foote, and Pagni, 1984). Figure 4-3 shows that approximately 1.5 times the stoichiometric ventilation is needed, below which significant amounts of CO and CH_4 were produced. Quasi-steady-state equilibrium did not occur until approximately 1500 s; for small fires at low ventilation rates, equilibrium did not occur until 2000 s. This long delay is primarily due to the large size of our enclosure, since the volume of air in the test cell

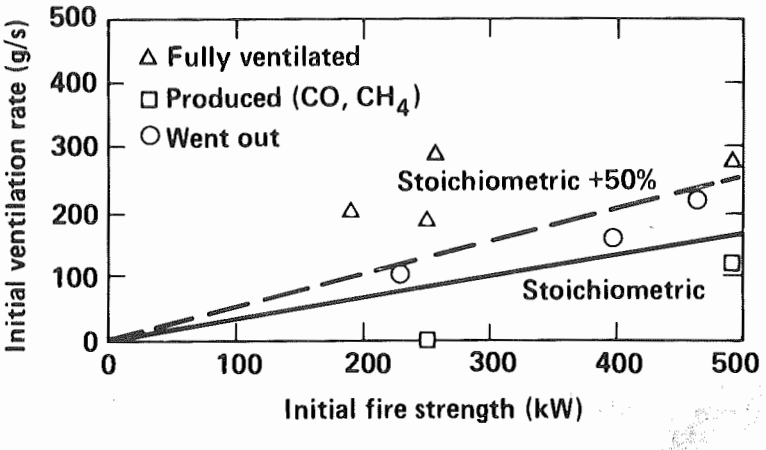

Figure 4-3. Plot of initial fire strength vs ventilation rate of LLNL forced-ventilated enclosure fire tests, illustrating the effect of the ventilation rate on fire efficiency.

Table 4-1. Validated 1983 model data at 500, 1000, 1500, and 2000 s.

	Am air temp. (°C)	Exit duct temp. (°C)	Avg. rake temp. (°C)	Avg. upper layer temp. (°C)	Ambient ceiling temp. (°C)	Rise in ceiling temp. (°C)	Avg. Steckler layer height (m)	Ventilation rate (g/s)	fire strength (kw)	Net energy out of room (kw)	% Energy lost to walls	Fuel consumed by CO_2CO (g/s)	O_2 consumed (g/s)	CO_2 (g/s)	CO (g/s)	CH_4 (g/s)
500 s																
Test 34	9	125	90	118	10	+40	1.77	200	*	*	*	*	*	*	*	*
Test 35	11	160	116	153	13	+56	1.70	190	*	*	*	*	*	*	*	*
Test 5	22	188	160	197	29	+73	1.62	118	*	*	*	*	*	*	*	*
Test 6	25	186	153	189	22	+73	1.63	185	*	*	*	*	*	*	*	*
Test 7	27	182	139	177	30	+57	1.67	350	*	*	*	*	*	*	*	*
Test 3	22	235	205	251	35	+126	1.70	115	*	*	*	*	*	*	*	*
Test 2	30	270	219	282	29	+133	1.81	170	*	*	*	*	*	*	*	*
Test 4	25	274	218	280	21	+134	1.75	235	*	*	*	*	*	*	*	*
Test 1	34	280	215	277	28	+107	1.75	310	*	*	*	*	*	*	*	*
1000 s																
Test 34	9	133	97	128	10	+54	1.81	195	*	*	*	*	*	*	*	*
Test 35	11	173	126	164	13	+79	1.70	185	*	*	*	*	*	*	*	*
Test 5	22	195	168	206	29	+96	1.65	115	*	*	*	*	*	*	*	*
Test 6	25	198	163	202	22	+96	1.66	180	*	*	*	*	*	*	*	*
Test 7	27	193	151	189	30	+73	1.64	335	*	*	*	*	*	*	*	*
Test 3	22	*	*	*	*	*	*	*	*	*	*	*	*	*	*	*
Test 2	30	264	218	274	29	+153	1.72	165	*	*	*	*	*	*	*	*
Test 4	25	278	221	286	21	+165	1.68	225	*	*	*	*	*	*	*	*
Test 1	34	293	232	294	28	+138	1.74	305	*	*	*	*	*	*	*	*
1500 s																
Test 34	9	140	105	137	10	+67	1.80	190	150	24	84	5.0	12.0	13.1	—	—
Test 35	11	177	132	171	13	+93	1.70	182	180	29	84	3.6	14.4	9.9	—	—
Test 5	22	201	175	212	29	+111	1.67	112	*	*	*	*	*	*	*	*
Test 6	25	207	170	211	22	+109	1.62	175	250	32	87	5.0	20.0	13.7	—	—
Test 7	27	199	163	199	30	+84	1.69	330	250	62	75	5.0	20.0	13.7	—	—
Test 3	*	*	*	*	*	*	*	*	*	*	*	*	*	*	*	*
Test 2	30	271	230	285	29	+172	1.79	160	400	42	89	8.0	32.0	20.6	1.5	1.8
Test 4	25	285	234	293	21	+180	1.65	220	465	61	87	9.3	37.2	24.5	0.9	0.5
Test 1	34	302	239	304	28	+158	1.78	300	490	84	83	9.8	39.2	26.9	—	—
2000 s																
Test 34	9	144	111	142	10	+74	1.78	187	150	24	84	5.0	12.0	13.1	—	—
Test 35	11	180	135	177	13	+104	1.75	180	180	29	84	3.6	14.4	9.9	—	—
Test 5	22	208	178	219	29	+123	1.75	110	230	21	91	4.6	18.4	12.1	0.5	0.4
Test 6	25	209	175	215	22	+119	1.61	175	250	32	87	5.0	20.0	13.7	—	—
Test 7	27	202	160	202	30	+93	1.70	325	250	62	75	5.0	20.0	13.7	—	—
Test 3	*	*	*	*	*	*	*	*	*	*	*	*	*	*	*	*
Test 2	30	271	234	285	29	+185	1.68	160	400	42	89	8.0	32.0	20.6	1.5	1.8
Test 4	25	291	243	304	21	+200	1.73	220	465	61	87	9.3	37.2	24.5	0.9	0.5
Test 1	*	*	*	*	*	*	*	*	*	*	*	*	*	*	*	*

allows free burning of small fires for significant periods of time, e.g., Test 0 was a 250-W fire with no ventilation at all, yet it burned for 500 s before reducing the available oxygen in the room to a concentration that would not support combustion.

Effects of Fire Parameters

We surveyed several new parameters during these tests. Tables 4-2 through 4-5 describe the importance of these parameters relative to room temperature and layer interface height. Much of our analysis focuses on the upper (or hot) layer temperature. We believe this to be the most important single enclosure fire parameter, since it represents the primary hazard to both life and property. Table 4-2 shows data from tests where the burner is located at different positions in the floor plane in the test cell. Figure 4-4 shows the three positions: Tests 9 and 10 at the west wall (position A); Tests 11 and 13a at the southeast corner (B); and Tests 2, 6, and 8 at the center (C). The average upper-layer temperatures are all similar at specified fire strengths. The only temperature variations between tests occur for TCs adjacent to fire plumes. Table 4-2 also shows data from tests where the fire strength was changed and the fire was elevated 1.0 m above the floor. In this comparison, the upper-layer temperatures are only slightly higher for tests with similar fire strengths.

Table 4-3 and Fig. 4-5 illustrate the effect of elevating the fire source off the center floor of the test cell. In five tests of the same fire strength, the burner was raised from the floor up to 2.5 m. Data collected in the exit duct (such as temperatures and gas concentrations) show little variation in the upper-layer temperature or the combustion gas composition for these tests. The average upper-layer temperature and ceiling surface temperature increases with fire source elevation. However, the temperature at the entrance to the exit duct exhibits a temperature difference of only 23°C. In Fig. 4-5 the oxygen concentrations at quasi-steady state are all the same; only the time to quasi-steady state changes as the burner is elevated. The oxygen concentration reaches equilibrium faster for the 2.5-m test because the upper layer is smaller, leaving less oxygen to be consumed.

The one parameter highly dependent on the fire elevation is the upper-layer interface height.

Table 4-2. Test with fire location and elevation changed at 2000 s.

Test	Burner height (m)	Initial fire strength (kW)	Location	Ambient temp. (°C)	Exit temp. (°C)	Avg. rake temp. (°C)	Avg. upper layer temp. (°C)	Ambient ceiling temp. (°C)	Rise in ceiling temp. (°C)	Avg. Steckler layer (m)
2	0.2	490	C	30	271	234	285	29	+185	1.68
9	0.2	490	WW	19	317	214	272	31	+136	1.95
11	0.2	490	SEC	21	253	199	279	20	+161	2.37
10	1.0	250	WW	21	235	153	221	31	+89	2.12
13A	1.0	490	SEC	25	270	192	305	33	+174	2.54
6	0.2	250	C	25	209	175	215	22	+109	1.61
8	1.0	490	C	24	281	203	301	28	+275	1.95

Table 4-3. Elevated tests at 2000 s.

Test	Burner height (m)	Ambient temp. (°C)	Exit temp. (°C)	Avg. rake temp. (°C)	Avg. upper layer temp. (°C)	Ambient ceiling temp. (°C)	Rise in ceiling temp. (°C)	Avg. Steckler layer (m)
2	0.20	30	271	234	285	29	+185	1.68
12	0.50	24	268	217	286	29	+233	1.97
8	1.00	24	281	203	301	28	+275	2.26
14	1.50	24	279	191	307	21	+334	2.48
16	2.50	27	294	169	333	34	+396[a]	3.02

[a] Sauriasen cracked, releasing the ceiling thermocouple from ceiling contact.

Table 4-4. Elevated tests with ventilation rate changed at 2000 s.

Test	Burner height (m)	Initial fire strength (kW)	Initial vent rate (g/s)	Ambient temp. (°C)	Exit temp. (C°)	Avg. rake temp. (C°)	Avg. upper layer temp. (C°)	Ambient ceiling temp. (C°)	Rise in ceiling temp. (C°)	Avg. Steckler layer (m)
5	0.2	250	150	22	208	178	219	29	+123	1.75
6	0.2	250	225	25	209	175	215	22	+119	1.61
7	0.2	250	425	27	202	160	202	30	+93	1.70
2	0.2	490	225	30	271	234	285	29	+185	1.68
4	0.2	490	300	25	291	43	304	21	+200	1.73
1	0.2	490	425	34	305	45	307	28	+163	1.75
14	1.5	490	225	24	279	191	307	21	+334	2.48
15	1.5	490	425	26	309	196	333	32	+347	2.62
16	2.5	490	225	27	294	169	333	34	+396*	3.02
17	2.5	490	425	26	308	171	357	37	+394*	3.12

Table 4-5. Test with vent pattern changed at 2000 s.

Test	Vent pattern (in/exit)	Ambient temp. (°C)	Exit temp. (°C)	Avg. rake temp. (°C)	Avg. upper layer temp. (°C)	Ambient ceiling temp. (°C)	Rise in ceiling temp. (°C)	Avg. Steckler layer (m)
7	Lo/Hi	27	202	160	202	30	+92	1.70
22	Hi/Hi	15	184	154	187	15	+100	2.15
26	Hi/Lo	17	138	177	208	10	+109	1.98
27	Lo/Lo	12	153	173	210	8	+112	1.48

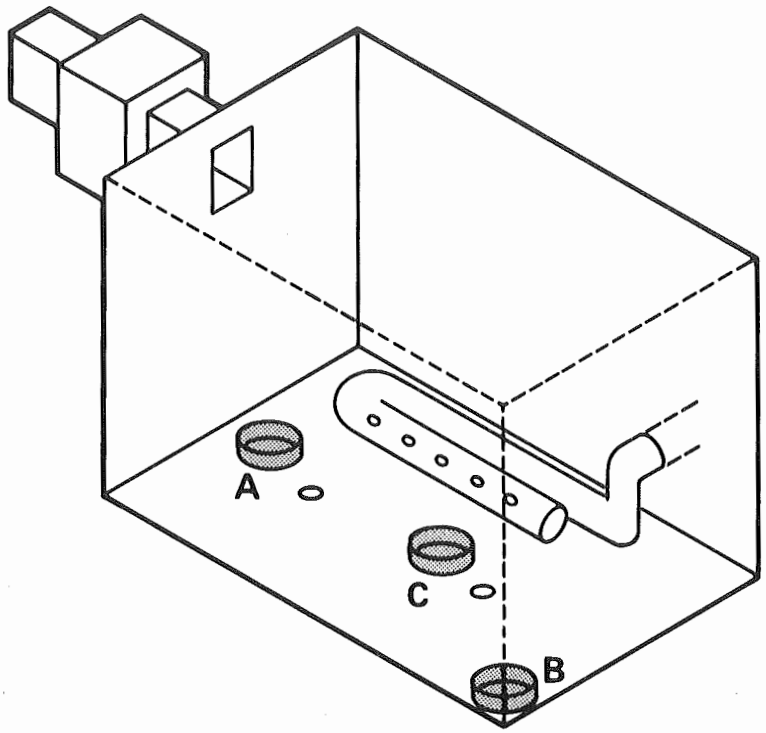

Figure 4-4. Three positions of burner in the fire-test cell.

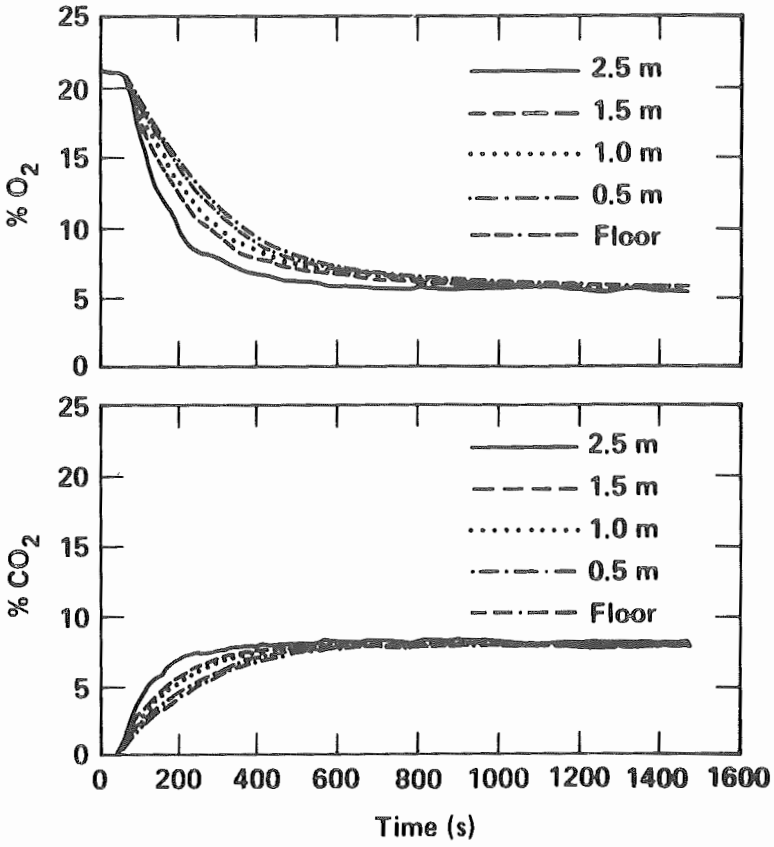

Figure 4-5. Effects of elevating the fire source from the floor of the test cell.

Table 4-3 shows that the interface rises as the fire is elevated. In these tests the hot layer attempts to fill the room but is stopped by the density difference of the cold and hot layer. Figure 4-6 illustrates this by plotting data from Table 4-4, showing that the fire elevation dictates layer height relative to fuel-surface elevation. The heat-release rate and ventilation rate have only a slight influence on the interface height. For the two tests at 0.2-m elevation, the layer heights are scattered around 1.70 m, showing little dependence on ventilation rate or heat-release rate. However, when the burner elevation is changed from 0.2 m to 2.5 m the effect is dramatic.

Changing the location of the inlet and outlet ducts also has a major effect on several fire parameters. Placing the exit duct high or low in the enclosure greatly changed the temperatures and gas concentrations measured in the exit duct. Table 4-5 lists temperatures and the upper-layer interface heights of four 250-kW fires, well ventilated at 425 g/s, each with a different ventilation pattern. For a low exit duct, the upper layer and ceiling temperature levels are higher than for a high exit duct. However, local temperatures in the test cell, such as the average rake temperature, change very little (~20°C). At conditions where the fire was slightly ventilation-limited (250 kW, 125 g/s), the effect of a high or low inlet duct was very important, e.g., with the inlet near the ceiling, the fire became so oxygen starved that it self-extinguished. Soon after the initial room air was consumed (~300 s), these fires flickered rapidly around the test cell in need of oxygen. Just before they went out, the flames burned blue instead of yellow and detached from the burner. For the worst-case ventilation pattern—that of high inlet and low outlet—a 250-kW fire required four times the stoichiometric amount of ventilation to sustain combustion. The output parameters of the fire are greatly affected by the location of the ventilation ducts. Any complete fire model should account for the location of these ducts, particularly the inlet duct.

We have not reported several tests because the data was not suitable for balancing: Tests 0, 3, 18, 19, 20, 21, 23, 24, 25, and 32 were extremely under-ventilated and did not run long enough for

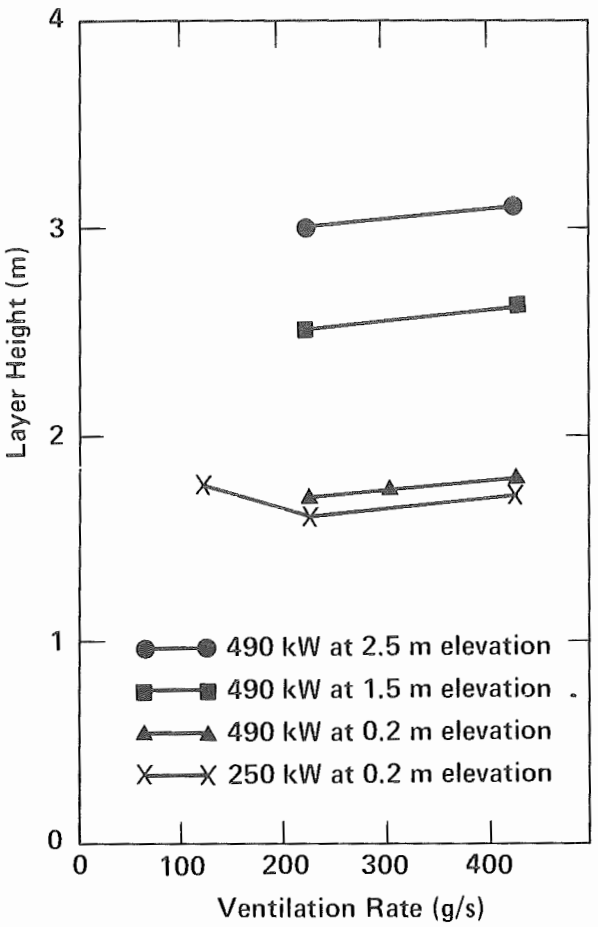

Figure 4-6. Plot of the ventilation rate vs layer height, showing that ventilation rate and heat-release rate have minor effects on the layer height releative to the fire-source elevation.

proper validation and comparison. Tests 29 and 30 were isopropanol pool fires for which we had difficulty reducing the data. The data for Test 31 was accidentally erased before it could be analyzed. Some tests simply have no basis for comparison with other tests, such as Tests 28 and 33. While these tests are not amenable for code validation, they are extremely useful for the description of fire behavior in forced-ventilated enclosures.

Conclusions of Forced-Ventilated Experiments

The 1983/1984 forced-ventilated enclosure tests have refined many of our conclusions from previous tests. We have found that in order to efficiently burn all the available fuel, 1.5 to 2.0 times the stoichiometric amount of air must be available to the fire. The walls of our enclosure absorb a large amount of the energy released by the fire (86% ± 5%). The large size of our enclosure means that quasi-steady-state equilibrium is not reached until at least 1500 seconds after the start of the fire.

These tests explored the effects of several new parameters. We found that the elevation of the fire source within the enclosure is the major determinant of the upper-layer interface height. Elevating the fire also reduced the time to quasi-steady state by reducing the volume of the upper layer. The lateral locations of the fire source on the floor affects only local temperatures and has no effect on parameters measured in the exit duct. The locations of the inlet and exit ducts, however, did have a major effect on the output parameters of the fire. When the inlet duct is placed near the ceiling, buoyancy effects severely inhibit combustion ventilation. Up to four times the stoichiometric amount of air may be needed to sustain burning. Placing the exit duct near the floor dramatically changed the parameters in the exit duct; the measured gas temperatures and the concentrations of combustion gases were both lower.

Though our test cell is uniquely designed for fire research, it is not dissimilar in material and construction to many modern laboratory and fabrication facilities. This is particularly true of facilities that contain toxic or highly energetic materials. Therefore, the results of our experiments can be applied to some establishments directly, and with certain modifications to many others.

Enclosure Fire Models

Two classes of fire models are in vogue for the prediction of fire conditions in enclosures: zone models and field models. The *zone* model assesses the effect of energy and mass transfer from a source (fire) to one or two homogeneous control volumes called zones. The *field* model is a type of zone model containing many (~1000) very small zones. This allows local conditions to influence properties and the response of adjacent zones, thus producing a potentially more realistic description of enclosure conditions. Zone models are simple and give adequate descriptions of enclosure fire conditions; whereas field models are more complex and capable of predicting local events, conditions in non-regular enclosures, and flow-pattern variations. Disadvantages of field models are the necessity for the (largely unavailable) detailed knowledge of physical phenomena and the need for huge computer capacities.

Selection of a Preliminary Model

Several research groups are already heavily involved in fire model development. We set out to identify an established modeling procedure that would fit the conditions found or expected in DOE energy-research facilities. Our selection was to be made by comparing data from the available models with benchmark measurements obtained in the LLNL fire-test cell. Table 4-6 lists the parameters for which these models were evaluated.

As shown in our FY 83 report, most of the models we investigated were unreliable for risk assessment in forced-ventilated enclosures. For the two most promising models, we proposed modifications to better simulate the behavior of forced-ventilated enclosure fires.

Code Modifications

Two of the computer models were modified by their authors to better predict the parameters of a forced-ventilated fire: the Harvard 5.3 code (Mitler, 1984) and the Cal Tech One-Layer code (Zukoski and Kubota, 1980). The improved version of the Harvard code used a higher specific heat in its plume calculation, allowing more heat to enter the hot layer. The Cal Tech code had two improvements: the surface area of the floor was included in the total area of heat-absorbing surfaces, and the assumed average wall conductivity was increased. These two improvements allowed more heat to be absorbed by the walls, thus reducing the rate at which the upper-layer gas temperature rises (a failing in the earlier version of this code).

Figures 4-7 and 4-8 show the results of these modifications for MOD9 (a 1982 test), plotted with the original predictions and actual data for comparison. In Fig. 4-7 the upper-layer prediction of the Harvard code is much better, though it is still about 100°C too low. The improved Cal Tech code predicts a lower temperature than before, yet still predicts too fast a rate of temperature rise, and at longer times it predicts an unrealistically high temperature. Figure 4-8 shows a similar comparison done with oxygen depletion. For this test, the oxygen prediction by the improved Cal Tech code is much better than the old one. This is not true for all the tests, however, and for all overventilated tests it does much worse. The improved Harvard code's prediction is much worse than the original prediction, and this code also does a worse job of predicting the upper-layer interface height than before. Thus, while the upper-layer temperature predictions of these codes are slightly improved, many of the other parameters are much worse. These codes still need extensive modifications before they will be reliable.

Table 4-6. Request for model predictions.

Using input data in Table 1 it is hoped that participating modelers will be able to predict time histories of the following parameters for comparison with collected experimental data:

1. **Mass flow at the inlet $\dot{M}(t)$ (g/s)**
2. **Fire strength, $\dot{q}_{fire}(t)$ (kW)**
3. **Gas temperature at the entrance to the exit duct, $T_d(t)$ (°C)**
4. **Gas temperatures throughout the room, $T_r(x,t)$ (°C)**
5. **Wall temperature of all surface walls, $T_2(x,t)$ (°C)**
6. **O_2, CO_2, H_2O, CO, and CH_4 concentrations at the entrance to the exit duct, $Y_{id}(t)$**
7. **O_2, CO_2, H_2O, CO, and CH_4 concentrations in the room, $Y_{ir}(t)$**
8. **Component heat flux to the room surfaces, $\dot{q}_{rad}(x,t)$, $\dot{q}_{conv}(x,t)$, $\dot{q}_{total}(x,t)$ (W/m^2)**
9. **Room pressure, $P_r(t)$ (Pascals)**
10. **Mass pyrolysis rate of the pool fires, $\dot{M}_f(t)$ (g/s)**

Temperature Correlation

In order to fulfill our project goals of providing a reliable method of risk assessment for DOE facilities, we developed a correlation to predict the upper-layer temperature of a fire in forced-ventilated enclosures. This correlation (known as the Simple Temperature Calculation, STC) reliably predicts the upper-layer temperatures of the fires we have done in our test cell. The method and form of the STC was developed by B. J. McCaffrey (McCaffrey, Quintiere, and Harkleroad, 1981). STC predicts upper-layer temperatures only at quasi-steady-state times. STC is absolutely empirical, so its value is to be suspect when applied to other enclosure fires. (For example, STC does not account for the elevation of a fire or the location of an inlet duct.)

STC is a simple equation that predicts the upper-layer temperature of a forced-ventilated enclosure fire using the maximum heat-release rate, ventilation rate, ambient-temperature surface area, and heating properties of the walls.

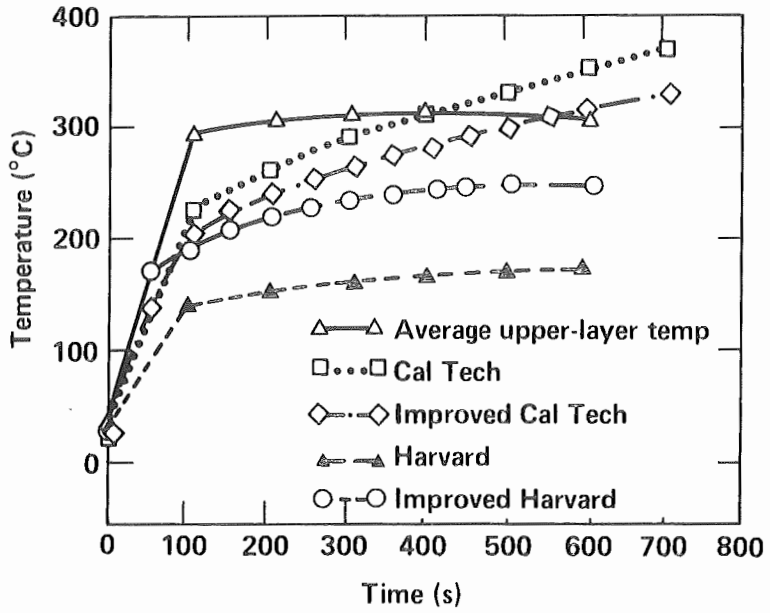

Figure 4-7. Upper-layer temperature predictions of various fire models, also showing LLNL forced-ventilated enclosure fire data. Note the improved accuracy.

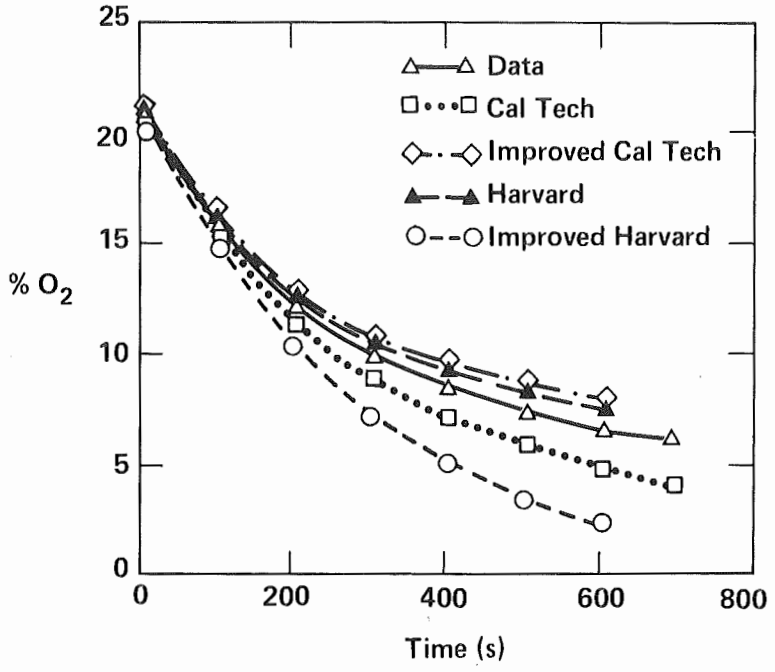

Figure 4-8. Oxygen depletion as predicted by various fire models with LLNL test-cell data, showing decreased accuracy.

$$\frac{T_u - T_a}{T_a} = 0.63\left[\frac{\dot{Q}_f}{M_i C_p T_a}\right]^{0.72}\left[\frac{\sqrt{K_w D_w C_w}\cdot A_w}{\sqrt{t}\cdot M_i C_p}\right]^{-0.36}$$

where

T_a = ambient temperature (K)
T_u = upper-layer temperature (K)
$\dot{Q}_f$ = maximum heat-release rate (kW)
M_i = ventilation rate (g/s)
A_w = total surface area of the walls, ceiling, and floor (m^2)
K_w = average conductivity of the walls, ceiling, and floor (kW/m K)
D_w = average density of the walls, ceiling, and floor (kg/m^3)
C_w = average specific heat of the walls, ceiling, and floor (kJ/kg K)
C_p = specific heat of air (kJ/kg K)
t = time (s)

STC has been found to be extremely accurate in predicting upper-layer temperatures in our test cell. Figure 4-9 is a plot of three upper-layer temperature curves (Test 4, Test 7, Test 34) vs predictions by STC. In all three cases the prediction is within 5%, or ±10°C, at long times. At early times for Test 4, the STC prediction is quite low, which is to be expected because this fire is under-ventilated; consequently, the fire strength changes with fire duration. For this prediction we used the quasi-steady-state heat-release rate, resulting in a low prediction at early times. Figure 4-10 is a similar plot of upper-layer temperatures from tests not used as part of the database for the correlation (Test 2, Test 8, Test 16). These tests were all severely under-ventilated, as the upper-layer temperature curves show. All three curves rise very quickly, then round off and drop as the heat-release rate drops. After 500 s, they begin a slow rise to quasi-steady state as the heat-release rate stabilizes. Again, our correlation under-predicts the temperature at early times, but is correct at later times. These tests all have the same ventilation and heat-release rate with the only difference between them being the fire elevation. STC has no parameter to change the fire elevation, so we simulated this by reducing the size of the room. We took the room height to be the distance from the burner to the ceiling.

This simple temperature correlation has proven itself to be reliable for a variety of tests in the LLNL test cell. We can use this correlation to make predictions about other fires, as we did above for Tests 2, 8, and 16, if we are careful. Figure 4-11 shows a plot of the correlation parameters X_1 vs X_2. On this plot is shown the entire

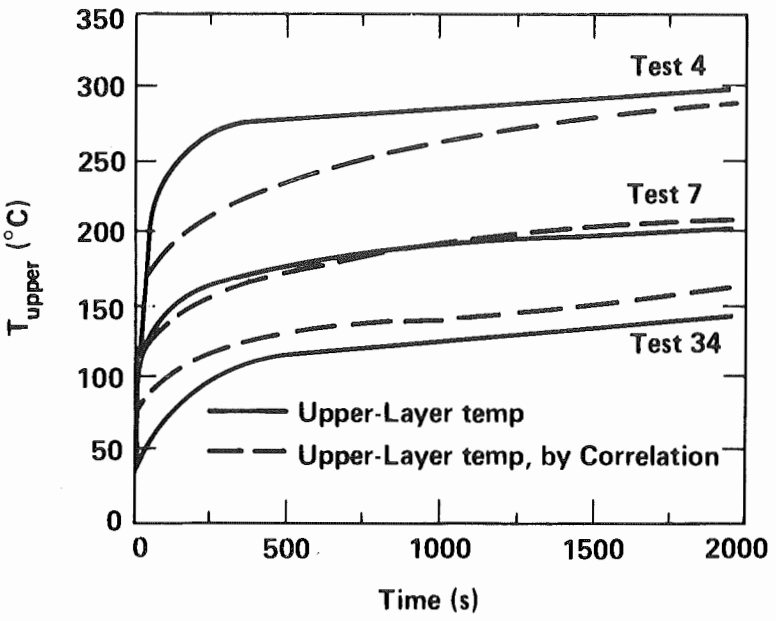

Figure 4-9. Upper-layer temperature curves for three tests, compared to predictions by STC, showing its accuracy over a wide range.

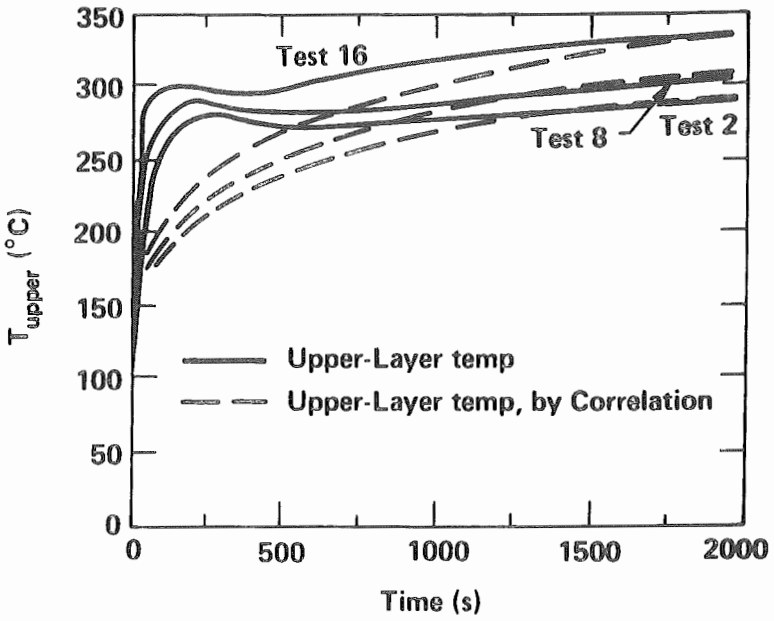

Figure 4-10. Upper-layer temperature curves for severely under-ventilated tests, compared to predictions by STC. These curves illustrate the correlation's ability to account for unique geometries.

range of possible fires as defined by the correlation. The cross-hatched region of the plot is the range X_1 and X_2 of the LLNL test cell. Our correlation is validated and works best for fires within this range. Using past experience, however, we can make predictions for fires in enclosures that fall outside this range.

Assessment of Current Enclosure Fire Models

Our validation procedures have showed that enclosure fire models are not yet at the stage of development where they can be practically employed for fire risk assessment. However, these models do show great promise and can currently be used to indicate trend changes when parameters such as ventilation, surface heat transfer constants, and enclosure dimensions are varied.

One major limitation in the use of zone models is that the relationship between enclosure size and fire size is not well defined. For example, we would expect that both the thickness and the temperature of the hot gas layer should be inversely proportional to the enclosure size for a fire with constant strength. This proportionality varies, however, depending on which dimension (vertical or horizontal) is changed. Moreover, as the enclosure dimensions increase for a fixed fire size, a point occurs beyond which heat losses to the enclosure surfaces may prevent a ceiling layer from forming, making the zone model boundary conditions invalid. Although we cannot describe the conditions that contribute to this situation, it is of real concern in the proper interpretation of zone model results for fire risk analysis.

Conclusion

Our goal has been to describe the main feature of a proposed fire risk analysis protocol, which will employ enclosure fire models as the focus of the analysis. We demonstrated that existing model algorithms are not yet developed to the stage where they can be used with confidence. In specific, limited cases, however, current models give results that can be used to assess generalized trends. By reducing output data to simplified terms of temperature and thermal-layer formation, in Appendix B we have described the procedure we will use in place of formalized models to drive our risk assessment protocol. Since this assessment scheme is designed in a modular sense, we will be able to replace our currently proposed procedure with formalized enclosure fire models as they become available. By continuing to improve this protocol, we will use the best contemporary procedures to assist in maintaining and improving DOE fire-loss records.

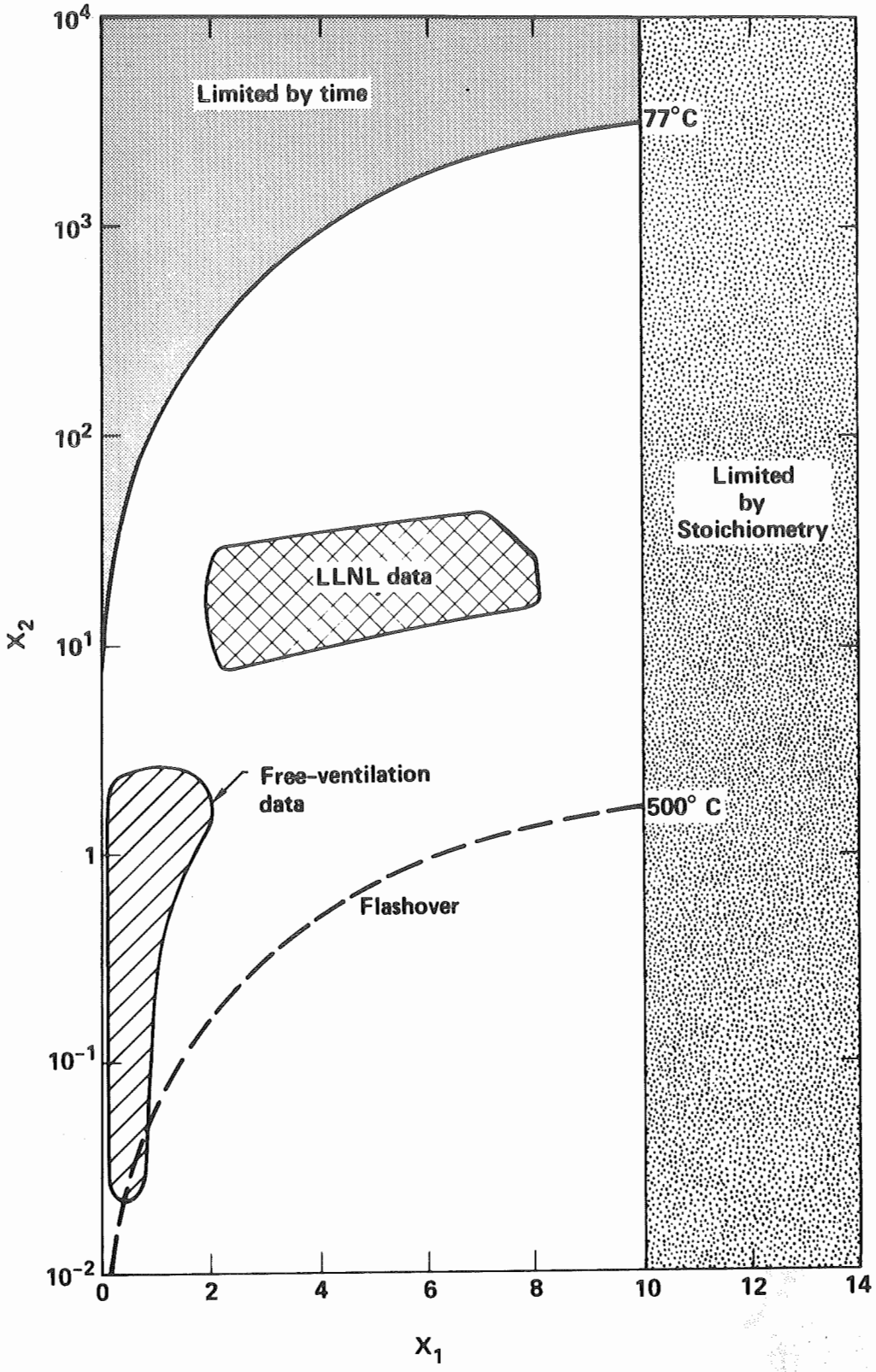

Figure 4-11. Plot of STC parameters X_1 and X_2, illustrating the expected range of application of the correlation for fire risk assessment.

Part 5:
Digraph-Fault Tree Methodology

Introduction and Background

This section gives an overview of the digraph-fault tree methodology used in our reliability analysis of the Mocho water-supply system which serves LLNL. Our methodology uses a simplified model of the Mocho system, and can be seen as a pattern for the analysis of other water-supply systems. For a more complete description of the methodology, consult Lapp and Powers (1977a,b), Allen and Rao (1980), and Lambert (1979).

A fault tree is a deductive logic model of a "Top Event," an undesired event or system state. A digraph (a "directed graph") is a symbolic multivalued-logic model useful for fault-tree analysis of control systems, and is always constructed with a Top Event in mind. The objective of the combined digraph-fault tree methodology is to systematically produce a fault tree for qualitative and quantitative evaluation of particular systems. For our analysis of the Mocho water-supply system, the Top Event was an inadequate supply of water in the event of a major fire at LLNL.

The Mocho system contains many control loops that maintain the water levels in the storage tanks and also alert the proper personnel in the event of low water level in the tanks. The digraph-fault tree methodology is useful in understanding how these control loops can fail, thereby causing an insufficient supply of water in the storage tanks.

Description of the Mocho Water-Supply System

Figure 5-1 shows the Mocho water-supply system to LLNL. The main source of water is the Hetch Hetchy Aqueduct, located 800 ft below ground at the Mocho pumping station. The water is first pumped to the surface and into the standpipes. The purpose of the standpipes is to prevent water hammer at pump discharge. The water flows by gravity from the standpipe to the storage tanks 1/2 mile south of LLNL on a hill above Sandia National Laboratories. The central control room for the system is located at LLNL in Bldg. 511. The system consists basically of two feedback subsystems: the water-level controls for the Mocho standpipes and for the storage tanks. Any two of the three pumps control the water level in the standpipes. Water level in the storage tanks is controlled by opening a valve that drains the standpipes. Gravity feeds water as needed from the storage tanks. Alarms, status indicators, and control signals are transmitted and received on a control console in Bldg. 511. Manual commands from the control console can open or close valves at the Mocho pumping station. Any abnormal condition, such as a high or low water level in the storage tanks or in the standpipes, or any pump failures, initiates an audible and visible alarm on the control console.

A standby water-supply system is available from the Zone 7 water district. This alternate water supply is used only during times when the Hetch Hetchy water is unavailable. The Zone 7 water supply must be activated by personnel on site.

Figure 5-2 is a simplified schematic which resembles the concept of the Mocho system. This schematic will be used to explain our digraph-fault tree methodology. The major differences between Figs. 5-1 and 5-2 are that Fig. 5-2 contains only one Mocho pump, one standpipe, and one storage tank. In addition, only two alarms are considered in the simplified schematic—low standpipe level and low storage-tank level. A low level in either the standpipe or the storage tank can lead to an insufficient supply of water to LLNL. For the simplified system, we assume that a low level in either case will result in the proper personnel valving in the alternate Zone 7 water supply.

Digraph Notation and Terminology

A digraph is a set of "nodes" and "connection edges." In the digraph, nodes represent variables. If one variable affects another variable, a directed arrow or edge connects the independent variable to the dependent one. The directed edge may be either a normal edge which indicates the relationship is normally true, or a conditional edge which indicates the relationship is true when another event (or condition) exists. Edges connecting any pair of nodes are mutually exclusive (i.e., only one edge is true at a given time).

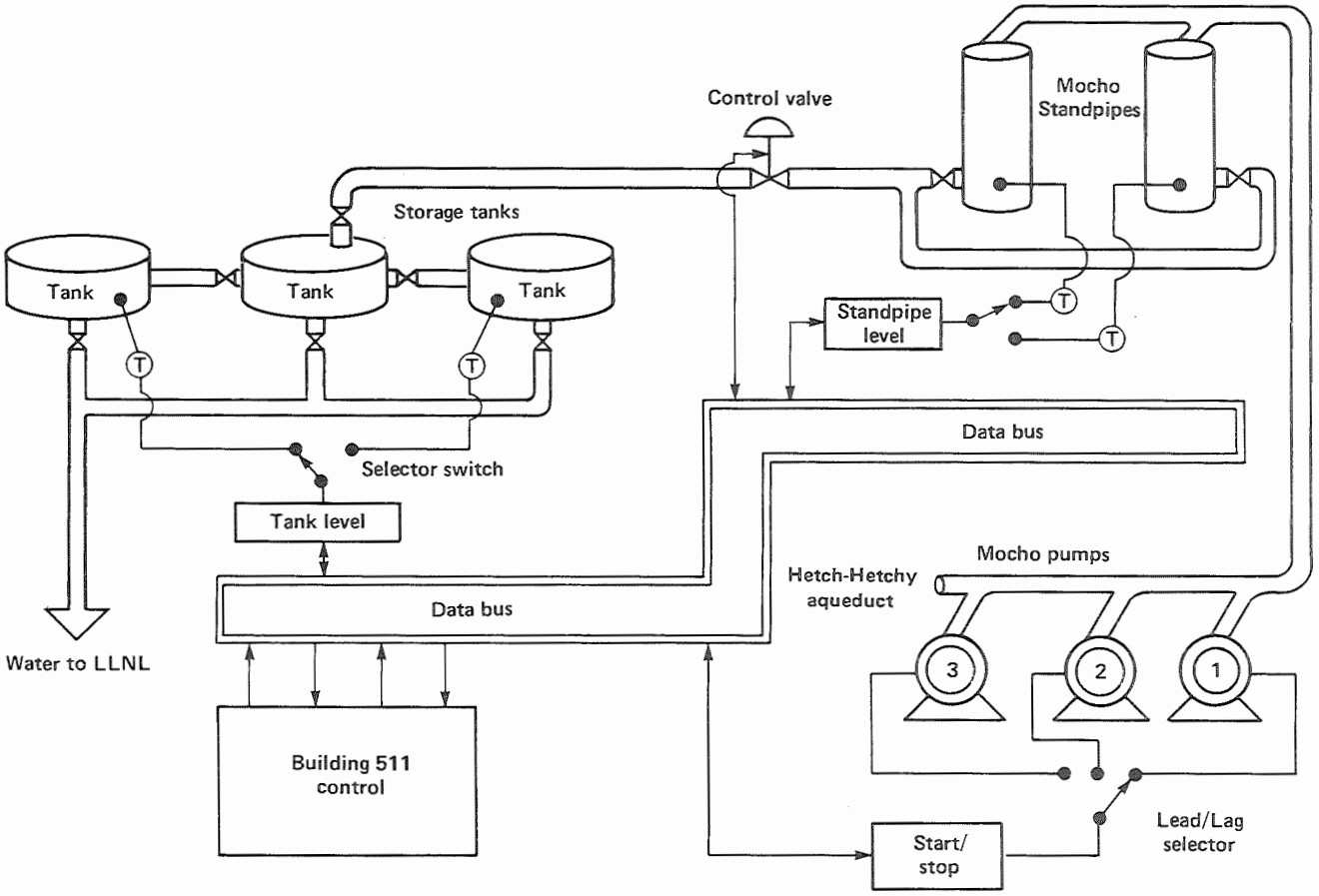

Figure 5-1. Schematic of the Mocho water-supply system.

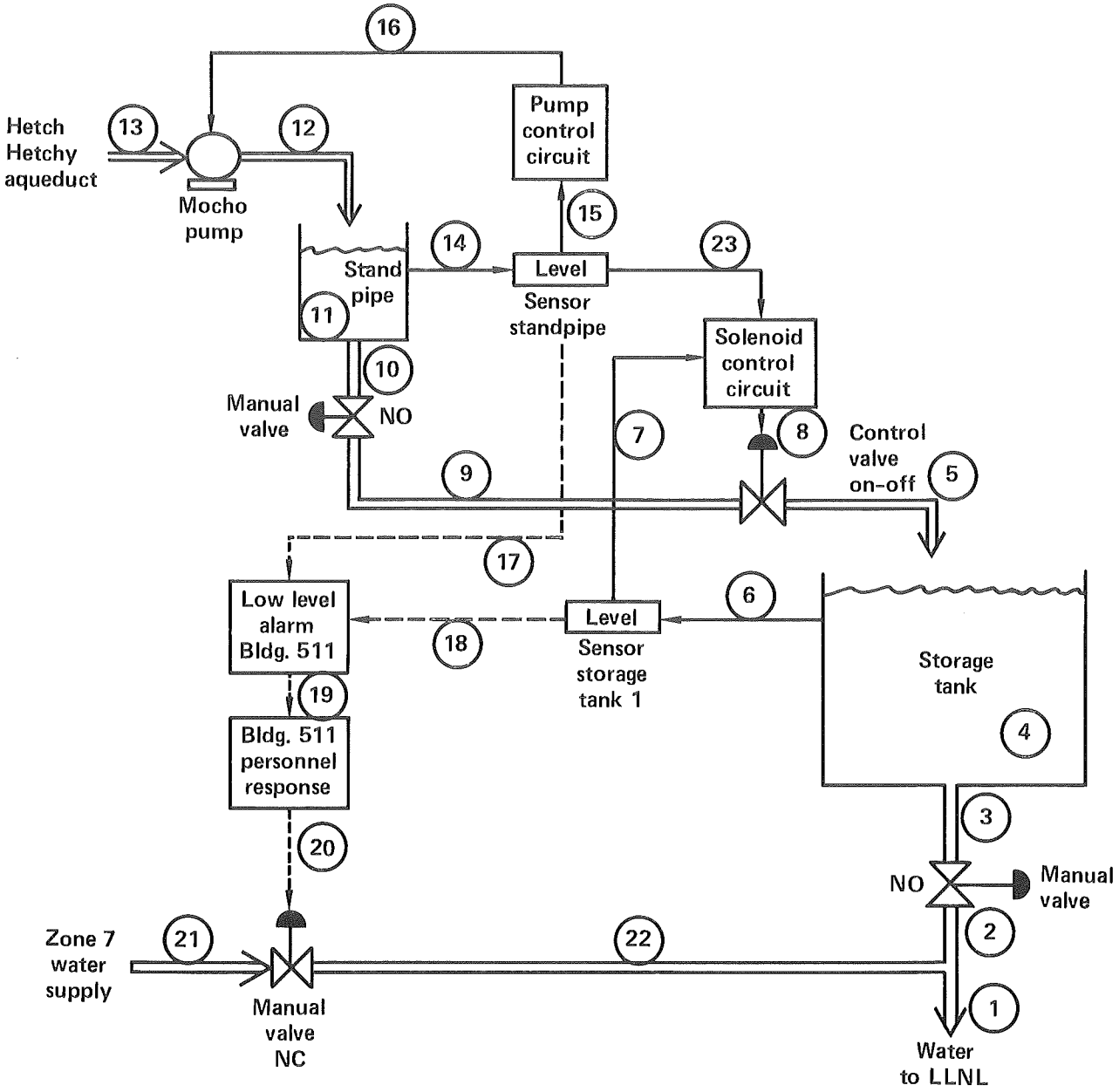

Figure 5-2. Simplified schematic of the Mocho system.

Numbers may be placed on the directed edge to represent the gains between the two events. These gains are based on the mathematical definition of gain, $\Delta Y/X$, where X and Y denote the independent and dependent variables or events, respectively. The magnitudes of the gains used in the digraphs for the assessment are quantized to three discrete values -1, 0, and $+1$, symbolizing a negative relationship, no relationship, and a positive relationship, respectively, between the independent and dependent variables.

Events are represented by alphanumeric labels on the nodes. For instance, "P2," "M3," "Fire at HX" represent pressure at location 2, mass flow rate at location 3, and fire at the heat exchanger. The direction of the deviation in the values of variables are denoted by "+" and "−". These deviations have magnitudes of "0" and "1". A magnitude of 1 indicates a range of values considered moderate; a magnitude of 0 symbolizes a true or expected range of values of the event. For instance, P2(0) represents the true or expected value

of pressure at location two, and M3 (+1) represents a moderate increase in mass-flow rate at location 3.

Lapp and Powers (1977a,b) use a five-level scheme for the representation of gains and values of variables. For our analysis of the Mocho supply system, three levels (−1, 0, and +1) were adequate.

Construction of the System Digraph

Unit Model Digraphs

The basic building blocks of the digraph-fault tree approach are unit model digraphs, which contain essentially the same information as in failure modes and effects analysis (below).

Figure 5-3 shows a unit model digraph for a pneumatic air-to-close regulating control valve (a proportional control valve). Regulating the controller air pressure at location 3 (represented by variable P3, as described above) will adjust the position of the valve, which will in turn regulate the flow cross-sectional area of the control valve, and thus control the mass-flow rate at location 2 (variable M2). Since the valve is air-to-close, increasing/decreasing P3 will decrease/increase M2, resulting in a −1 gain between P3 and M2. A gain of −1 implies that M2 (the independent variable) and P3 (the dependent variable) will have the relationship represented in Fig. 5-3.

Failure Modes and Effects Analysis (FMEA)

We performed a detailed failure modes and effects analysis (FMEA) on the Mocho system, with input from LLNL personnel. The results of this study provided much of the information needed for the construction of the digraph and the fault tree and for the probabilistic evaluation of the fault tree. The advantage of a FMEA is that personnel can provide the required information for the analysis without having a knowledge of the digraph-fault tree procedure.

Table 5-1 presents a portion of our FMEA conducted for this study.

The System Digraph

The nodes in Fig. 5-2 represent location nodes for the system digraph presented in Fig. 5-4. The Top Event variable considered in the system digraph is mass flow to LLNL (the integral of mass-flow rate over time). The cycles in the digraph show two basic feedback loops:

- The storage-tank level control loop, nodes L4, S6, S7, S8, and M5.
- The standpipe-tank level control loop, nodes L11, S14, S15, S16, and M12.

As described in Fig. 5-4, the variables L, M, and S represent water level, mass flow, and electrical signal, respectively. The dashed lines in the system digraph represent corrective branches to two negative feedforward loops. A low standpipe level generates a low-voltage signal, S14, which generates an alarm in Bldg. 511. For either alarm,

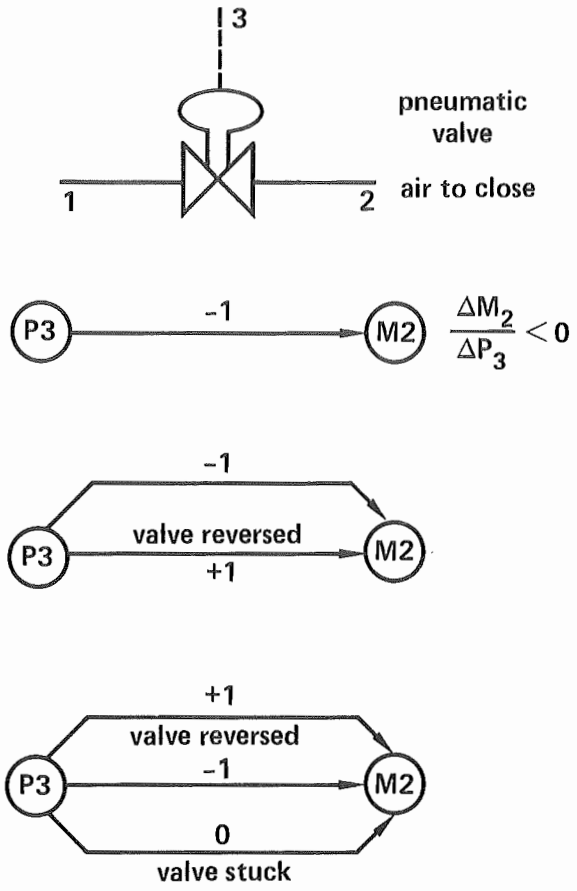

(domain) P3	(range) M2
−0	+1
0	0
+1	−1

Figure 5-3. Unit model digraph for pneumatic air-to-close regulating control valve.

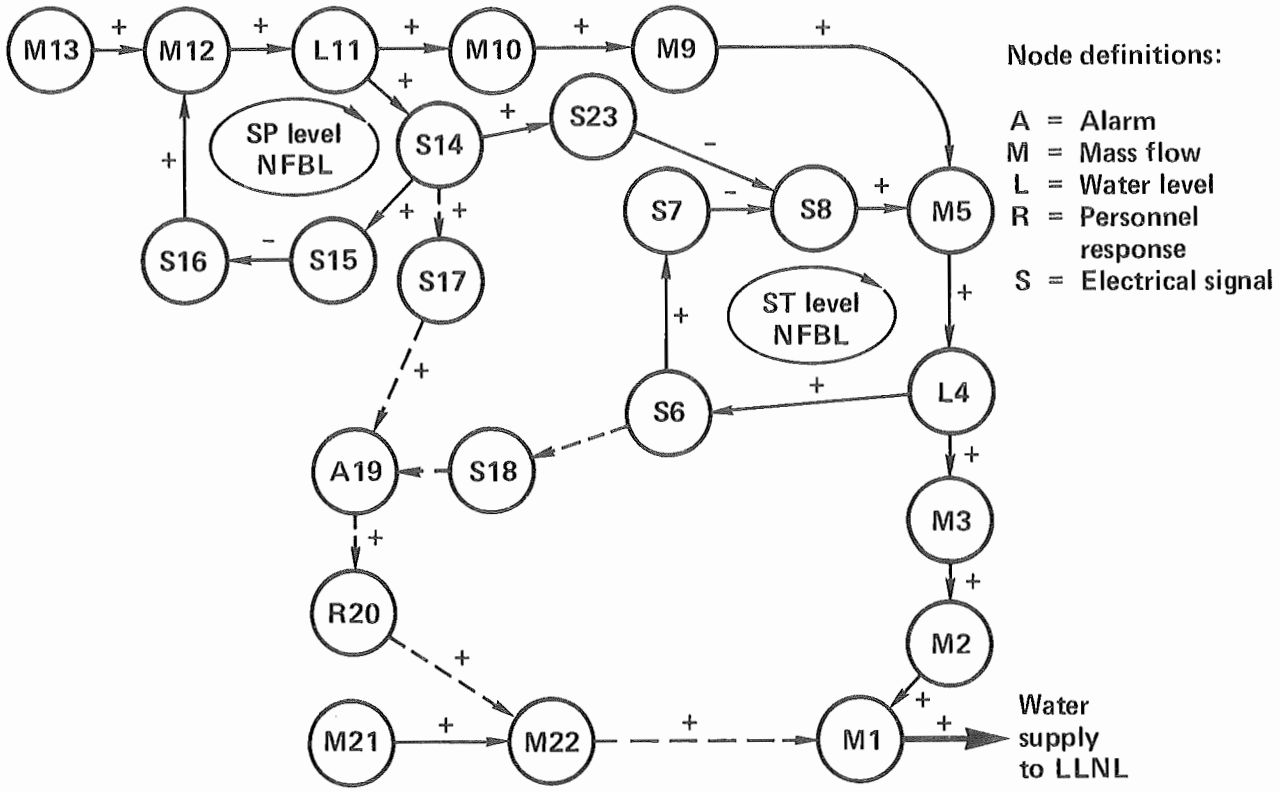

Figure 5-4. The Mocho system digraph shows two basic feedback loops: the storage tank level and the standpipe level.

personnel will valve in Zone 7 and restore an adequate water supply. For our Mocho supply system analysis, the negative feedforward loops (NFFLs) consist of a causative branch(es) and a corrective branch(es). Figure 5-4 shows two NFFLs with the following causative branches:

- Nodes S6, S7, S8, M5, L4, M3, M2, and M1 (causes low storage-tank level).
- Nodes S14, S23, S8, M5, L4, M3, M2, and M1 (causes low standpipe level, which causes the control valve to close, which in turn causes low storage-tank level).

We see that NFFLs fan out on a node (called the start node of the NFFL) and converge on a downstream node (the end node of the NFFL). The start nodes to the NFFLs in the system digraph are S6 and S14, and the end node in both cases is M1.

Incorporation of Failure Modes into the System Digraph

Figure 5-5 shows the digraph for the LLNL water-supply system with the failure modes included from the FMEA in Table 5-1. This digraph shows two types of failure modes:

- Input disturbances to the negative feedback loop (NFBL) designated by primary nodes (nodes which have no inputs).
- Failure modes designated by the zero-gain events (indicated by the symbol "0:").

The above failure modes appear as basic events in the fault tree, and represent the limit of resolution of the analysis. Input disturbances cause either a low standpipe level or a low storage-tank level. The zero-gain events deactivate the corrective branch of the negative feedforward loop so that personnel will fail to take corrective action in the event of a low level in either the storage tank or standpipes.

It is important to note that if the storage tank drain valve is closed, then the tank level will rise to its normal value, and then the control valve will close. The relationship which describes this on the digraph is represented by a reverse arrow from nodes M3 to L4. In this case, an adequate level in the storage tank will be maintained, but

Table 5-1. Portion of the failure modes and effects analysis conducted on the Mocho water-supply system.

Title: Mocho water system				System : Mocho control system Subsystem :					
Item* Identif.	Function	Failure Mode	Failure Cause	Failure effect on			Failure Detection Method	Mean Time to Failure	Mean Time to Repair
				Comp. or Func. Assembly	Next Higher Assembly	System			
⑥ Pressure transducer storage tank	Measures water level in storage tank	Variable resistance high	Random failure	High voltage generated	On-off control valve will be closed too long	Low storage tank level	Low water pressure LLNL	0.4 yr^{-1}	3 hours
⑭ Pressure transducer standpipe	Measure water level in standpipe	Variable resistance high	Random failure	High voltage generated	Mocho pump will run much shorter time	Low standpipe level	Eventual low storage tank level alarm	0.4 yr^{-1}	5 hours
⑯ Pump control CCT -- start relay	Starts Mocho pump	Starting relay contacts stick	Random failure	Start signal not generated	Mocho pump will not start	Low standpipe level	Low level standpipe alarm	0.4 yr^{-1}	8 hours
⑯ Pump control CCT -- shunt relay	Detects imbalance in voltage	Shunt relay trips open	Random failure	No control voltage	Mocho pump will not start	Low standpipe level	Low level standpipe alarm	6 yr^{-1}	2 hours
㉓ Solenoid control circuit	Opens & closes control valve	Control relay residual magnetism	Random failure	Relay sticks	Causes control valve to be closed too long	Low storage tank level	Low storage tank alarm	0.067 yr^{-1}	2 hours
⑩ Manual drain valve	Isolates standpipe	Left in closed position	Human error maintenance	Standpipe will fill to normal level	Cannot drain standpipe	Low standpipe level	Low standpipe level alarm	0.067 yr^{-1}	2 hours
③ Manual drain valve	Isolates storage tank	Left in closed position	Human error maintenance	Tank will fill to normal level	Cannot drain storage tank	Will drain system down stream of manual valve	Low water pressure LLNL	0.067 yr^{-1}	1 hour
⑰ Low standpipe level alarm module	Generates alarm in Bldg. 511	Inactive	Random failure	Cannot notify personnel in Bldg. 511 of low standpipe level			Test	0.067 yr^{-1}	3 hours
⑱ Low storage tank level module alarm	Generates alarm in Bldg. 511	Inactive	Random failure	Cannot notify personnel in Bldg. 511 of low storage tank level			Test	0.067 yr^{-1}	3 hours
⑫ Mocho pump failure	Pumps water from Hetch Hetchy	Fails to start	Random failure	Cannot pump water to standpipe	Low standpipe level	Inadequate water supply	Low standpipe level	0.133 yr^{-1}	8 hours

*Number refers to location on schematic in Fig. 2

the pipes downstream from the manual valve will be drained, leading to a dry condition. In this case, an alarm will not be generated. Closing the storage-tank drain valve is a single event leading to inadequate supply of water.

Fault Tree Synthesis Algorithm

The fault tree synthesis algorithm defines how a control loop can cause or pass a disturbance, resulting in an occurrence of the Top Event. Here, the Top Event is a disturbance in the top node variable (i.e., M1 = −1). For the fault tree analysis of the Mocho water-supply system, we are concerned with events that can cause an inadequate supply of water. Causes of an inadequate water supply can be component failures resulting in a low storage-tank level or low standpipe level; these component failures may include failures on control devices on the NFBL, or disturbances external to the NFBL. The fault tree in Fig.

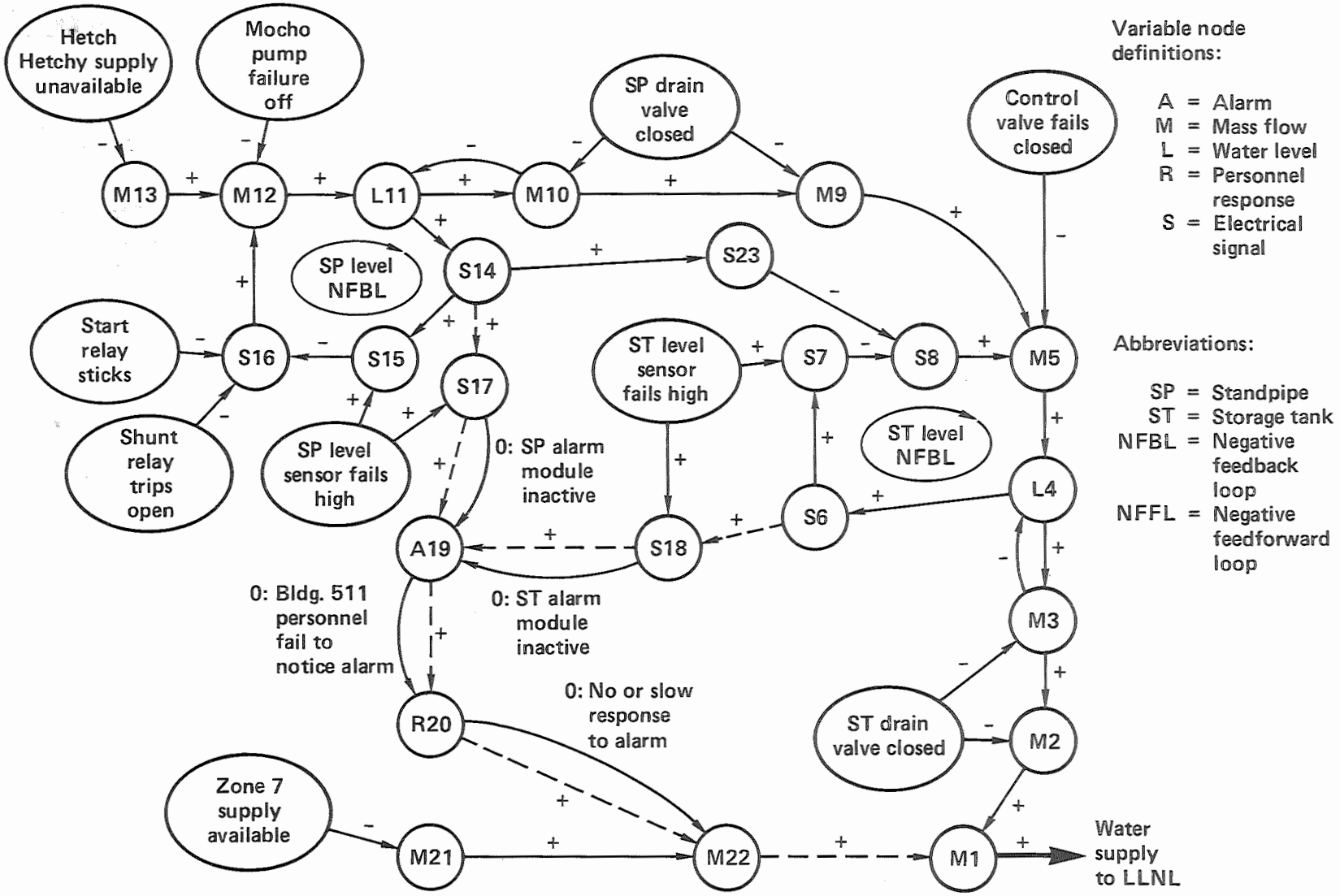

Figure 5-5. The Mocho system digraph showing the failure modes included from the Failure Modes and Effects Analysis in Table 5-1.

5-6 displays these failures. In addition, failure of LLNL personnel to take action is represented by zero-gain events which cause the NFFLs to fail. As stated previously, another cause of insufficient water supply is the closure of the storage-tank drain valve. In this case no storage-tank level signal is generated, which automatically fails the NFFL.

The tank-level sensor failing high also has a similar effect. This sensor performs both a control function and a monitoring function, and its failure generates a low level in the storage tank without generating an alarm in Bldg. 511. Examining the fault tree in Fig. 5-7, we see that the level sensor failing low appears as input to both sides of an AND gate. The failure of the standpipe-level sensor has the same effect, resulting in a failure of the storage-tank level, since the inventory of water in the standpipe will be low at all times.

Even if NFFLs work as intended (i.e., personnel in Bldg. 511 respond correctly to an alarm), there will be a time lag before water can be valved in from Zone 7 (represented by the basic event "no or slow response to alarm"). This dead time in the system leads to additional unavailability of the water supply. Results of the detailed reliability assessment (Hasegawa and Lambert, 1985) showed that the other zero-gain events which fail the NFFLs did not dominate the analysis from a probabilistic viewpoint.

Conclusions

This study points out some useful features of the digraph-fault tree methodology, including the incorporation of system dynamics and consideration of the topology of system variables. The Mocho supply system was a very complicated system to understand and model. Use of the digraph-fault tree analysis made the reliability analysis of this system manageable and gave insights generally not obtainable from a conventional fault-tree analysis.

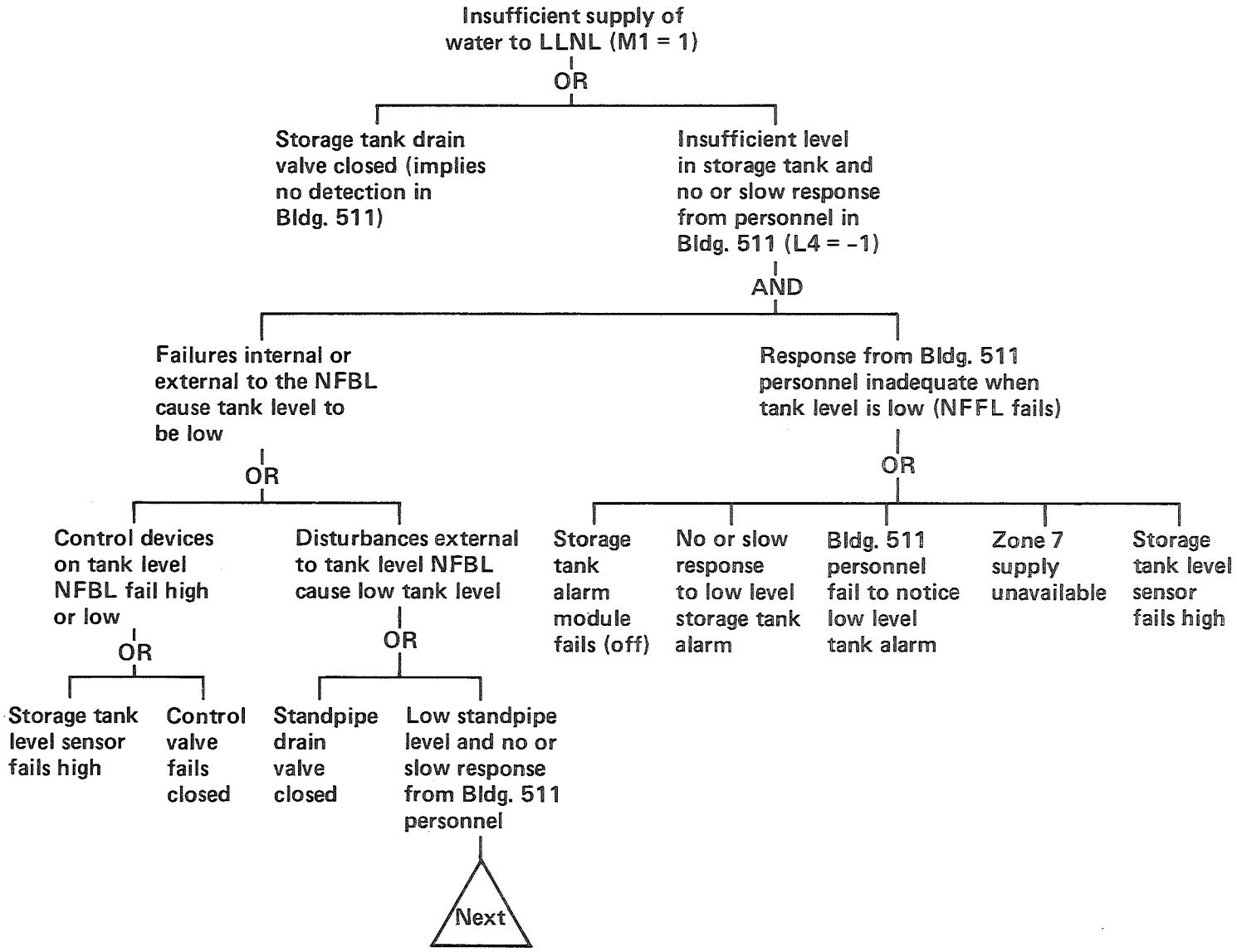

Figure 5-6. Fault tree of Mocho water-supply system, following the effects of an insufficient supply of water to LLNL.

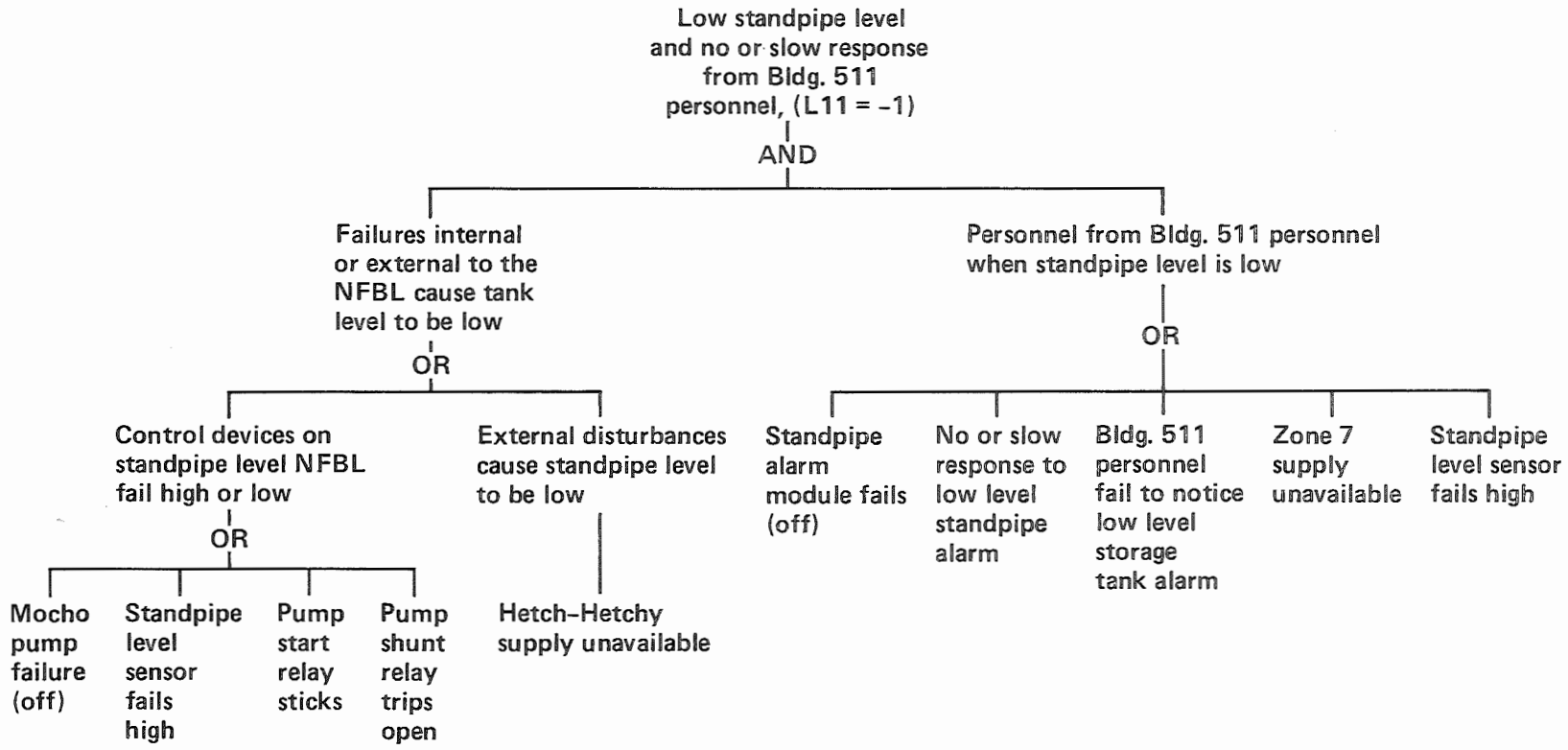

Figure 5-7. Fault tree showing the effects of a low standpipe level and no or slow response from B-511 personnel to valve in the alternate water supply.

Part 6: Conclusions

As outlined in Table 6-1, the ideal approach to fire risk assessment consists of six categories of analysis. To date, our research has concentrated on only the second, third, and fourth categories from the table, but even with this truncated list, we were quite productive in the areas of physical research. In the highly qualitative areas of risk analysis and interpretation, our approach was far more generalized. Appendix A of this report details our ideal risk analysis protocol. Several factors complicate this ideal procedure, chiefly lack of time. Very few of the facilities subject to our analysis are simple in either design or content. Any analysis must have adequate time to:

- Define the facility mission and the details of operation.
- Conduct a detailed site analysis, preferably before project completion.
- Establish locations and spacial relationships of critical areas and components as perceived by key personnel.
- Do operations necessary to fire-risk and potential-damage assessment of critical areas and components.
- Establish lost-time estimates defined by key personnel.

We have accomplished such an analysis, as demonstrated in the TMX Upgrade risk assessment section in our FY 83 Year-End Report. In this analysis, we provided information on potential loss based only on critical space analysis and on the perception of responsible operating personnel.

We have studied heat-release rates as determined from large-scale cable fire tests. These results indicate that for fuel load conditions in typical experimental facilities, fires will never produce a hot-layer temperature that will cause significant fire spread (325°C), but will insure sprinkler activation (~70°C) in less than 300 s. We used our heat-release rate data as input to study available fire models in order to determine the conditions under which these models may be accurately employed; using the results from this study, we have produced a fire risk-assessment protocol for facilities, described in Part 4 of this report.

In addition to risk analysis for total facilities, we have also developed similar procedures for single systems, most notably an analysis of the LLNL water-supply system. This analysis expands on the fault-tree procedures we employed early in this project to define operational characteristics and the reliability of enclosure-fire management systems. By using digraphs to augment the fault-tree analysis, we were able to relate the system dynamics and the interaction of system variables in order to determine the reliability of the key parameters of water-supply control circuits. The details and background of this analysis are contained in Part 5 of this report.

Weight-loss rate from the full-scale cable fire tests ranged from 11 to 42 g/s, and heat-release rate ranged from 100–1000 kW. In our smoke test at Fort Cronkhite, the average weight-loss rate was about 33 g/s, which gives us an idealized

Table 6-1. General flow of systems approach to fire risk.

1.	**Define natural boundaries of activity zones.**
	a. Walls, halls, wings, floors
	b. HVAC circuit separations, flow separations
	c. Cross zoning of fire-management systems.
	d. Passive fire barrier systems.
	e. Activity separation systems.
2.	**Define components and areas of critical importance to the facility.**
	a. Degree of life-hazard potential.
	b. Capital loss (direct cost and indirect factors).
	c. Programmatic delay.
	d. Loss of competitive currency.
3.	**Analyze fire risk and fire management capability in critical areas.**
	a. Potential for substantial ignition event.
	b. Fire growth and heat-release rate analysis.
	c. Fire detection and suppression reliability analysis.
	d. Fire detection and suppression effectiveness analysis.
	e. Research into unusual condition of fire risk potential.
4.	**Assess potential loss in each critical zone.**
	a. Programmatic delay
	b. Capital loss (direct cost and indirect factors).
5.	**Apply current guidelines and codes with regard to effectiveness to prevent potential loss.**
	a. LLNL guidelines
	b. DOE guidelines
	c. UBL guidelines
	d. Cal/OSHA and Federal OSHA guidelines.
6.	**Define appropriate contemporary and cost-effective procedure to improve total facility fire safety.**

heat-release rate of 1150 kW. For the mixture of polyurethane and neoprene, the actual heat-release rate depends on the efficiency of burning and the energy required to gasify the polymer. From various articles in the literature (Tewarson, 1980) the efficiency of burning is approximately 80%; therefore, the actual heat-release rate in the Fort Cronkhite tests was about 900 kW, a value within the range of our cable fire tests. Smoke transport from this source through the 12-ft high, 180-ft long tunnel indicates optical density of 0.214/ft near the open end of the tunnel. The maximum reduction in pH from 5.46 to 4.08 (measured acid strength produced by aerosol solution in calibrated water traps) was of sufficient concentration to cause severe corrosion of metals had they been located at the exit of the tunnel. This test series was conducted in a constrained volume—the smoke generated was conveyed 180 ft down a 12-ft high by 13-ft wide tunnel to the outside. If the fire was set in the middle of a very large enclosure, concentration at the 180-ft radius would be about one percent of the tunnel value. Using smoke-plume dilution algorithms from smoke filling relationships (Cetegen, Zukoski, and Kubota, 1982), we project the smoke concentration of a 180-ft radius to be about 300 ppm for this fire. This is not enough smoke to cause corrosion, but it is 15 times the alarm threshold concentration for smoke detectors. Thus, both experiment and analytical results couple to indicate the potential for corrosive damage and the potential for alarm by calculation of smoke dilution in the condition produced by our smoke fate experiments.

In our final report of this project, we will combine these related analytical procedures into an ideal and practical protocol for fire risk assessment. This protocol will be flexible in order to address different facilities. Other protocol components can be added as needed.

Acknowledgments

The authors are indebted to many individuals who assisted and encouraged the work sponsored in this report. Principally, Dr. Arnold A. Weintraub, who maintained a firm rein on this project to ensure its pertinence and application to overall fire safety of the Department of Energy. Our consultants: Professors Patrick Pagni and Carlos Fernando-Pello from the University of California, Berkeley, and Professor Edward Zukoski from the California Institute of Technology, and Dr. Howard Lambert, private consultant, were major contributors and guides in various areas of research. Finally, the yeoman efforts of Technical Information Department editors, Kevin J. Anderson, for this year's report, and Gorgiana M. Rotter, for the previous year-end reports, and also Elaine Bosserman, Executive Secretary for the Special Projects Division, must be celebrated. They were all untiring but forgiving, qualities that grace few people whose work is bound by deadlines.

Bibliography

D. J. Allen and M. S. M. Rao (1980), "New Algorithms for the Synthesis and Analysis of Fault Trees," *I&EC Fundamentals*, **19**, 79–85.

R. L. Alpert and E. J. Ward (1982), *Evaluating Unsprinklered Fire Hazards*, Factory Mutual Research Corporation, FMRC Tech Report 01836-2.

N. J. Alvares, K. L. Foote, and P. J. Pagni (1984), "Forced Ventilation Enclosure Fires," *Combustion Science and Technology* **39**, 55–81.

B. M. Cetegen, E. E. Zukoski, and T. Kubota (1982), "Entrainment of Flame Geometry of Fire Plumes," Ph.D. thesis, California Institute of Technology, Pasadena, CA.

K. L. Foote, P. J. Pagni, and N. J. Alvares (1985), "Temperature Correlations for Forced-Ventilated Compartment Fires," Lawrence Livermore National Laboratory, Livermore, CA, UCRL-92818.

H. K. Hasegawa, N. J. Alvares, A. E. Lipska-Quinn (1982), D. G. Beason, K. L. Foote, and S. J. Priante, *Fire Protection Research for Energy Technology Projects: FY 81 Year-End Report*, Lawrence Livermore National Laboratory, Livermore, CA, UCRL-53179-81.

H. K. Hasegawa, N. J. Alvares, A. E. Lipska-Quinn, D. G. Beason, S. J. Priante, and K. L. Foote (1983), *Fire Protection Research for DOE Facilities: FY 82 Year-End Report*, Lawrence Livermore National Laboratory, Livermore, CA, UCRL-53179-82.

H. K. Hasegawa, N. J. Alvares, A. E. Lipska-Quinn, D. G. Beason, K. L. Foote, S. J. Priante, and K. Staggs (1984), *Fire Protection Research for DOE Facilities: FY 83 Year-End Report*, Lawrence Livermore National Laboratory, Livermore, CA, UCRL-53179-83.

H. K. Hasegawa and H. E. Lambert (1985), *Reliability Study on the Lawrence Livermore National Laboratory Water-Supply System*, Lawrence Livermore National Laboratory, Livermore, CA, UCRL-92057.

H. E. Lambert (1979), "Comments on the Lapp-Powers Computer Aided Synthesis of Fault Trees," *IEEE Transactions on Reliability* **28**, 6.

S. A. Lapp and G. J. Powers (1977), "Computer-Aided Synthesis of Fault Trees," *IEEE Transactions on Reliabilty*, R-26, p. 2–13 (April 1977).

S. A. Lapp and G. J. Powers (1977), "The Synthesis of Fault Trees," *Nuclear Systems Reliability and Risk Assessment*, J. B. Fussell and G. R. Burdick, eds., (Society for Industrial and Applied Mathematics, Philadelphia, PA), pp. 778–799.

B. J. McCaffrey, J. G. Quintiere, and M. P. Harkleroad (1981), "Estimating Room Temperatures and the Likelihood of Flashover Using Fire Data Correlations," *Fire Technology* **17**(2), 98–119.

H. E. Mitler (1984), "Zone Modeling of Forced-Ventilation Fires," *Combustion Science & Technology* **39**, 83–106.

J. G. Quintiere, K. Steckler, and D. Corley (1984), "An Assessment of Fire-Induced Flows in Compartments," *Fire Science and Technology* **4**(1), 1–4.

A. Tewarson (1980), "Physico-Chemical and Combustion Pyrolysis Properties of Polymeric Materials," National Bureau of Standards, Gaithersburg, MD, NBS-GCR 80-295 (December 1980).

E. E. Zukoski and T. Kubota (1978), "A Computer Model for Fluid Dynamic Aspects of a Transient Fire in a Two-Room Structure," (2nd Ed.), California Institute of Technology Report, prepared for U.S. Dept. of Commerce, National Bureau of Standards, Gaithersburg, MD.

E. E. Zukoski and T. Kubota (1980), "Two-Layer Modeling of Smoke Movement in Building Fires," *Fire and Materials* **4**(19).

KJA/sg

Appendix A
Outline for Ideal Risk Analysis Protocol

Title: Fire risk assessment and the definition of appropriate fire management procedures in DOE experimental facilities.

Scope: Our philosophy regarding the interaction of experimental goals and fire safety procedures:

- The successful completion of the experiment is paramount.
- Fire prevention and fire countermeasures *must not* interfere with experimental goals.
- Fire prevention and fire countermeasures must be more than capable of fighting the analyzed fire risk.
- Non-experimental facilities (including computer rooms) are already adequately analyzed by current DOE codes and regulations.

Approach: Methodology for applying this protocol to enclosures housing experimental facilities:

1. *Pre-visit Analysis*

   Review mission of facility

   a. Define components to meet goals:
      - control rooms
      - diagnostic systems
      - power systems
      - super-conducting systems
      - neutral beam systems
      - laser systems

   Review required subsystems

   a. Those unusual in experimental situations
      - shielding
      - cooling or heating
      - reservoirs for special fluids or gases
   b. Those usual in experimental situations
      - HVAC
      - environmental control
      - standard power and lighting
   c. Inspect geometric arrangement of systems and subsystems
   d. Note the range and distribution of materials required
      - enclosure construction
      - experimental construction

   Review facility planning documents

   a. Pert charts and resource management
   b. Critical path networks
   c. Time schedule planning both for purchasing and construction
   d. Review SARs

2. *Identify Critical Components and Unit Spaces*

   From enclosure dimensions, ventilation, and enclosure heat-transfer constants, predict fire heat-release rate required to:

   - attain sprinkler fuse temperature in ceiling layer
   - attain average polymer degradation temperature in ceiling layer (~300°C)
   - produce a ceiling layer thickness of one-half the total enclosure height
   - produce a one-half-thickness ceiling layer with temperature potential to do structural damage to experimental component or to enclosure.

From enclosure dimensions, ventilation, and plume velocity theory, predict the fire heat-release rate required to:

- activate smoke detectors (average)
- attain sufficient concentration to spread smoke to adjoining critical space enclosures
- attain sufficient concentration to cause potential for smoke corrosion of corrosion-sensitive experimental and diagnostic units
- define a fire-management system with the capability for overkilling the predicted fire spread and smoke production scenarios

Special case for fire management of facilities during construction, remodeling, and experimental replacement procedures.

3. *Site-Inspection Analysis*
   Identify and contact appropriate facility technologists and safety personnel.
   - Review facility planning documents with appropriate site personnel; rationalize data to current status.
   - Characterize "as-built" facilities to "as-planned" documents.
   - Confirm identification of critical spaces and components.
   - Inspect and perform dimensional analysis of confirmed critical spaces and components.
   - Define areas of high fire potential that may impact a critical space or spaces (if any).
   - Define flammable materials parameters in critical spaces:
     — ease of ignition (critical temperature, 13 number, heat of vaporization)
     — flame-spread rate
     — heat-release rate f(geometry)
     — smoke-release rate
     — excess pyrolyzate production
   - Compare upper-layer WT produced by flammable materials to destructive/detection loads predicted from enclosure data in the pre-visit analysis.
   - Contrast existing and predicted fire-management system with that predicted by the site visit.
   - Identify specific trouble spots, specifically those relating to fire/smoke spread and the capability of fire-management system overkill.

4. *Report*
   Report the results of the analysis in a concise form to establish: areas where current procedures provide a confident level of risk mitigation; areas where fire risk conditions provide an unusual hazard in terms of flammable materials, critical equipment corrosion susceptibility, or fire-management system compromise; and areas where future materials of unknown composition are required to complete the experimental goals.
   - Recommend procedures to provide a confident level of risk mitigation in the specified area.
   - Provide a statement of critical assumptions and conjecture.
   - Provide a statement of areas where (in our analysis) fire protection systems are unnecessary.
   - Provide a statement describing how future fire analysis procedures can improve confidence of fire risk projects.

Appendices:

A. NFPA Decision Tree modified to address conditions in enclosures housing large DOE experiments.
B. Project management critical path networks as an aid to identify critical items of the experiment.
C. Upper-limit flammability of polymeric materials common to contemporary experiments.
D. Upper-limit flammable output of polymeric materials common to contemporary experiments.
E. Range of corrosive components (potential maximum) in pyrolyzates of polymeric materials common to contemporary experiments.

F. Comparison of enclosure fire model results to experimental data.
G. Delimitation of model output to specific upper-layer temperature and upper-layer depth.
H. Dimensional limits for enclosure fire model application.
I. Correlation of smoke transport with ceiling jet estimates.
J. Fire management systems, attributes and limitations and passive countermeasures.
K. Specific problems relative to the primary design of the experimental enclosure (i.e., is a building designed specifically to house an experiment, or is the experiment placed in an enclosure originally designed for another purpose?)
L. Contrast of fire risk during construction, experimental assembly, and calibration, and during experimental operation.

Appendix B
Using Models to Define Fire Risk

We are convinced that mathematical modeling is the most logical approach to defining interactive fire conditions in enclosures. To this purpose, we have chosen to adopt a set of simplified modeling procedures that combine theoretical and semi-empirical approaches to fire-plume entrainment theory. With these algorithms, we attempt to describe three important parameters produced by enclosure fires:

1. Temperature rise in the hot layer, suggested by a procedure developed at the National Bureau of Standards (NBS), and refined for forced-ventilated conditions at LLNL (Simple Temperature Correlation).
2. Position of the interface between hot and cold layer, using a simplified Cal-Tech code (Zukoski and Kubota, 1978; Cetegen, Zukoski, and Kubota, 1982).
3. Limit values for ceiling jet dynamics by modified semi-empirical plume entrainment calculations developed at Factory Mutual (Alpert and Ward, 1982).

Combined use of these separate relationships (as outlined in Table B-1) enables us to decide whether or not zone model predictions are useful in different enclosures containing fires of variable size. For example, if fire size and room dimensions are within specific ranges, such that the hot layer exceeds a predetermined temperature level, we can apply zone model procedures for defining the fire risk. The operational potential of fire detection and suppression circuits can also be estimated; if these limits are not reached, then the fire-spread potential is limited to regions near the initial fire plume.

The prediction protocol shown in Table B-1 gives the steps we use to assess the level of fire risk possible in DOE enclosures. First, the time to formation of a significant upper layer is estimated using Eq. (1). If the estimated layer-formation time is greater than 300 s (5 min),* then the enclosure is considered to be much larger than the fire. In this case, the fire is either slow-growing, or isolated to a specific item, and thermal threat to the enclosure is minimal. We do, however, want to consider the localized effects that might lead to a small nonhazardous fire growing into a large uncontrollable fire. For the localized fire, we use Eqs. (2.1)–(2.3) to estimate the temperature of the ceiling directly above the fire and the radiant flux from the fire to adjacent objects. We have not yet addressed smoke production from small fires, which is a very important factor to be discussed in the future.

If Eq. (1) estimates a layer-formation time of less than 300 s, then we are able to use Eqs. (1.1)–(1.2), which predicts upper-layer temperature rise and upper-layer thickness, respectively, to evaluate the fire risk to the whole enclosure. We define upper-layer temperatures which are critical to hazard evaluation in an enclosure fire: at 70°C, sprinklers may activate; at 325°C substantial pyrolysis of most combustible polymers probably occurs; and at 500°C flashover may occur. These three temperatures define four ranges of fire hazard. Enclosures with predicted upper-layer temperatures below 70°C represent little hazard; those below 325°C represent minor hazards; those below 500°C represent major hazards; and those above 500°C represent severe hazards.

Criteria for Using Fire Models

Both temperature- and time-dependent conditions control our analysis protocol. Necessary criteria for applying current enclosure-fire model codes are summarized below.

If $T_{upper} > 70°C$; $t_{fire} = 300$ s, we use the **Case 1** procedure in Table B-1;

If $T_{upper} < 70°C$; $t_{fire} = 300$ s, we use the **Case 2** procedure in Table B-1,

---

* National laboratory fire department response times are estimated to be no greater than 5 minutes.

Table B-1. Steps for defining thermal risk in enclosure fires.

Calculate time to layer formation[11]

$$t = \frac{20A_c}{\dot{Q}^{1/3}H_r^{2/3}} \qquad (1)$$

t = time to layer depth equal to half room height[a]
A_c = area of room ceiling
$\dot{Q}$ = heat-release rate of fire source
H_r = room height

[a]If $t > 300$ s, then use only *Case 2*.
If $t < 300$ s, then use *Case 1* and *Case 2*.

Case 1. Hot layer forms within 300 s (5 min):

1.1 Calculate maximum upper-layer temperature at 1800 s.[8,12]

$$T_u = \frac{14.5\ Q^{2/3}}{(A_w \dot{m})^{1/3}\,(kpc)^{1/6}} + 300$$

T_u = bulk temperature of upper layer
$\dot{m}$ = mass-flow rate of air available for burning
kpc = thermal constants of interior surfaces; k = thermal conductivity; p = density; c = heat capacity
A_w = internal surface area of enclosure

1.2 Calculate layer depth (Zukoski and Kubota, 1978).

$$h_1 = 1.95\,\frac{\dot{Q}^{2/5}}{(T_u - 27)^{3/5}}$$

h_1 = altitude of interface between hot and cold layer

Case 2. Hot layer not formed within 300 s:

2.1 Define height of fire plume (Cetegen, Zukoski, and Kubota).

$$H_f = 0.21\,\dot{Q}^{1/3}$$

H_f = height of fire plume

2.2 Define ceiling jet velocity and maximum temperature: (region of plume stagnation on ceiling surface; $r^{6.2}H_f$) (Alpert and Ward, 1982).

$$V_c = 0.79\,\frac{\dot{Q}^{1/3}}{H_r^{5/4}}$$

$$T_c = 159\,\frac{\dot{Q}^{2/3}}{H_r^{2/3} + 27}$$

V_c = maximum ceiling jet velocity
T_c = maximum ceiling jet temperature
H_r = room heat

2.3 Calculate radiant exposure (horizontal) from fire plume to adjacent objects.

$$\dot{Q}_r = \frac{\dot{Q}}{617}$$

$\dot{Q}_r$ = radiant flux level at 3 m from center of plume

Sample Application of Fire-Risk Protocol

Figure B-1 shows two views each of the control room and the accelerator bay for the Engineering Test Accelerator (ETA) Facility attached to Bldg. 435 at LLNL. This facility is a fairly typical example of an experiment that has been in active operation for several years. We applied our analysis protocol to these enclosures to predict the critical output parameters of temperature and layer height for a 400-kW fire symmetrically located in the enclosure. The variable input parameters were the thermal properties of the interior surface (ignoring the floors) and the ventilation rate (in the control room only). Fire strength was estimated based on the known composition of electrical insulation of the majority of cable in the ETA Facility. Similar materials used in experiments conducted in our fire test cell helped us to establish 400 kW as a representative fire strength.* Figure B-2 shows the relative sizes of the ETA main bay and our fire test cell.

Tables B-2a and B-2b list both input and output parameters for the ETA main bay and control room. Only ventilation of the control room is varied in Table B-2a, and we assume interior surfaces to be all concrete. Table B-2b has the same ventilation variation; however, in this case thermal constants of interior surfaces are selected to best duplicate the materials contained in the ETA Facility. Both tabular and graphic displays show that the upper-layer temperature in both large and small enclosures is highly dependent on surface heat transfer and ventilation; for large rooms this effect is less. In both the control room and the main bay, the layer temperature never attains levels that would suggest fire spread using a 400-kW fire.

---

* See large-scale cable fire data, Part 3 of this report.

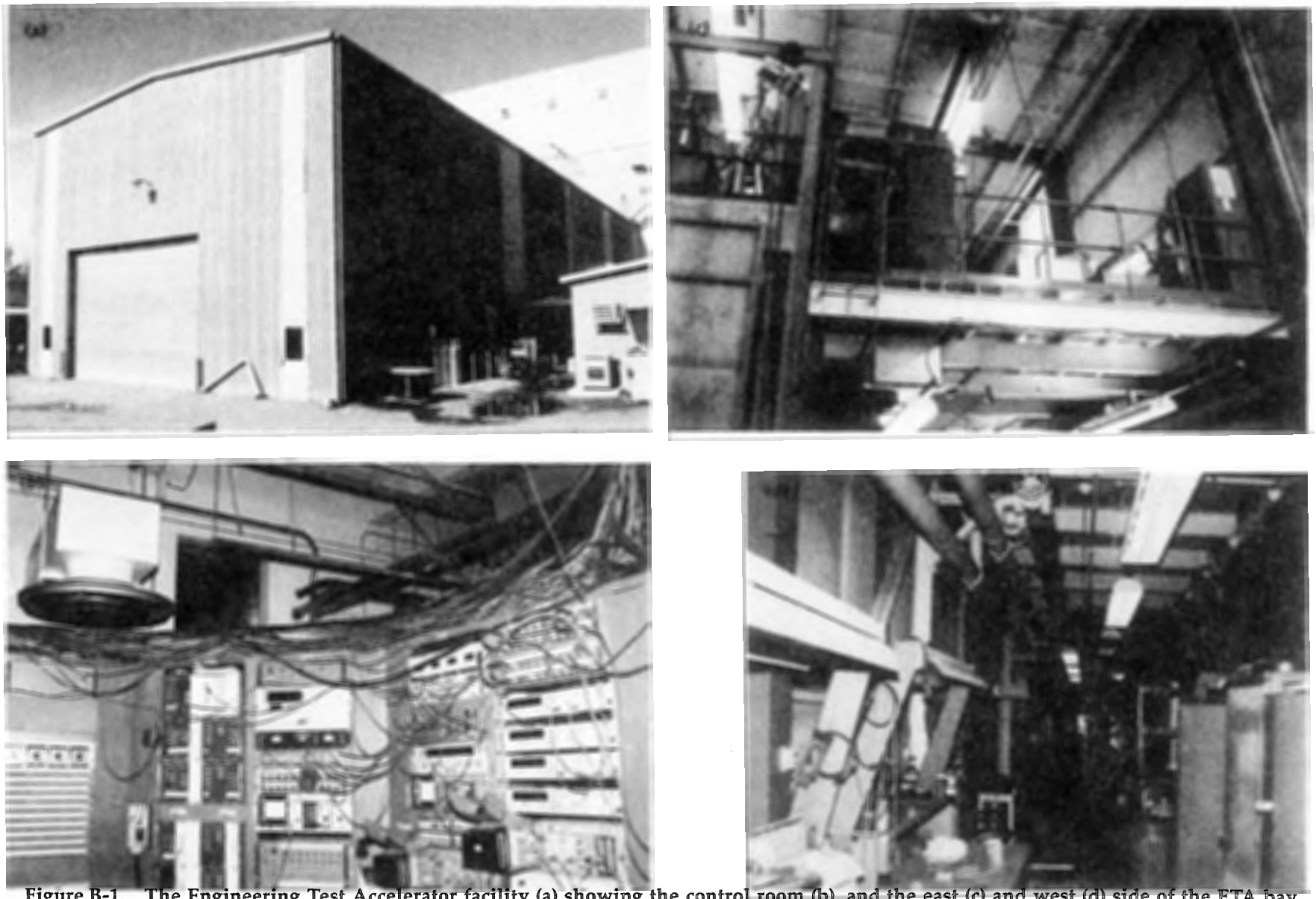

Figure B-1. The Engineering Test Accelerator facility (a) showing the control room (b), and the east (c) and west (d) side of the ETA bay.

Table B-2a. Prediction of hot-layer temperature and plume radiation in ETA facility enclosure surfaces assumed to be thick concrete.

Building	ETA test chamber	ETA control room	ETA control room
Height (m)	14	4	4
Width (m)	15	5	5
Length (m)	52	9.5	9.5
Ventilation (g/s)	2000	2000	2000
Fire potential (kW)	400	400	400
kpc of walls	2.88	2.88	2.88
Est. flame height (m)	231	2.31	2.31
Est. plume temp. at ceiling (°C)	113	884	884
Est. plume velocity at ceiling (m/s)	2.14	3.67	3.67
Est. plume smoke concentration at ceiling (%)	—	—	—
Est. radiant exp. to object 3 m away (kW)	0.65	0.65	0.65
Est. time to formation (s)	74	10	10
Est. upper layer temp. at 300 s (°C)	61	114	155
Est. upper layer temp. at 1800 s (°C)	73	144	199
Est. layer interface height at 300 s (m)	2.57	1.47	1.17
Est. layer interface height at 1800 s (m)	215	1.23	0.98
Est. time to 70°C (sprinkler activation) (s)	>1800	<300	<300
Est. time to 325°C (plastic pyrolysis) (s)	>1800	>1800	>1800
Est. time to 600°C (flashover) (s)	>1800	>1800	>1800

Table B-2b. Prediction of hot-layer temperature and plume radiation in ETA facility enclosure surfaces of ETA *in situ* properties.

Building	ETA test chamber	ETA control room	ETA control room
Height (m)	14	4	4
Width (m)	15	5	5
Length (m)	52	9.5	9.5
Ventilation (g/s)	2000	2000	2000
Fire potential (kW)	400	400	400
kpc of wals	0.00178	0.179	0.179
Est. flame height (m)	231	2.31	2.31
Est. plume temp. at ceiling (°C)	113	884	884
Est. plume velocity at ceiling (m/s)	2.14	3.67	3.67
Est. plume smoke concentration at ceiling (%)	—	—	—
Est. radiant exp. to object 3 m away (kW)	0.65	0.65	0.65
Est. time to formation (s)	74	10	10
Est. upper layer temp. at 300 s (°C)	145	165	230
Est. upper layer temp. at 1800 s (°C)	185	213	300
Est. layer interface height at 300 s (m)	1.23	1.11	0.88
Est. layer interface height at 1800 s (m)	1.02	0.93	0.74
Est. time to 70°C (sprinkler activation) (s)	>1800	<300	<300
Est. time to 325°C (plastic pyrolysis) (s)	>1800	>1800	>1800
Est. time to 600°C (flashover) (s)	>1800	>1800	>1800

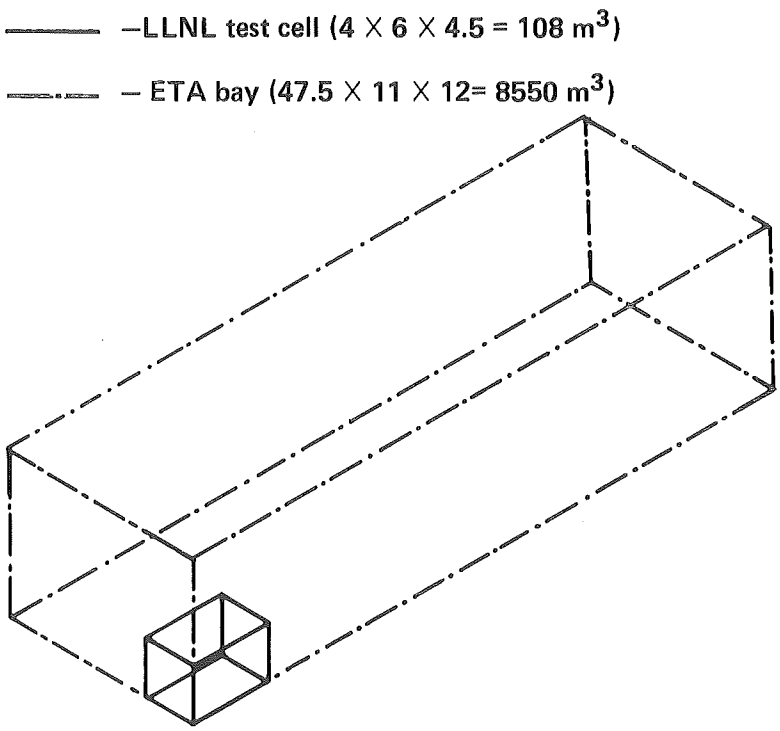

Figure B-2. Relative sizes of ETA bay, LLNL test cell, and other enclosures.